Electrospinning of Biocompatible Polymers

Bc. Lenka Vítková

Master's thesis
2019

Tomas Bata University in Zlín
Faculty of Technology

Univerzita Tomáše Bati ve Zlíně
Fakulta technologická
Ústav fyziky a mater. inženýrství
akademický rok: 2018/2019

ZADÁNÍ DIPLOMOVÉ PRÁCE
(PROJEKTU, UMĚLECKÉHO DÍLA, UMĚLECKÉHO VÝKONU)

Jméno a příjmení:	**Bc. Lenka Vítková**
Osobní číslo:	**T17305**
Studijní program:	**N2808 Chemie a technologie materiálů**
Studijní obor:	**Materiálové inženýrství**
Forma studia:	**prezenční**
Téma práce:	**Elektrostatické zvlákňování biokompatibilních polymerů**

Zásady pro vypracování:

1. **Vypracujte rešerši na zadané téma diplomové práce.**
2. **Připravte roztoky na bázi hyaluronanu, polyvinylalkoholu, polyethylenoxidu a jejich kombinace.**
3. **Na zařízení pro elektrospinnig proveďte experimenty a připravte několik typů nanovláken.**
4. **Proveďte analýzy nanonvláken a diskuzi k výsledkům.**

Rozsah diplomové práce:

Rozsah příloh:

Forma zpracování diplomové práce: **tištěná**

Seznam odborné literatury:

1. **Lukáš, D. et al.: Physical principles of electrospinning (Electrospinning as a nano-scale technology of the twenty-first century),** *Textile Progress* **, 41 (2), 59-140, 2009.**

Vedoucí diplomové práce: **doc. Mgr. Aleš Mráček, Ph.D.**
Ústav fyziky a mater. inženýrství

Datum zadání diplomové práce: **1. února 2019**

Termín odevzdání diplomové práce: **17. května 2019**

Ve Zlíně dne 22. února 2019

L.S.

doc. Ing. Roman Čermák, Ph.D.
děkan

doc. Mgr. Aleš Mráček, Ph.D.
ředitel ústavu

Příjmení a jméno: Vítková Lenka Obor: Materiálové inženýrství

PROHLÁŠENÍ

Prohlašuji, že

- beru na vědomí, že odevzdáním diplomové/bakalářské práce souhlasím se zveřejněním své práce podle zákona č. 111/1998 Sb. o vysokých školách a o změně a doplnění dalších zákonů (zákon o vysokých školách), ve znění pozdějších právních předpisů, bez ohledu na výsledek obhajoby [1)];
- beru na vědomí, že diplomová/bakalářská práce bude uložena v elektronické podobě v univerzitním informačním systému dostupná k nahlédnutí, že jeden výtisk diplomové/bakalářské práce bude uložen na příslušném ústavu Fakulty technologické UTB ve Zlíně a jeden výtisk bude uložen u vedoucího práce;
- byl/a jsem seznámen/a s tím, že na moji diplomovou/bakalářskou práci se plně vztahuje zákon č. 121/2000 Sb. o právu autorském, o právech souvisejících s právem autorským a o změně některých zákonů (autorský zákon) ve znění pozdějších právních předpisů, zejm. § 35 odst. 3 [2)];
- beru na vědomí, že podle § 60 [3)] odst. 1 autorského zákona má UTB ve Zlíně právo na uzavření licenční smlouvy o užití školního díla v rozsahu § 12 odst. 4 autorského zákona;
- beru na vědomí, že podle § 60 [3)] odst. 2 a 3 mohu užít své dílo – diplomovou/bakalářskou práci nebo poskytnout licenci k jejímu využití jen s předchozím písemným souhlasem Univerzity Tomáše Bati ve Zlíně, která je oprávněna v takovém případě ode mne požadovat přiměřený příspěvek na úhradu nákladů, které byly Univerzitou Tomáše Bati ve Zlíně na vytvoření díla vynaloženy (až do jejich skutečné výše);
- beru na vědomí, že pokud bylo k vypracování diplomové/bakalářské práce využito softwaru poskytnutého Univerzitou Tomáše Bati ve Zlíně nebo jinými subjekty pouze ke studijním a výzkumným účelům (tedy pouze k nekomerčnímu využití), nelze výsledky diplomové/bakalářské práce využít ke komerčním účelům;
- beru na vědomí, že pokud je výstupem diplomové/bakalářské práce jakýkoliv softwarový produkt, považují se za součást práce rovněž i zdrojové kódy, popř. soubory, ze kterých se projekt skládá. Neodevzdání této součásti může být důvodem k neobhájení práce.

Ve Zlíně .....

.....

[1)] zákon č. 111/1998 Sb. o vysokých školách a o změně a doplnění dalších zákonů (zákon o vysokých školách), ve znění pozdějších právních předpisů, § 47 Zveřejňování závěrečných prací:

(1)Vysoká škola nevýdělečně zveřejňuje disertační, diplomové, bakalářské a rigorózní práce, u kterých proběhla obhajoba, včetně posudků oponentů a výsledku obhajoby prostřednictvím databáze kvalifikačních prací, kterou spravuje. Způsob zveřejnění stanoví vnitřní předpis vysoké školy.

(2)Disertační, diplomové, bakalářské a rigorózní práce odevzdané uchazečem k obhajobě musí být též nejméně pět pracovních dnů před konáním obhajoby zveřejněny k nahlížení veřejnosti v místě určeném vnitřním předpisem vysoké školy nebo není-li tak určeno, v místě pracoviště vysoké školy, kde se má konat obhajoba práce. Každý si může ze zveřejněné práce pořizovat na své náklady výpisy, opisy nebo rozmnoženiny.

(3)Platí, že odevzdáním práce autor souhlasí se zveřejněním své práce podle tohoto zákona, bez ohledu na výsledek obhajoby.

[2)] zákon č. 121/2000 Sb. o právu autorském, o právech souvisejících s právem autorským a o změně některých zákonů (autorský zákon) ve znění pozdějších právních předpisů, § 35 odst. 3:

(3) Do práva autorského také nezasahuje škola nebo školské či vzdělávací zařízení, užije-li nikoli za účelem přímého nebo nepřímého hospodářského nebo obchodního prospěchu k výuce nebo k vlastní potřebě dílo vytvořené žákem nebo studentem ke splnění školních nebo studijních povinností vyplývajících z jeho právního vztahu ke škole nebo školskému či vzdělávacího zařízení (školní dílo).

[3)] zákon č. 121/2000 Sb. o právu autorském, o právech souvisejících s právem autorským a o změně některých zákonů (autorský zákon) ve znění pozdějších právních předpisů, § 60 Školní dílo:

(1) Škola nebo školské či vzdělávací zařízení mají za obvyklých podmínek právo na uzavření licenční smlouvy o užití školního díla (§ 35 odst. 3). Odpírá-li autor takového díla udělit svolení bez vážného důvodu, mohou se tyto osoby domáhat nahrazení chybějícího projevu jeho vůle u soudu. Ustanovení § 35 odst. 3 zůstává nedotčeno.

(2) Není-li sjednáno jinak, může autor školního díla své dílo užít či poskytnout jinému licenci, není-li to v rozporu s oprávněnými zájmy školy nebo školského či vzdělávacího zařízení.

(3) Škola nebo školské či vzdělávací zařízení jsou oprávněny požadovat, aby jim autor školního díla z výdělku jím dosaženého v souvislosti s užitím díla či poskytnutím licence podle odstavce 2 přiměřeně přispěl na úhradu nákladů, které na vytvoření díla vynaložily, a to podle okolností až do jejich skutečné výše; přitom se přihlédne k výši výdělku dosaženého školou nebo školským či vzdělávacím zařízením z užití školního díla podle odstavce 1.

ABSTRAKT

Tato diplomová práce si klade za cíl najít způsoby produkce nanovláken kyseliny hyaluronové pomocí elektrostatického zvlákňování z polymerního roztoku. Kyselina hyaluronová je biopolymer vlastní lidskému tělu, a je široce studována pro možnost využití v medicínských aplikacích, jako je tkáňové inženýrství a distribuce léčiv. Především v tkáňovém inženýrství byla prokázána nezastupitelnost nanostruktur pro úspěšnou podporu růstu buněk. Elektrostatické zvlákňování je pokročilá metoda výroby nanovláken, která může být převedena do výroby ve velkém měřítku. Cílem experimentální části této práce je určit parametry roztoku a procesní parametry zajišťující úspěšnou tvorbu nanovláken obsahujících kyselinu hyaluronovou.

Klíčová slova: kyselina hyaluronová, polyvinylalkohol, poly(ethylen oxid), elektrostatické zvlákňování z roztoku, rozpouštědlo

ABSTRACT

The current Master’s thesis is devoted to finding means to produce hyaluronic acid nanofibers via polymer solution electrospinning. Hyaluronic acid is a biopolymer own to human body, and is widely investigated for potential use in medical applications, such as tissue engineering and drug delivery. Especially in tissue engineering, nanostructures have been found essential to successfully sustain cell growth. Electrospinning is a progressive method of nanofibers fabrication, with potential to large scale production modification. The experimental part of the current thesis aims to determine solution and processing parameters necessary to successfully electrospun nanofibers containing hyaluronic acid.

Keywords: hyaluronic acid, polyvinylalcohol, poly(ethylene oxide), solution electrospinning, solvent

Acknowledgements

I would like to thank my supervisor doc. Mgr. Aleš Mráček PhD. for his guidance throughout the work on this thesis. I would also like to thank Ing. Lenka Musilová PhD. for her very appreciated help during the experimental work on this thesis.

I hereby declare that I have worked out my Master's thesis independently and on the basis of literature and sources listed in Bibliography.

I hereby declare that the print version of my Master's thesis and the electronic version of my thesis deposited in the IS/STAG system are identical.

"Getting an education was a bit like a communicable sexual disease. It made you unsuitable for a lot of jobs and then you had the urge to pass it on."

Terry Pratchett

CONTENTS

INTRODUCTION…….…….. **11**

I. THEORETICAL PART

1 FUNDAMENTALS OF ELECTROSPINNING……...……. **13**

1.1 Electrohydrodynamics……...……... **13**

1.1.1 Electrospinning onset…….. **14**

1.1.2 Flow in an external electric field…….…… **16**

1.2 Electrospinning setup……... **18**

1.3 Electric wind effect…….. **19**

1.4 Parameters of electrospinning process……. **19**

1.4.1 Solution parameters…… **19**

1.4.2 Processing parameters…….…… **23**

1.4.3 Ambient parameters…….……... **23**

1.5 Core-shell fibers…….….. **23**

1.5.1 Co-axial electrospinning…….…… **24**

1.5.2 Self-organized phase separation…….…… **24**

1.6 Applications……. **25**

2 MATERIALS CONSIDERATION…… **26**

2.1 Hyaluronic acid…… **26**

2.1.1 Properties…… **26**

2.1.2 Electrospinning……... **26**

2.2. Polyvinyl alcohol……. **27**

2.2.1 Properties…… **27**

2.2.2 Electrospinning……... **28**

2.3 Poly(ethylene oxide)…… **28**

2.3.1 Properties…….……... **28**

2.3.2 Electrospinning……... **28**

3 ANALYSIS METHODS…… **28**

3.1 Solution analysis…….. **29**

3.1.1 Tensiometry……. **29**

3.1.2 Viscometry…….. **29**

3.1.3 Conductometry…… **30**

3.1.4 Density measurement…….. **30**

3.2 Fiber analysis…… **30**

3.2.1 Scanning electron microscopy…… **30**

3.2.2 Fluorescence confocal microscopy……..……... **31**

II. EXPERIMENTAL PART

4 AIM OF WORK…… **33**
5 SAMPLE PREPARATION…… **33**
5.1 Chemicals…… **33**
5.2 HA oxidation and fluorescent labeling of HA and PVA…… **33**
5.2.1 HA oxidation…… **33**
5.2.2 HA fluorescent labeling…… **34**
5.2.3 PVA fluorescent labeling…… **34**
5.3 Solution preparation…… **34**
5.4 Electrospinning equipment…… **35**
6 SAMPLE ANALYSIS…… **36**
6.1 Viscometry…… **36**
6.2 Conductometry…… **36**
6.3 Density measurement…… **36**
6.4 Tensiometry…… **36**
6.5 SEM analysis…… **36**
6.6 Fluorenscent confocal microscopy…… **36**
7 RESULTS…… **36**
7.1 Single Mw HA solutions…… **36**
7.2 Mixed Mw HA solutions…… **50**
7.3 HA/PEO bi-component blend solutions…… **54**
7.4 HA/PVA bi-component blend solutions…… **60**
8 DISCUSSION…… **65**
8.1 Electrospinning of single Mw HA solutions…… **65**
8.2 Electrospinning of mixed Mw HA solutions…… **67**
8.3 The influence of HA Mw on HA/PEO bi-component solutions and their spinnability…… **68**
8.4 The influence of BAC concentration on spinnability of HA/PVA bi-component solution…… **69**
CONCLUSION…… **71**
BIBLIOGRAPHY…… **72**
LIST OF ABBREVIATIONS…… **78**
LIST OF FIGURES…… **79**
LIST OF TABLES…… **82**

INTRODUCTION

Electrospinning is a thin fiber fabrication method. It was first described in 1902 by Cooley and Morton [1], [2],when the effect of strong electric field on liquids was observed. Deformation of free liquid surface and disintegration of droplets occurs at sufficient electric field strength [3]. The deformation is caused by elongation of the material at high rates. In case of polymer solution or melt, solidification of material occurs during electric field driven elongation, and fibers of tens to hundreds of nanometers in diameter are formed. Typically, non-woven fiber mats are produced due to whipping instability taking place in the process. The method is being studied and new approaches are arising, as well as deeper understanding of the electrospinning phenomenon.

Electrospinning of biocompatible polymers is desirable due to potential use in medicine, pharmacy and cosmetics. Nanofibers are a promising material in tissue engineering for various types of tissue [4]–[6]. Nanofibers based drug delivery systems make use of enormous specific surface of nanofibers, possibility of functional group addition to the fiber fundamental material, and encapsulation of a material inside a core-shell structured fibers. This area is being studied by many researchers, such as Agarwall et al., 2008, Rogina, 2014, Vikram and Vasanthakumari, 2016, and Burke et al., 2017, [4], [7]–[9]. Cosmetic industry is already making use of electrospun biocompatible polymer fibers. This is mainly due to inherent hydrophilicity of biopolymers, as well as large specific surface area of nanofibers. These qualities make the nanofibers excellent hydration agents. Other uses of nanofibrous non-woven mats include mechanical filters, or sensors [10].

The currents thesis aims to experimentally determine the conditions allowing a polysaccharide hyaluronic acid (HA) to be spun by direct current electric field. This have been done by several research groups, such as Um et al., 2004, Liu et al., 2011 or Brenner et al., 2012 [11]–[13]. In the current thesis, a novel approach to solvent selection is applied. Electrospinning of bi-polymer blend solutions is applied as well.

In theoretical part of the thesis, the process of polymer solution electrospinning is described. The influence of various parameters is reviewed with respect to relevant literature. The electrospinning process is not fully understood yet, and the significance of respective parameters is being discussed among the experts. The current thesis gives a review of physical phenomena playing a part in electrospinning process and theories of electrospinning onset and jet flow. Theoretical background on the material choice and analytical methods is also given in this part of the thesis.

The experimental part gives the details of materials, their chemical modification and electrospinning process. The results of polymer solution analysis are given and discussed with respect to resulting fiber analysis.

I. THEORETICAL PART

1 FUNDAMENTALS OF ELECTROSPINNING

In electrospinning, a fiber is formed via uniaxial stretching of a viscoelastic material. This is done using electric force. A polymer jet is formed when the repulsive electrostatic force induced in the liquid overcomes the surface tension. Solidification is achieved via rapid solvent evaporation due to enormous specific surface area of the fibers, and path length being enlarged by so-called whipping instability. The method inherently leads to continuous fiber formation, which ends only when the material is consumed [7], [14].

1.1 Electrohydrodynamics

Liquid body behavior in an external electric field is described by electrohydrodynamics. The existence of electrospinning phenomenon can be explained using several physical concepts, which will be discussed in this section [14].

Maxwell's first law of electrostatics gives the relation for electric field magnitude as follows:

$$\vec{\nabla}\,\vec{E}=\frac{\rho}{\varepsilon} \tag{1},$$

where ρ denotes the charge density and ε denotes electric permittivity. An electric field is a conservative field, therefore a scalar potential φ exists, for which the following equation applies:

$$\vec{E}=-\,grad\,\varphi \tag{2}.$$

The hydrodynamic processes associated with electrospinning take place in the surface layer of the liquid. Therefore capillary forces, described by surface tension, and electric bi-layer formation have to be taken into account.

Surface tension is defined as the force needed to enlarge the surface area of a liquid by an area unit. A widely accepted explanation for its existence is through omnidirectional intermolecular forces. In the bulk of homogeneous liquid, all the intermolecular forces cancel each other out. The surface is commonly an interface of gas and liquid phases. The intermolecular forces acting in a gas are considerably lower than in a liquid. This situation leads to an imbalance of forces at the interface, with the resultant force acting perpendicular to liquid surface, in the direction out of the liquid. In agreement with the lowest energy principle, the surface of a liquid will always assemble in a shape with the lowest surface area possible, thus minimizing the force acting on the surface [15].

Conductivity in a liquid is typically provided by free ions. In a static electric field, the charges gather at the surface, thus increasing charge density at the surface. This increased charge density attracts particles of opposite charge in the surrounding of a charged surface, due to which an electric bi-layer is formed. As a result of this phenomenon, the potential is constant and field intensity is zero inside conductive bodies with high free charge concentration. The bi-layer thickness is typically in the range of tens of nanometers and the charge density is multiple times higher in comparison to the bulk, therefore the molecules in the surface layer are affected by the external electric field more. In electrospinning, electric bi-layer can be understood as the reason for only the surface molecules to be drawn from the liquid [14].

Electric pressure is generated due to difference in strength of electric field generated by the surface charge, and electric field generated by the charge in the bulk of the liquid and elsewhere in the

space. As was stated above, electric field inside the bulk of the liquid is shielded by the surface electric field, therefore it remains constant. A relation for electrostatic pressure can be written as follows:

$$p_e = \frac{\varepsilon E^2}{2} \quad (3),$$

where ε denotes electric permittivity and E denotes total electrostatic intensity acting on the liquid [14].

The onset of electrospinning can be in the most general way assumed when the electric pressure overcomes the capillary forces. The process will be discussed in more details in the following section.

1.1.1 Electrospinning onset

Theory of electrospinning onset have been developed via analysis of liquid bodies disintegration. When a liquid droplet is subjected to an electric field, a spike-like structure is observed [14]. The spikes are the precursors of spray/jet formation. The charge density is concentrated at the small radius. The problem of electric potential near the tip of the spike was investigated by Taylor [3], and led to the electrospinning cones being named Taylor cones. Taylor considered a fairly conducting liquid cone of a semi-vertical angle 2θ in an external electrostatic field.

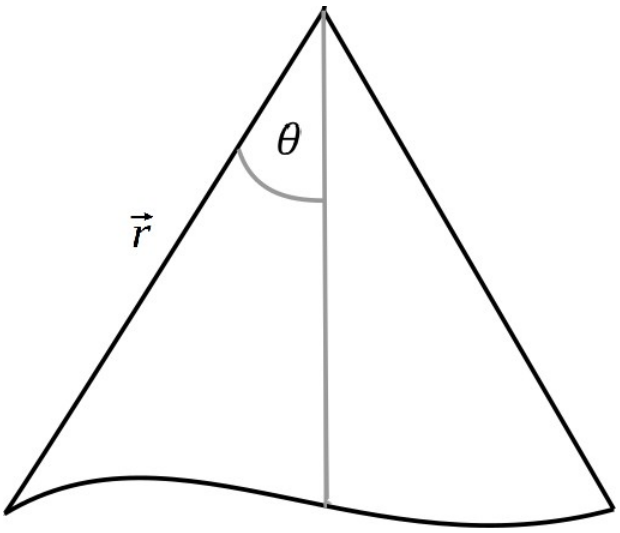

Fig. 1: Taylor cone scheme

In his work, he determined the potential near the cone tip as

$$\varphi = \varphi_0 + A\sqrt{r}\,P_{1/2}(\cos\theta) \quad (4),$$

where φ_0 denotes the potential at the angle θ limiting to zero, A is a constant, r denotes the radial distance from the origin and $P_{1/2}(\cos\theta)$ is the fractional order Legendre polynomial of the half-angle of the cone. To satisfy the condition of a constant potential at the surface of the cone, the Legendre polynomial has to be equal to zero, which gives the angle θ = 49.3°. As the eq. (4) was found by considering the balance between capillary and electrostatic pressure, Taylor managed to determine a critical voltage, i.e. the lowest voltage sufficient to draw a fluid from a capillary:

$$V_c = 4\ln\left(2\frac{h}{R}\right)\cdot\left(1{,}3\pi R\gamma\right)\cdot\left(0{,}09\right) \quad (5),$$

where h [m] denotes the tip-to-collector distance, R [m] denotes the outer radius of the capillary, and γ [mN·m^{-1}] denotes the surface tension. It is ought to remember that eq. (5) was derived considering a fairly conducting fluid in a capillary, and therefore is not generally valid.

Taylor cones are formed on free liquid surface, as well as at the capillary tip. This phenomenon is explained by self-organization induced by electrostatic field. Charges of the same sign are introduced to the liquid surface, resulting in a repulsive force. This force causes the original roughly hemispherical shape to flatten and create a rim. In this rim, a stationary wave is formed, which gives a rise to a Taylor cone formation and start of jetting [14].

The wave in the case of electrospinning is governed by gravity, electrostatic field, and capillary forces arising from surface tension and non-zero curvature of the surface. The stationary wave then follows the dispersion law, which can be derived as

$$\omega^2 = \left(\rho g + \gamma k^2 - \varepsilon E_0^2 k\right)\frac{k}{\rho} \quad (6),$$

where ω denotes angular frequency, ρ denotes liquid mass density, g denotes gravity acceleration, γ denotes surface tension, k denotes wave number, ε denotes dielectric permittivity and E_0 denotes the magnitude of applied electric field [14]. As implied in the previous paragraph, the critical parameter for electrospinning is the electric field strength. According to the theory of fastest forming instability, as derived by Lukáš et al. [16], an unstable wave is formed at the limiting boundary condition $kh \to \infty$, h being the thickness of a planar liquid layer. This leads to (ωt-kh) reaching zero. A critical electric field can be found as

$$\sqrt[4]{4\gamma\rho\frac{g}{\varepsilon^2}} \quad (7).$$

If capillary length a is defined as

$$a = \sqrt{\frac{\gamma}{\rho g}} \quad (8),$$

the instability growth can be analyzed similarly to the aforementioned approach, using the condition of equality of capillary and electric pressures. In this case, capillary length is defined by capillary pressure and can be unified with a typical radius of curvature. This condition is conveniently defined by dimensionless electrospinning number, as follows:

$$\Gamma = \frac{a\varepsilon E_0^2}{2\gamma} \quad (9).$$

As a result of definition, electrospinning number Γ is equal to 1 at the critical electric field E_c. Therefore, electrospinning may occur only for $\Gamma > 1$ [14], [17].

Since the electrospinning onset via fastest forming instability theory derived by Lukáš et al. [16] for free liquid surface concludes in equilibrium of capillary and electrostatic pressure, it can be used to describe the capillary electrospinning as well. It gives the condition that electrospinning from a capillary may occur only if the capillary diameter $2r$ is equal to or greater than the wavelength of a

fastest growing instability [14]. This makes the fastest forming instability theory a more generalized approach to the problem of electrospinning onset.

Rayleigh instability

Electrospinning onset and jet formation is closely related to Rayleigh instability. This instability takes place if the surface tension of a fluid cylinder of a certain volume is higher than the surface tension of several droplets of the same volume. Perturbations of various wavelengths occur on the surface of the liquid jet, consequently leading to disintegration of the jet into isolated droplets in an avalanche effect matter. Rayleigh instability therefore hinders the stable jet formation and results in electrospraying. The initial stage of electrospinning can be achieved only when the Rayleigh instability formation is prevented by external electric field. The effect of this instability drops with higher conductivity of the fluid [14].

1.1.2 Flow in an external electric field

As implied earlier, polymer solution is subjected to strong extensional stress during electrospinning. It has been shown that Newtonian approximation gives inaccurate results [18]. Viscoelastic behavior of polymers has a non-negligible effect on the jet behavior in high elongation rate, such as in electrospinning. The jet path from spinneret towards collector can be split into two regions – stable and whipping jet region. These will be discussed separately.

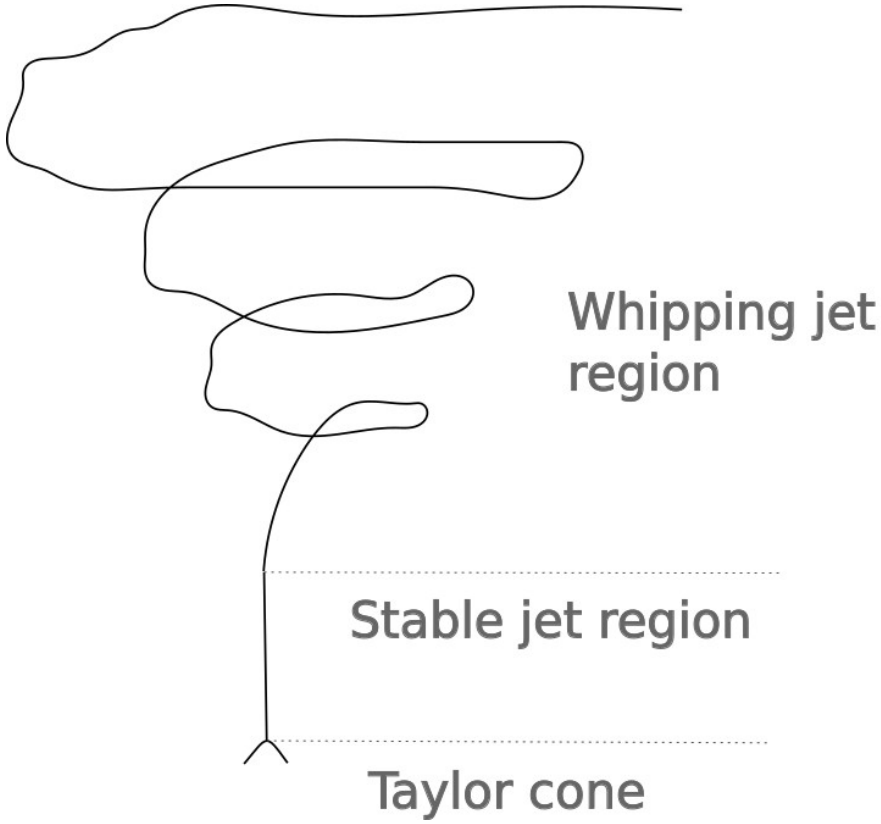

Fig. 2: A scheme of electrospinning jet path

Stable jet region

At the initial part of electrospinning, the jet path remains rather straight, so as to the stable jet region name. In this region, the jet behavior is a result of viscoelastic forces prevailing over inertia. Three stages can be found in this phase of spinning:

a) I. pseudo – Newtonian,

b) II. strain hardening,

c) III. pseudo-steady [18].

The pseudo-Newtonian stage refers to low strain and it is typically described using Newtonian fluid approximation. Trouton ratio (η_e/η) in this region equals 3 [18].

In strain hardening stage, the jet behavior is a result of electromechanical and viscoelastic stresses acting on the fluid. Strain hardening due to locking up of the chains via entanglement knots is a typical feature of this stage. Strain hardening aids stability and cohesion in the forthcoming stages of electrospinning and therefore governs the success of the process. It is argued that strain hardening can occur in any polymer at deformation rates sufficient to ensure entanglement network strengthening [19]. To enhance strain hardening, branching of polymer and increase in polydispersity can be introduced [20]. Palangetic et al., 2014, suggest higher polydispersity can increase the spinnability of a polymer solution [21]. This is based on higher elasticity of polydisperse system over monodisperse, which leads to fewer instabilities being formed.

For pseudo-steady stage of stable jet region, it is typical that the tensile stress settles at a given value, although thinning of the jet continues. The electric field can be described by the far-field value $E = UH^{-1}$, where E denotes electric field intensity, U denotes voltage and H denotes distance between the opposite electrodes. In the previous regions on the other hand, the electric field intensity decreases gradually from the tip of a Taylor cone to the far-field value. Jet inertia and tangential electric forces overcome the viscoelastic forces, making them negligible. As a result, transition to whipping region occurs [18].

Whipping jet region

The rapid bending, or whipping, of a jet in the latter region of electrospinning path can be devoted to Earnshaw's theorem, which claims: *"A charged body placed in an electric field of force cannot rest in a stable equilibrium under the influence of the electric forces alone."* vide Jeans, 1908 [22]. Rapid elongation of the jet continues. Reneker and Yarin, 2008, state up to 10 000 times elongation [23]. The intrinsic Coulombic forces overcome the interaction of the jet and external electric field greatly, making the latter negligible. The Coulombic forces acting along the axis of a unidimensional jet exceed the transverse ones, resulting in jet elongation [14].

Kinetic energy required to keep the elongated jet moving in straight direction would be too high, therefore coiling of the jet occurs due to bending instability. The coil typically increases in diameter as it approaches the collector. Higher-order bending instabilities may occur as well, creating a fractal pattern of the resultant fiber. Each bending, or whipping, instability causes yet more rapid elongation. If third-order bending instabilities occur, the diameter of the fiber can be of fractions of micron. Elongation leads to increase in surface area and accelerates solvent evaporation. Elongation typically stops when complete drying of the fiber is achieved [14], [23].

Reneker and Yarin, 2008, identified the main influences on whipping instability during electrospinning using computational modeling. These include electric bending force, viscoelastic stresses and gradual increase in elongation viscosity caused by solvent evaporation. The effects found negligible in their model include gravity, air viscosity and jet surface tension [23].

Branching and bead-on-string instabilities

Typical instabilities of electrospun jet, besides the bending instability, include a bead-on-string instability and branching instability. Both are a result of Rayleigh instability, which was described earlier. With respect to the wavelength of a critical perturbation, the jet is either stabilized, or destabilized by the excess electrical charges on the fluid jet surface and consequent elongation flow [23].

High excess of surface charge produces branches on the original jet. A stable shape of a liquid in an external electric field is a cylinder. However, sufficient charge density is able to stabilize quasi-stable states of matter, creating cylindrical undulations on the original jet. These undulations are carried in the outward direction to a lower potential. If the energy difference is sufficient to create additional surface area, branching occurs. Multiple branches can be formed on a single jet [23].

Except for undulations, a disintegration of the jet into droplets may occur due to Rayleigh instability, as was described in 1.1.1. As the droplets are elongated in strong electric field, a fluid bridge is created between the droplets and a bead-on-string structured fiber is formed. In contrast to branching, bead-on-string instabilities are formed when the jet charge density is low. Stabilization against bead formation is possible via increasing solution viscoelasticity or using ionic additives, such as inorganic salts, to increase the conductivity of electrospinning solution [23].

1.2 Electrospinning setup

The conventional electrospinning setup consists of a high direct current (DC) voltage power supply, a single-nozzle spinneret and a static grounded collector, as can be seen in fig. 3.

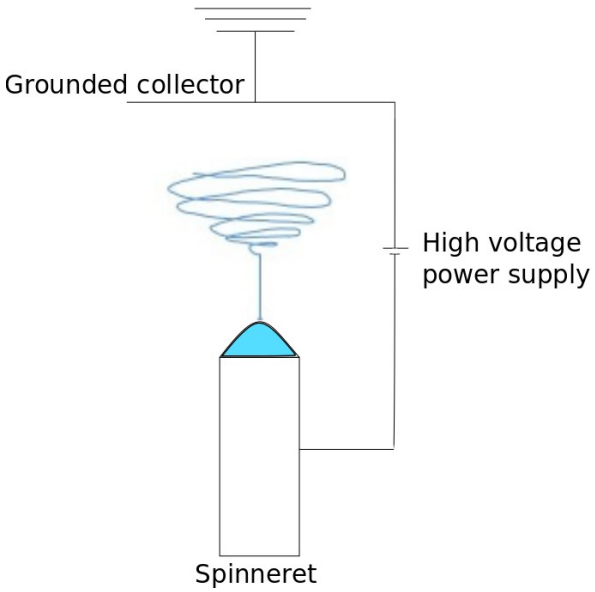

Fig. 3: Conventional DC electrospinning setup scheme

For many applications it is advantageous to modify this setup [24]. Typical modifications involve the use of alternating current (AC) voltage [24], needleless spinneret or multi-jet spinneret, and a collector allowing alignment of the resulting fibrous mat, such as a rotating collector. Electrospinner modifications are out of the scope of the current thesis. Further information on this topic can be found for example in Teo and Ramakrishna, 2006, Nayak et al., 2012, or Alghoraibi and Alomari, 2018 [24]–[26].

1.3 Electric wind effect

Electric wind is in general present in asymmetric capacitors, which applies to a typical DC electrospinner too. As stated earlier, the electric field is not constant through the whole spinning area, but reaches a maximum at the vicinity of small charged bodies, i.e. needles, Taylor cones, liquid droplets etc. The electric field achieves sufficient strength for ionisation of ambient gas and ion acceleration. This results in gas fluxes. According to Lukáš et al., 2009, the electric wind velocity is comparable to the velocity of jet motion. Therefore it can alter the path of the jet significantly and sway it away from the collector. The spinneret and collector create electric wind of opposite charges. If the electric wind velocity of the collector is high enough, the fibers will not reach the collector, as the electric wind overcomes the attractive Coulombic forces [14].

1.4 Parameters of electrospinning process

In general, the process parameters can be divided into three groups: solution parameters, processing parameters and ambient parameters. Unlike processing and ambient parameters, solution parameters, such as viscosity, concentration, molecular weight (M_w) or conductivity, cannot be controlled independently, as they influence one another [7]. In this thesis, the main focus is on the solution parameters.

1.4.1 Solution parameters

Electrospinning process is highly dependent on both solvent, and polymer characteristics, as well as their interactions. Some of the most important solution parameters will be discussed in the following section separately.

Polymer chain in a solution

The conformation and relaxation of a polymer chain in a solution is highly dependent on the polymer chain composition, and interactions of the polymer chain to the solvent molecules respective to interactions among polymer segments, or solvent molecules to each other. The basic concepts relevant to electrospinning process will be discussed in this section.

Polymer solubility

The ability of a polymer to dissolve in a certain solvent, or solvent mixture, is given by the Gibbs free energy of mixing, defined as follows:

$$\Delta G_M = \Delta H_M - T\,\Delta S_M \qquad (10),$$

where H_M denotes the enthalpy of mixing, T denotes the thermodynamic temperature and S_M denotes the entropy of mixing [27]. Systems in equilibrium tend to minimize their free energy, therefore mixing is only possible in such systems, which give negative change in Gibbs free energy. The entropy of polymer solution is always higher compared to a polymer in solid state. Therefore the term $-T\Delta S_M$ is always negative. The overall change in Gibbs free energy is mainly governed by the change in enthalpy. This change is given by

$$\Delta H_M = N_1 \varphi_2 \Delta \varepsilon - T\,\Delta S_M \qquad (11),$$

where N_1 denotes the number of solvent molecules, φ_2 denotes the volume fraction of a polymer and $\Delta\varepsilon$ denotes the energy change [28]. Energy change is a term expressing the energy interaction of a

polymer to solvent, polymer segment to polymer segment and solvent to solvent combined. These interactions are conveniently described using dimensionless polymer-solvent interaction parameter:

$$\chi = \frac{\Delta \varepsilon}{k_B T} \quad (12),$$

where k_B is the Boltzmann constant [28]. Interaction parameter χ is tabelized for many polymer-solvent pairs at infinite dilution.

Hildebrand in 1950, followed by Hansen in 2000, made an attempt to estimate relative miscibility of systems based on the strength of respective intermolecular forces. Hansen assumed three components of the solubility parameter: a dispersion force component (f_D), a polar interaction component (f_P) and a hydrogen bond component (f_H). In a 3D Cartesian plot, a sphere of solvents can be found for every respective polymer, with the solvent quality declining from the center to the edges. As a general rule, a good solvent allows polymer chains to uncoil and stretch, whereas in bad solvent compact coils and microscopic clumps of polymer are formed. Hansen solubility parameters can be also graphed in a 2D triangular Teas graph, where the solubility of a polymer can be mapped conveniently. Luo et al., 2010, used Teas graph mapping to find suitable solvents and solvent mixtures for electrospinning of polymethylsilsesquioxane (PMSQ) [29]. Solvent quality governs the degree of chain entanglements in a polymer solution. This topic will be further discussed later. Experimental experience shows that a good solvent does not ensure spinnability. On the contrary, better spinnability was observed by several researchers for lower quality solvents, see [14], [20], [29], [30].

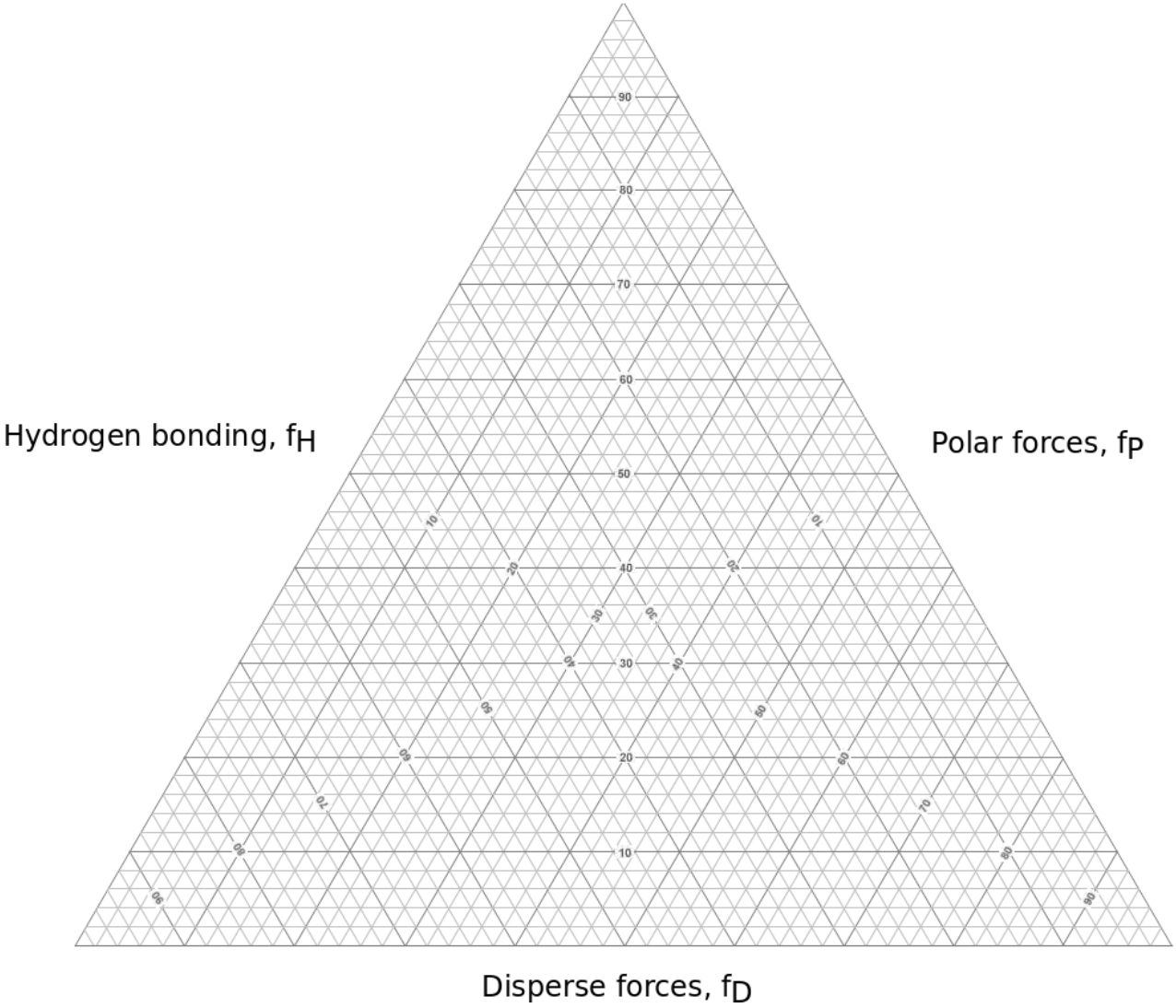

Fig. 4: Teas graph – a ternary plot designed to depict fractional solubility parameters of solvents derived from Hansen solubility parameters

Chain entanglements

A common parameter to describe the behavior of a polymer chain in a solution is intrinsic viscosity, i.e. the limiting viscosity at zero concentration approximation. Intrinsic viscosity $[\eta]$ is closely related to polymer M_w through Mark-Houwink equation:

$$[\eta] = K M_w^a \tag{13},$$

where K and a are constants dependent on polymer, vide Tanford, 1961 [31]. It is generally believed that the number of chain entanglements is a crucial parameter for successful spinning, however, clear understanding of minimum entanglements is still missing. A straightforward way to describe the degree of chain overlap, which can serve as a good approximation of chain entanglement number, is so-called Berry number, defined as follows:

$$Be = c \cdot [\eta] \tag{14},$$

with c being the molar concentration of polymer [32]. Shenoy et al., 2005, proposed an alternative way to determine the entanglement number in solution:

$$(\eta_e)_{sol} = \frac{\varphi_p M_w}{M_e} \quad (15),$$

where φ_p is the volume fraction of polymer in solution, M_w is the molecular weight of the polymer, and M_e the entanglement molecular weight, which corresponds to the average molecular weight between entanglement junctions. This model should be more appropriate for use in semi-dilute polymer solutions, because Berry number is derived using sphere hydrodynamics model. This model is accurate only in dilute solutions [20]. Both approaches work with the assumption, that solution viscosity rises with the number of entanglements. It is likely the reason viscosity is sometimes used as a determining solution parameter for successful electrospinning process [7], [14], [33].

A common assumption in electrospinnability models is that a minimum of one entanglement per chain is necessary for a stable jet formation. Using this assumption, a critical concentration can be easily taken from Berry number, resulting in

$$c_{cr} \approx \frac{1}{[\eta]} \quad (16).$$

However, Shenoy et al., 2005, report a minimum number of entanglements for complete jet stabilization to be 2,5 entanglements per chain [20]. Above the critical concentration, fiber diameter increases with concentration [7], [14], [20]. In a poor solvent, the critical concentration have been observed to decrease [20]. Malkin et al., 2017, reported spinnability of solutions below critical concentration. They identified two contribution to solidification of the fibers – solvent evaporation and extension induced polymer-solvent demixing [30]. Such approach is advantageous for solutions in which high M_w of a polymer prevents attaining the critical concentration due to high viscosity [7], [20], [29], [30].

Chain entanglements are a function of M_w, as well as concentration. Therefore, the critical concentration has to be related to a given M_w [12], [13]. In the case of Berry number assumption, the effect of molecular weight is represented within the definition of limiting viscosity number (see eq. 13).

Surface tension

The origin of surface tension was discussed in section 1.1. In a typical electrospinning solution, surface tension is mainly governed by the solvent. However, additives, such as surface active substances or salts, as well as the polymer-solvent interaction, can have a significant impact on it [34].

The effect of surface tension is in the most general approximation described by dimensionless electrospinning number, which was defined by eq. (9) in section 1.1.1. High surface tension prevents the jet to be ejected at low fields. It has been demonstrated that increase of electric field strength can lead to instabilities formation and result in beaded structures [7]. Surface tension determines the polymer tendency to create the lowest specific surface area possible. Therefore, the tendency to form beads, or bead-on-string structures increases with the increase of surface tension [20]. On the other hand, Reneker and Yarin, 2008, found the surface tension forces negligible in their model, and attribute the main contribution to bead-on-string and branching instabilities formation to Rayleigh instability influence and polymer chain related characteristics, mainly

elasticity of the solution, and corona discharge, which is governed by the solution conductivity [23]. The role of surface tension in electrospinning thus needs further investigation in order to be fully understood.

Electric conductivity

Electric conductivity is the measure at which an electric charge can pass through a material. In a liquid, conductivity is typically governed by free ions. It increases with the number of ions per volume unit and with the ion drift velocity. Ion drift velocity is the product of ion mobility and magnitude of applied electric field. Ion mobility is proportional to the charge of a single ion and diffusion coefficient, and inversely proportional to Boltzmann constant and thermodynamic temperature [35], [36].

Conductivity of a solution is closely related to the surface charge density. It helps increase the electrospinning number by increasing the electric energy and increase the stability of a spinning jet [37]. Higher conductivity prevents the fluid cylinder from undergoing Rayleigh instability [14], [23]. Ionic polymers act on their own as a conductivity-increasing media, which makes them advantageous in terms of electrospinning. Ions of small diameters have greater charge density and higher ionic mobility, leading to higher elongation force. The addition of inorganic salts results in smaller fiber diameter, as well as higher spinnability [38].

1.4.2 Processing parameters

Among the most important processing parameters, electric field strength and tip-to-collector distance stand out. The tip-to-collector distance needs to give sufficient time for the jet to dry off before it reaches the collector [7]. By the nature of an electric field, the field strength is inversely proportional to the separating distance squared. In general, it is advantageous to use the lowest tip-to-collector distance possible, hence minimizing the applied voltage. The use of higher electric field strength leads to thinner fibers. In too high fields, instabilities may occur in form of non-uniform fibers, bead-on-string structures, or complete disruption of the jet [7].

1.4.3 Ambient parameters

By ambient parameters, mainly temperature, pressure and humidity are understood. These influence the rate of solvent evaporation during spinning and conductivity of the environment. Pressure is negligible in most experiments. Humidity and temperature affect the solvent evaporation rate and therefore have a significant impact on electrospinning process [7], [21].

1.5 Core-shell fibers

A core-shell structure is a type of a composite, that has a distinct boundary between the core and shell phase. Typically, the chemical nature of the phases is different. Core-shell structure enables tuning of mechanical properties, such as stiffness, toughness, optical properties and other [7]. It allows hollow body fabrication via selective dissolution of core component [39]. In terms of electrospinning, it provides a tool to use this technique with materials which are normally not electrospinnable, including materials of low molecular weight. In principle, an electrospinnable polymer is used as a template for the non-electrospinnable component to be drawn at [40]. It can be used for encapsulation of non-solid state matter, such as liquid-crystalline substances [41]–[43]. Core-shell structured fibers have a potential to be used as sensors, drug delivery systems or in

microscale electronic devices, for example batteries. An important field of research is also fabrication of nanotubes [44].

1.5.1 Co-axial electrospinning

A common way to fabricate core-shell structured fibers is the use of co-axial spinneret. The apparatus typically consists of multiple (at least two) nozzles and separate fluid distribution channels. A double-nozzle spinneret is not sufficient to ensure core-shell structure formation. A viscous pressure due to viscosity difference is necessary to keep the core encapsulated within the shell. The respective solutions have to be immiscible, or partly immiscible in order to create a stable Taylor cone. Due to shear stress being generated at the core/shell interface, it is necessary for the viscous forces acting at the shell fluid to overcome the interfacial surface tension. In practice this can be ensured by maintaining the shell fluid viscosity to be lower than the core fluid viscosity [43], [44].

Pursue for large scale fiber fabrication drives the research to find alternatives to nozzle-based spinneret, as only one Taylor cone develops in such devices and, consequently, only one fiber is drawn at a time. Vysloužilová et al., 2017, described a device where dual nozzle is replaced with a dual slit. The separate channels for each fluid are preserved. The device is capable of creating multiple jets at the same time, increasing the productivity of the process greatly [39].

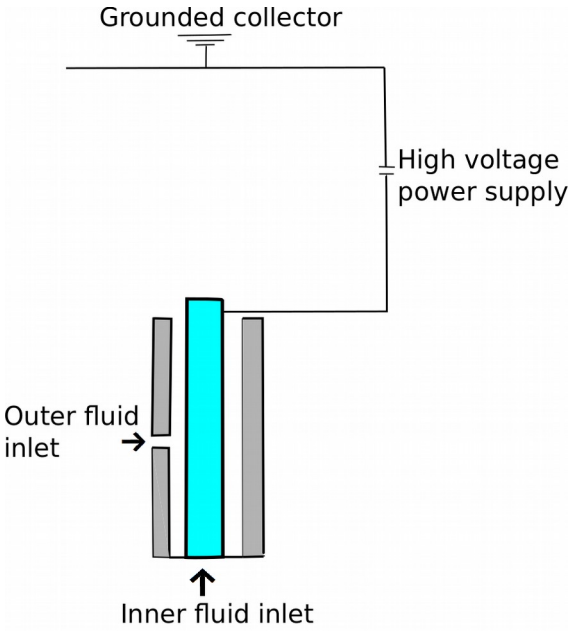

Fig. 5: Co-axial electrospinning setup scheme

1.5.2 Self-organized phase separation

A single nozzle electrospinning of core-shell fibers is possible for certain immiscible materials. The materials are present in the nozzle or drop in the form of an emulsion. A continuous fiber with a long range core-shell structure is created via rapid stretching of core material droplet inside the shell material. A force capable to ensure encapsulation of one material within the other has to exist. This can be done via electric field induced separation, which requires the phases to possess opposite charges. At the formation of Taylor cone and jet spinning, the fluid with higher electric susceptibility will be drawn towards the outer edge by electric force, creating the shell layer. More

common approach is to take an advantage of difference in viscous force. The higher viscosity polymer will be encapsulated inside the lower viscosity polymer in high elongation rates, as to ensure an even velocity profile of the jet as a whole. The electric field induced phase separation is less advantageous also due to fast discharge of many common electrospinning solutions [44], [45]. Ma et al., 2017, have produced core-shell structured chitosan/HA fibers via phase separation with the use of build-in electric field [46].

There are several issues to be addressed in co-axial electrospinning. A good concentricity of the spinneret needs to be ensured. Mutual adherence of the materials may cause problems in some cases, however this effect can be minimized by inner nozzle modification. Flow rate balance of respective fluids is necessary to eliminate fiber diameter fluctuations. These problems vanish in single nozzle electrospinning devices. They also allow for simple transformation into large scale fabrication [45], [47].

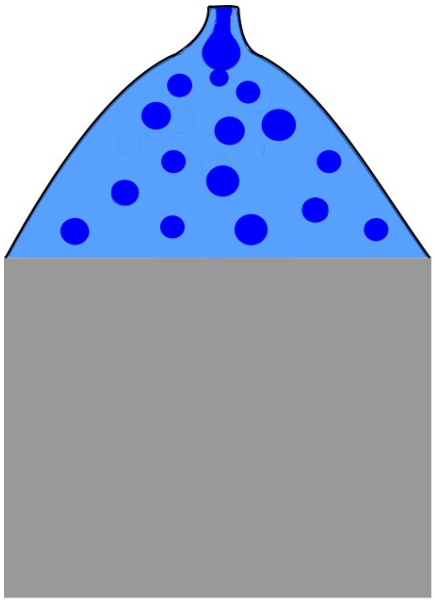

Fig. 6: A scheme of core-shell electrospinning of an emulsion

1.6 Applications

As an inexpensive technology with potential to produce large volumes of nanofibers in a short time, electrospinning is extremely desirable to be used in industry, and has already found applications. Highly porous structures with large specific surface area make it suitable for sensor and membrane manufacturing [45], [48]–[50]. Recent advances show promising results in tissue engineering and drug delivery [5], [6].

Commercial solutions to electrospun nanofibers and non-woven mats production are available. As an example, NanospiderTM and 4SPIN® technology can be listed. NanospiderTM was developed and patented by Jirsák et al., 2005, and is commercially produced by Elmarco s.r.o. 4SPIN® technology is used by Contipro a.s. for electrospinning of biopolymers including various proteins and HA.

2 MATERIALS CONSIDERATION

In natural fibers, uni-directional orientation is formed by specific growth direction. Man-made fiber fabrication techniques typically involve uni-directional stretching using various kinds of force. The material characteristics need to be carefully tailored to fulfill the requirements of the given method, but some generic guidelines can be found for suitable polymer choice. Linearity of polymer chains allows for alignment in a certain direction, therefore creating a fiber. A sufficient cohesion of the chains is necessary to prevent fiber breakup. The cohesive force, as well as the ability to align, grows along with the polymer length [51].

Materials for solution electrospinning can be classified in several perspectives, such as solvent nature, biocompatibility, biodegradability, ionic character etc. For the purpose of this thesis, biocompatible and water soluble polymers were used.

2.1 Hyaluronic acid

HA, sometimes denoted hyaluronan alongside sodium hyaluronate, is a polar biopolymer found in animal tissue, namely synovial fluid and extracellular matrix. It can be harvested in M_w up to milions of g·mol^{-1}. Its biocompatibility makes it desirable for use in medicine and cosmetics. HA is used in synovial fluid replacement in rheumatology. It is widely used in eye surgery, wound healing and drug delivery. Lately it is being used in cosmetics as a moisturizing agent [52].

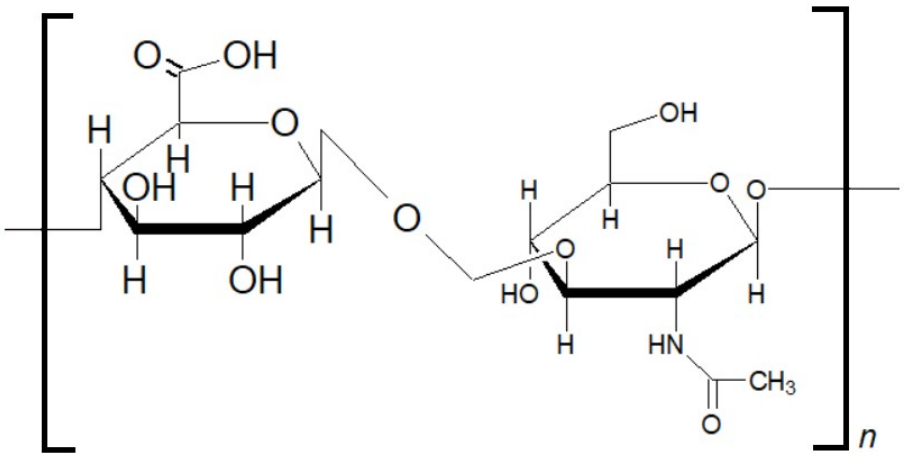

Fig. 7: HA structure formula

2.1.1 Properties

HA is a polysaccharide consisting of (1,4)-β linked D-glucoronic and (1,3)-β linked N-acetyl-D-glucosamine units. The chain primary structure is linear, but chemical cross-linking is possible. HA is water-soluble in low concentrations and highly hygroscopic in dry state. It is prone to degradation by oxygen and UV light. It can serve as a scavenger or free radicals [52]. HA displays behavior of a polyelectrolyte. Polyelectrolytes are characterized by dissociating groups in their repeating units. Therefore the polymer molecules are present in the form of ions in a solution [6], [53].

2.1.2 Electrospinning

Attempts to fabricate HA nanofibers via electrospinning have been many. The role of solvent, concentration and Mw is being investigated. The challenges are mainly high viscosity at very low

concentrations, high surface tension of HA aqueous solutions, and insufficient solvent evaporation rate. Um et al., 2004, performed electrospinning of HA from acidic solution. They observed positive effect of adding low molecular weight HA to high molecular weight HA, thus controlling the viscosity. Ethanol (EtOH) addition had a positive effect as well. However, satisfactory outcomes were achieved only when an air blowing system was attached to the electrospinning apparatus. This ensured high solvent evaporation rate and provided the system with additional pulling force to form the jet [11]. Uppal et al., 2010, report electrospinning of HA from aqueous solution with the addition of cocamidopropyl betaine as surfactant. 1 wt.% - 4 wt.% solutions were spun using DC voltage ranging from 12,5 kV to 15 kV [54]. HA was also successfully spun from N,N,-dimethylformamide (DMF) based solutions [13].

2.2 Polyvinyl alcohol

Polyvinyl alcohol (PVA) is a biocompatible water-soluble polymer. It was first synthesized by Herman and Haehnel, 1924, by polyvinylacetate hydrolysis. It cannot be produced via polymerization, as the monomer is unstable. PVA is easily spun into fibers from aqueous solution by various methods, such as wet spinning, dry spinning or air-gap spinning. Using cross-linking reactions or surface modifications, the fibers can be made water-insoluble. Macro-scale PVA fibers are used for rope or fishing net fabrication due to low elongation and high tenacity. The -OH groups in the structure provide good adhesion to natural rubber and PVA can therefore be used as reinforcement agent in rubber products. Due to biocompatibility, PVA has found applications in medicine, e.g. as surgical threads [55], [56].

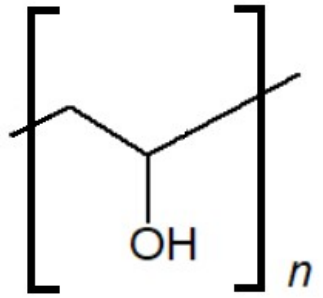

Fig. 8: PVA structure formula

2.2.1 Properties

PVA is a polar polymer due to -OH groups. In relaxed state it is amorphous, but when stress is applied, the oriented molecules tend to crystallize. There are strong intermolecular forces present. The number of -OH groups governs PVA sensitivity to water. PVA is soluble in water, however, the rate of solution is very low at room temperature. Therefore it is usually dissolved at 70°C or higher temperature. The decomposition temperature is below melting temperature, melt processing is therefore impossible. In dilute PVA solutions in air atmosphere, the surface tension decreases gradually until an equilibrium is reached. This is partially due to diffusion of PVA molecules to the surface of the liquid. It also appears, that molecules association, and oxidation take place at the liquid-air interface [55], [57].

2.2.2 Electrospinning

PVA is a desirable material for electrospinning. It can be easily spun from aqueous solutions. The critical concentration appears to be 10 wt.% at molecular weight around 93 kDa. Shenoy et al., 2005, found a correlation between pre-treatment of PVA with temperature above 95°C and lower tendency to form a stable jet. They estimate a connection to physical gelation occurring in aqueous PVA solution [33].

2.3 Poly(ethylene oxide)

Poly(ethylene oxide) (PEO) is a linear synthetic polyether. It displays nonionic character. It is synthesized via catalytic polymerization of ethylene oxide. This reaction provides material of very high M_w, up to milions of $g \cdot mol^{-1}$. PEO is soluble in cold water at any M_w, and miscible with ionic or amphoteric liquids. It creates hydrogen bonds due to -OH terminal groups [58], [59].

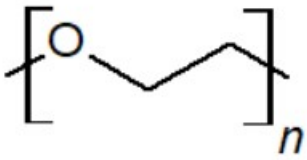

Fig. 9: PEO structure formula

2.3.1 Properties

PEO is a semicrystalline polymer due to linearity. Partial negative charge located on the oxygen atoms causes PEO to act as a proton acceptor, and form blends with proton donating polymers [60]. PEO is used as a plasticizer in polymer processing, a water soluble lubricant, or an antistatics in urethane rubber production. It can be processed as a thermoplastic via extrusion techniques [59], [60].

PEO is highly biocompatible, with extremely low cytotoxicity and imunogenicity. Although it is not biodegradable, it can be easily excreted from living organisms. Due to these properties, PEO is highly desirable in medicine and pharmaceutical applications. It is United States Food and Drug Administration (FDA) approved for number of applications in medicine. It has a potential to create 3D structures, such as hydrogels, making it a suitable material for scaffolds in tissue engineering [58], [61], [62].

2.3.2 Electrospinning

PEO can be easily spun from multiple solvents, the commonly used being water, EtOH, DMF or chloroform. Due to high spinnability it is desirable in research of electrospinning phenomena. For this purpose it was used by Reneker and Yarin, 2008, Shenoy et al.,2005, Yan et al., 2011, Son et al., 2004, and many others [20], [23], [63], [64]. It is a common choice as a dragging polymer for biopolymers with low spinnability, such as chitosan, collagen or HA [58].

3 ANALYSIS METHODS

The electrospinning solutions, as well as the obtained fibers, were analyzed to determine correlations between solution parameters, electrospinning process and resulting fiber morphology. A theoretical background of the analysis methods is given in this section.

3.1 Solution analysis

As stated in 1.4.1, there are several solution parameters affecting the electrospinning process. Theoretical background of the measurement methods used in the experimental part of the thesis is given in this section.

3.1.1 Tesiometry

Surface tension can be measured using number of techniques. These include capillary rise method, stalagmometry, force based methods such as Wilhelmy plate method, or optical methods based on drop shape analysis. In this section, a pendant drop measurement method will be described in more details, since it is the method used in the experimental part of the current thesis.

A pendant drop measurement uses the curvature of the drop profile to determine the tension on the interface of two phases, i.e. surface tension. Typically, a specifically heavier liquid is suspended into a specifically lighter phase, air or other gas most frequently. A direct consequence of surface tension existence is Laplace pressure generation, i.e. a difference in pressure outside and inside the liquid droplet. Laplace pressure can be described using the following equation:

$$\Delta p = \gamma \left(\frac{1}{R_1} + \frac{1}{R_2} \right) \quad (18),$$

where γ denotes interfacial tension, and R_1 and R_2 denote radii of horizontal and vertical circles of curvature, respectively [65]. If there are no other forces acting on the droplet, its shape is spherical. Due to gravity, a hydrostatic pressure contributes to the inner pressure of the liquid and deforms the original sphere. The hydrostatic pressure is defined as follows:

$$\Delta p_{hyd} = \Delta \rho \, g \, l \quad (19),$$

where $\Delta\rho$ denotes the difference in densities of the respective phases, g denotes gravitational acceleration and l denotes vertical distance between measuring point and needle opening. The deviation from spherical shape is therefore given by the relationship between the surface tension and weight of the drop. With the knowledge of density difference between the phases, and the dimensions of the droplet, it is possible to calculate the surface tension from the shape of the droplet [65], [66].

3.1.2 Viscometry

Two separate kinds of viscosity are defined – kinematic and dynamic viscosity. Kinematic viscosity is the way to express gravity influence on the flow. Dynamic viscosity as the measure of resistance to flow was first thoroughly described by Newton. He found the shear stress to be directly proportional to dynamic viscosity and shear rate of a fluid in shear flow [67]. Fluids can be divided into two groups – those which maintain constant dynamic viscosity at any given shear rate, so called newtonian fluids, and those in which dynamic viscosity is a function of shear rate, so called non-newtonian fluids. Several measurement techniques have been developed to measure the dynamic viscosity in both newtonian and non-newtonian fluids. The most common include capillary viscometers, rotational rheometers or the falling sphere method, also known as Hoppler viscometry. Special techniques to measure dynamic viscosity in elongation flow exist as well [68].

Rotational rheometer is probably the most common device used for to viscometry in polymer science. They are capable of measurement in wide range of shear rates. In principle, a rotating part of the rheometer creates shear stress on the sample, resulting in shear flow at a certain rate. The viscous behavior of the sample results in torque, which can be measured. Common geometries are plate-plate, cone-plate, and cup and bob geometry [68].

3.1.3 Conductometry

Conductivity is defined as the reciprocal value of electric resistance. A straightforward means to measure it is therefore by taking an advantage in Ohm's law, which states

$$I = \frac{U}{R} = U \cdot \sigma \qquad (21),$$

where I denotes the electric current, U denotes voltage, R denotes electric resistance and σ denotes electric conductivity. By putting a voltage of a known magnitude onto an electrode submerged in a conductive fluid, the current can be measured. Conductivity of the fluid can be directly determined using this knowledge [69].

3.1.4 Density measurement

Density is defined as the mass to volume ratio. The most common measurement technique for liquid density measurement is direct measurement of a mass and volume. To avoid fluctuations due to temperature, ultrasonic measurement technique may be used [70]. In the current thesis, oscillating U-tube method was used, and therefore will be described in more details in this section.

The oscillating U-tube method is based on the resonance frequency shift induced by change in mass of a body. A glass U-tube of a defined volume and resonance frequency is filled with the liquid sample, thus changing its overall mass and average density. Oscillations at a characteristic frequency are induced in the U-tube. Resonance frequency shift is detected and used to calculate the density of the sample [71].

3.2 Fiber analysis

Nanofibers can be evaluated from many points of view – mechanical performance analysis, biological activity, surface activity etc. In this thesis, the focus is on morphology, therefore the fiber analysis is reduced to microscopic analysis. The principles of microscopic methods used in the experimental part of the current thesis will be briefly described in the following subsections.

3.2.1 Scanning electron microscopy

Electron microscopy makes use of wave character of accelerated electrons. The accelerating voltage ranges from 0.1 keV to 50 keV. The elementary interactions between the sample and electron beam are elastic and inelastic scattering. These interaction cause a gradual loss of energy, hence a limit of depth of information in scanning electron microscopy (SEM). The depth of information depends on the electron beam energy, and sample density. Typically it lies between 10 nm – 10 μm. There are several phenomena contributing to SEM imaging. The most important include secondary electrons, backscattered electrons and Auger electrons [72].

The secondary electrons are the outcome of inelastic collisions, in which the electron is excited to a sufficient energy level allowing it to overcome the work function. Low energy is typical for secondary electrons, the typical values being 2-5 eV [72].

Backscattered electrons are produced by elastic interactions of primary electron beam. Multiple scattering causes the electrons to lose energy, leading to very broad energy range (50 eV up to 0,8 times the original accelerating voltage) [72].

Auger electrons are one of the possible outcomes of electron deexcitation. If an electron from lower energy level leaves the electron shell, a higher energy level electron fills its position. The difference in energy can be either converted to a photon, resulting in X-ray emission, or it can be transferred to another electron, providing it with sufficient energy to overcome the work function. The latter mechanism refers to Auger electron generation [72].

3.2.2 Fluorescence confocal microscopy

Confocal microscopy is a modification of optical microscopy. In contrast to conventional wide field microscopy, it uses focused light beams to scan the sample. This way the sample is sectioned in a non-invasive way, which allows the instrument to construct a 3D image. In general, confocal microscopy is not limited to fluorescent samples, however, it is convenient to join these techniques, especially in biological applications. Fluorescence microscopy maximizes the contrast and helps to remove out-of-focus light, thus increasing the resolution [73].

Fluorescence is a quantum phenomenon taking place in certain molecules. Essentially, an electron is excited to a higher energy state by a photon absorption. After that, deexcitation to ground energy state occurs, accompanied by photon emission. The emitted photon’s wavelength is longer than the originally absorbed photon, i.e. the energy is lower. This is due to radiationless relaxation processes. The difference of wavelengths of absorbed and emitted photon is referred to as the Stoke’s shift. The magnitude of Stoke’s shift is highly dependent on fluorescent molecule structure. In most instruments, the excitation light is in the range of visible or UV light, the emitted light alike [74].

II. EXPERIMENTAL PART

4 AIM OF WORK

The current thesis aims to find solutions containing HA of various M_w, which can be spun into nanofibers using DC electric field. The solutions are then characterized with respect to parameters vital to electrospinning process.

5 SAMPLE PREPARATION

The following section gives the description of chemical modifications which were performed on some polymers used. It also gives detailed description of electrospinning solutions preparation, and the specifications of electrospinning experimental device.

5.1 Chemicals

Polymers and solvents

HA of the following M_w: 124 kDa, 243 kDa, 370 kDa, 600 kDa, 1 180 kDa and 1 500 kDa was kindly gifted by Contipro a.s. PVA 89-98 kDa, 99+% hydrolyzed, and PEO of M_w 300 kDa and 600 kDa respectively were purchased from Sigma Aldrich.

Demineralized (DEMI) water was prepared usign Milipore Direct-Q 3UV system. EtOH absolute Spectranal and propan-2-ol (IPA) puriss p.a., ACS reagent were purchased from Sigma Aldrich. Methanol (MeOH) p.a. was purchased from Lach:Ner.

Benzethonium chloride (BAC) ≥97 % was purchased from Sigma Aldrich.

Chemicals for modification of HA and PVA

Disodium hydrogen phosphate dodecahydrate ≥99%, 4-acetamido-TEMPO (4-Ac-TEMPO) free radical, 97%, dimethyl sulfoxide (DMSO) ACS reagent, ≥99,9%, Nile Blue A, dye content ≥75 %, NaBH3CN reagent grade, 95%, pyridine anhydrous, 99,8%, fluorescein isothyocyanite isomer (FITC) ≥90% and dibutiltin dilaurate ≥95% were purchased from Sigma Aldrich. Sodium bromide pure was purchased from Lachema a.s. Na2S2O3·5 H2O pure was purchased from Lach:Ner. Sodium hypochlorite solution pure was purchased from Penta. NaCl PharmaGrade was purchased from SAFC.

5.2 HA oxidation and fluorescent labeling of HA and PVA

Oxidation of HA was performed in order to find out the influence of such chemical modification on electrospinning performance. It also allows for fluorescence labeling using Nile Blue to be done. Fluorescence labeling of HA and PVA was done in order to examine the structure of fibers obtained from bi-component blend solution electrospinning using fluorescence microscopy.

5.2.1 HA oxidation

Oxidation of HA was performed following modified procedure published by Huerta-Angeles et al., 2012 [75]. Briefly, 1 g of HA 600 kDa was dissolved in 100 ml of DEMI water by stirring for 24 hours at 50°C. Sodium bromide, 0,129 g, and disodium hydrogen phosphate, 0,771 g, were added to the solution. After cooling the solution to 5°C, 5 mg 4-Ac-TEMPO pre-dissolved in 500 µl DEMI water, and 450 µl sodium hypochlorite were added. The reaction was carried for 45 minutes under

nitrogen atmosphere. Then the reaction was stopped by adding 2 ml of 5% Na2S2O3 solution. The product was dialysed for three days and then dried via lyophilization in yield 95,5 %.

5.2.2 HA fluorescent labeling

Oxidized HA (HA-ox) was labeled with Nile Blue fluorescent dye by following modified procedure published by Šmejkalová et al., 2017 [76]. 2 wt.% HA-ox solution was prepared by dissolving 0,5 g of HA-ox in DEMI water. The solution was stirred for 24 hours at 50°C. 92 mg of Nile Blue was dissolved in 5 ml DMSO by stirring for 5 minutes at room temperature. The Nile Blue solution in DMSO was poured into the HA-ox solution. The reaction was carried for 5 hours in darkness at 25°C. After that, 79 mg NaBH3CN was added, and the reaction was left to carry on over the night. During the process the mixture was kept in darkness. After the reaction terminated, the remaining Nile Blue was washed out using excess IPA. Further cleaning was performed via dialysis in NaCl solution for 5 days and the product was isolated by lyophilization in yield 78,2 %.

5.2.3 PVA fluorescent labeling

Fluorescent labeling of PVA using FITC was performed following modified procedure published by Kaneo et al, 2005 [77]. 0,5 g of PVA (M_w = 89-98 kDa) were dissloved in combination of 66,6 ml DMSO and 416,6 µl pyridine by stirring for 24 hours at 80°C. 83 mg of FITC and 31 µl dibutiltin dilaurate were added to the solution and the reaction was carried for 2 hours at 95°C in darkness. After the reaction terminated, free dye was washed out using excess IPA. The final product was obtained by lyophilization in yield 88 %.

5.3 Solution preparation

HA of various M_w was dissolved in binary or ternary solvent mixtures. The dissolving was done at 50°C under vigorous stirring for 48 hours regardless the HA M_w and solvent mixture, to obtain completely homogenized solution [78]. The optimal binary and ternary solvent mixtures were found experimentally by changing the respective solvents ratio. The solvent mixtures chosen for the experiments are H_2O:IPA at weight ratio 10:7, and H_2O:EtOH:MeOH at weight ratio 5:5:1. The solutions were prepared at various weight concentrations.

Solution of mixed M_w HA was prepared in a way corresponding to the procedure described in the previous paragraph. Binary solvent mixture of H2O and EtOH at weight ratio 4:3 was used. HA of Mw 124 kDa, 243 kDa, 370 kDa and 600 kDa was used in the first round of experiments. For second round of experiments, HA of M_w 1,18 MDa and 1,5 MDa were added to explore the influence of high M_w fractions on electrospinning process. The weight fractions of each M_w were equivalent in both cases.

HA/PVA blend solution was prepared by the following procedure: 2 wt.% HA and 1 wt.% PVA solutions were prepared separately in DEMI water. Dissolving of PVA was done by stirring it in DEMI water at 80°C for at least 5 hours. BAC aqueous solution of various weight concentration (see table 1) was added into PVA solution and stirred. HA solution was then added to PVA solution with BAC and stirred at room temperature for 1 hour to ensure complete homogenization of the solution [78].

Table 1: Contents of HA/PVA blend solutions with addition of BAC

BAC concentration of the original solution [wt.%]	Respective components contents in resulting solutions		
	HA 600 kDa [wt.%]	PVA 89-98 kDa [wt.%]	BAC [wt.%]
1	1,1	0,44	0,006
2	1,1	0,44	0,013
5	1,1	0,44	0,033
10	1,1	0,44	0,065

HA/PEO blend solutions were prepared by mixing the polymers at 1:1 ratio, adding it to DEMI water and then stirring vigorously at room temperature for 48 hours. The weight concentration was adjusted to 2 wt.% in all cases, considering the desired outcomes of the experiments. This procedure was done regardless the Mw of respective polymers used [58], [64].

For the purpose of confocal microscopy, HA/PVA and HA/PEO blend solution containing fluorescent labeled polymers were prepared. The procedure does not differ from those described above. In HA/PVA blend solution, the content of BAC was 0,065 wt.%, FITC labeled PVA (PVA-FITC) made up 4 % of PVA content, and Nile Blue labeled HA (HA-NB) content made up 4 % of HA content. For HA/PEO blend solution, 600 kDa PEO was chosen. HA-NB made up 5 % of 600 kDa HA content.

5.4 Electrospinning equipment

A home-made electrospinner was used to conduct electrospinning experiments. It consists of a high DC voltage power supply Spellman SL150, a grounded metal collector and a simple rod metal spinneret. The collector's diameter is 40,3 mm, the spinneret is 8 mm in diameter. The setup corresponds to the typical setup sketched in fig. 3. The tip-to-collector distance is interchangeable. In the experiments, the tip-to-collector distance was kept at 76 mm. The experiments were conducted in air atmosphere at room temperature and humidity, and normal pressure. The fibers were collected using a recycled paper target, in order to ensure good adhesion.

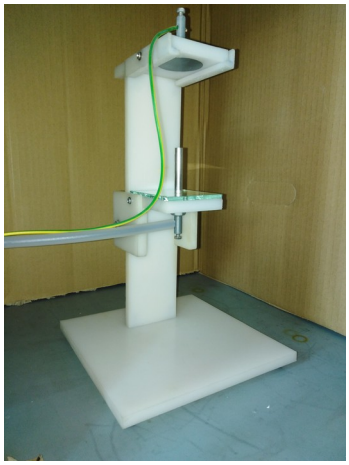

Fig. 10: Electrospinning device used in experimental part of the current thesis (high voltage power supply not in picture)

6 SAMPLE ANALYSIS

Specifications of analytical methods used in the experiments are given in the following section.

6.1 Viscometry

Dynamic viscosity was determined using rotational rheometer Malvern Kinexus pro+ with cup and bob geometry. The measurements were conducted at 25°C at 11 different shear rates ranging from 0,1 s-1 to 10 s-1.

6.2 Conductometry

A portable conductometer Mettler Toledo Seven2Go Pro was used to determine the conductivity of the solutions. Each solution was measured three times at room temperature.

6.3 Density measurement

Density of the solutions was determined using Anton Paar DMA 5000M. The measurement was conducted three times for each sample at 25°C.

6.4 Tensiometry

The surface tension was determined using Krüss Drop Shape Analyzer DSA 100. Three separate drops of each sample were measured. Each drop was measured 30 times with 1 s delay between the measurements. Dixon's Q-test was used to exclude the outliers. The measurement was conducted at 25°C in air atmosphere.

6.5 SEM analysis

Fiber morphology analysis was done using Phenom Pro X scanning electron microscope in backscattered electrons mode. The samples were sputtered with a layer of gold prior to the analysis. The acceleration voltage was 10 kV. 5 000 times and 10 000 times magnification was used. Optical analysis of the images was done using ImageJ software.

6.6 Fluorescent confocal microscopy

Olympus FLUOVIEW FV3000 Laser Scanning Microscope with coherent light sources of the following wavelengths: 405 nm, 488 nm, 561 nm and 640 nm, was used for fluorescence confocal microscopy.

7 RESULTS

The results of solution and fiber analysis are presented in the following section.

7.1 Single M_w HA solutions

It was not possible to electrostatically spun HA of any M_w from solely aqueous solution. Binary and ternary solvent mixtures were found experimentally, given respect to literature [29], [30]. Upper and

lower limiting, as well as ideal concentrations were determined for each solvent mixture and HA M_w. The criteria evaluated in suitability for electrospinning are the following:

a) complete solvent evaporation at given tip-to-collector distance,

b) formation of stable jet instead of particle formation,

c) number of Taylor cones formed,

d) speed of complete material consumption.

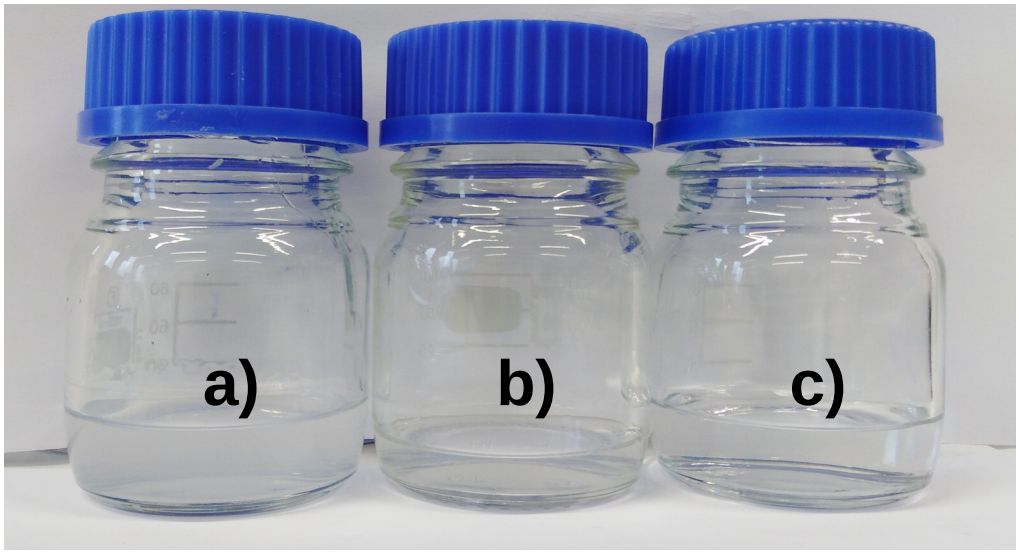

Fig. 11: Solutions of 0,6 MDa HA in H2O:IPA 10:7, a) 3,2 wt.%, b) 2,3 wt.%, c) 1,3 wt.%

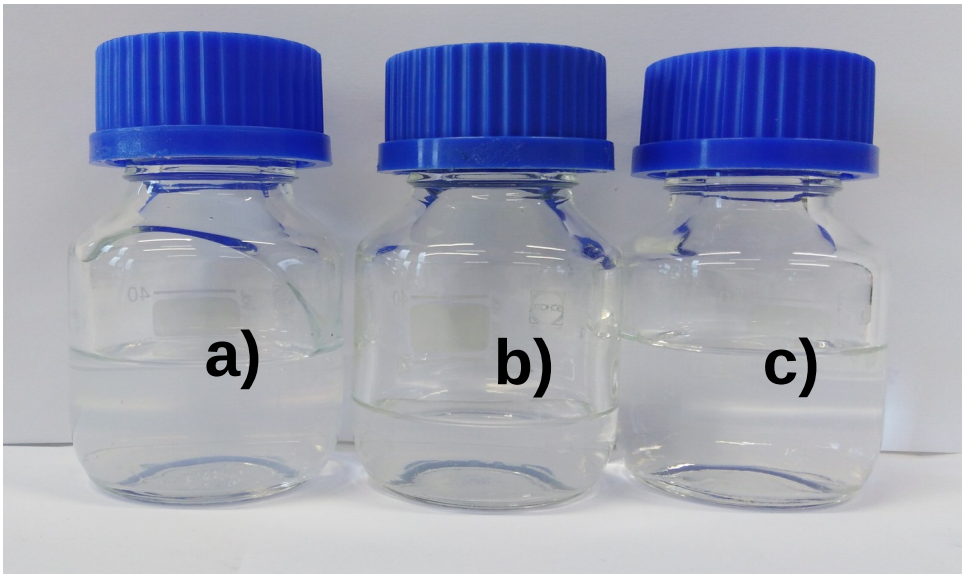

Fig. 12: Solutions of 1,18 MDa HA in H2O:IPA 10:7, a) 2,9 wt.%, b) 1,2 wt.%, c) 1,0 wt.%

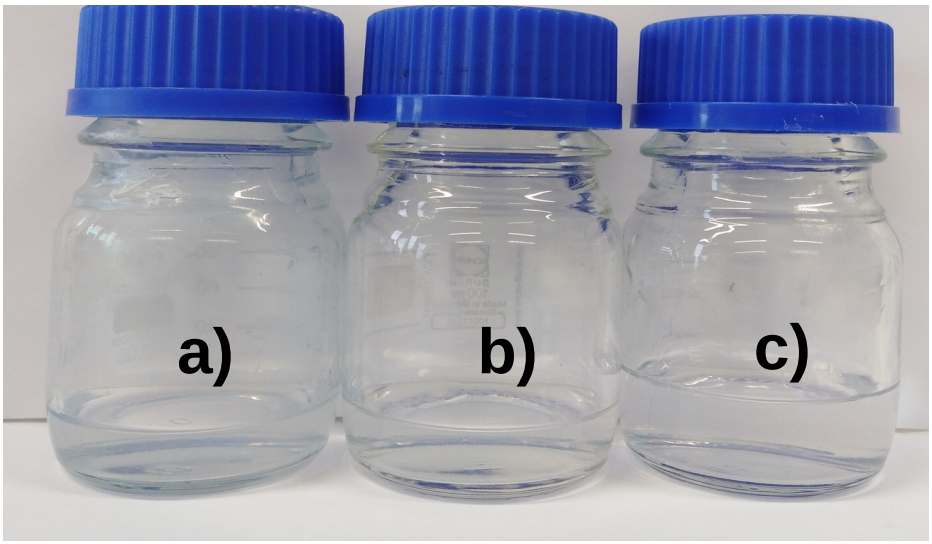

Fig. 13: Solutions of 0,6 MDa HA in H2O:EtOH:MeOH 5:5:1, a) 2,8 wt.%, b) 2,4 wt.%, c) 0,7 wt.%

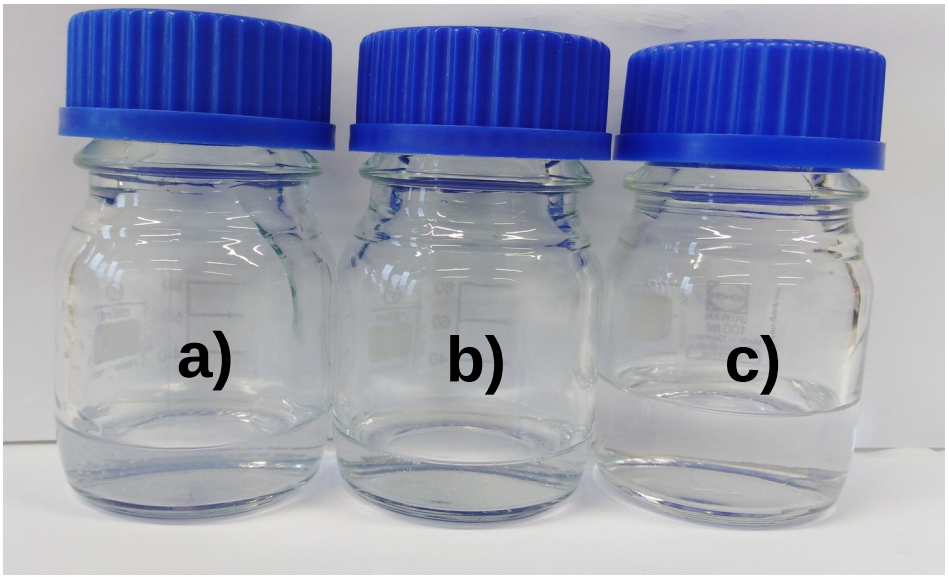

Fig. 14: Solutions of 1,18 MDa HA in H2O:EtOH:MeOH 5:5:1, a) 2,3 wt.%, b) 2,2 wt.%, c) 1,5 wt.%

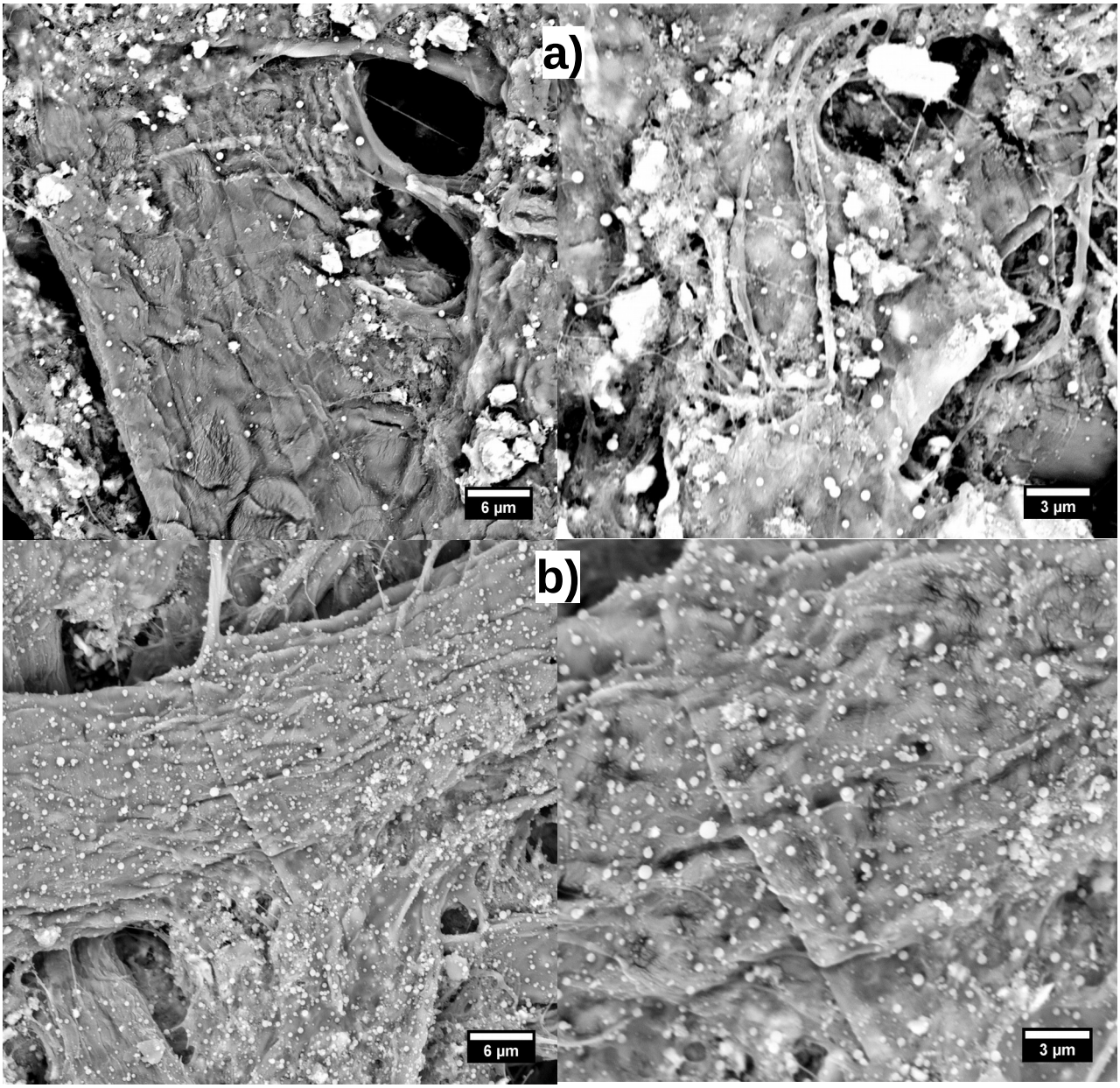

Fig. 15: SEM micrographs of HA 0,6 MDa H2O:IPA 10:7 3,2 wt.% solution fibers; a) non-oxidized HA, spinning voltage 20,5 kV b) HA-ox, spinning voltage 17,1 kV

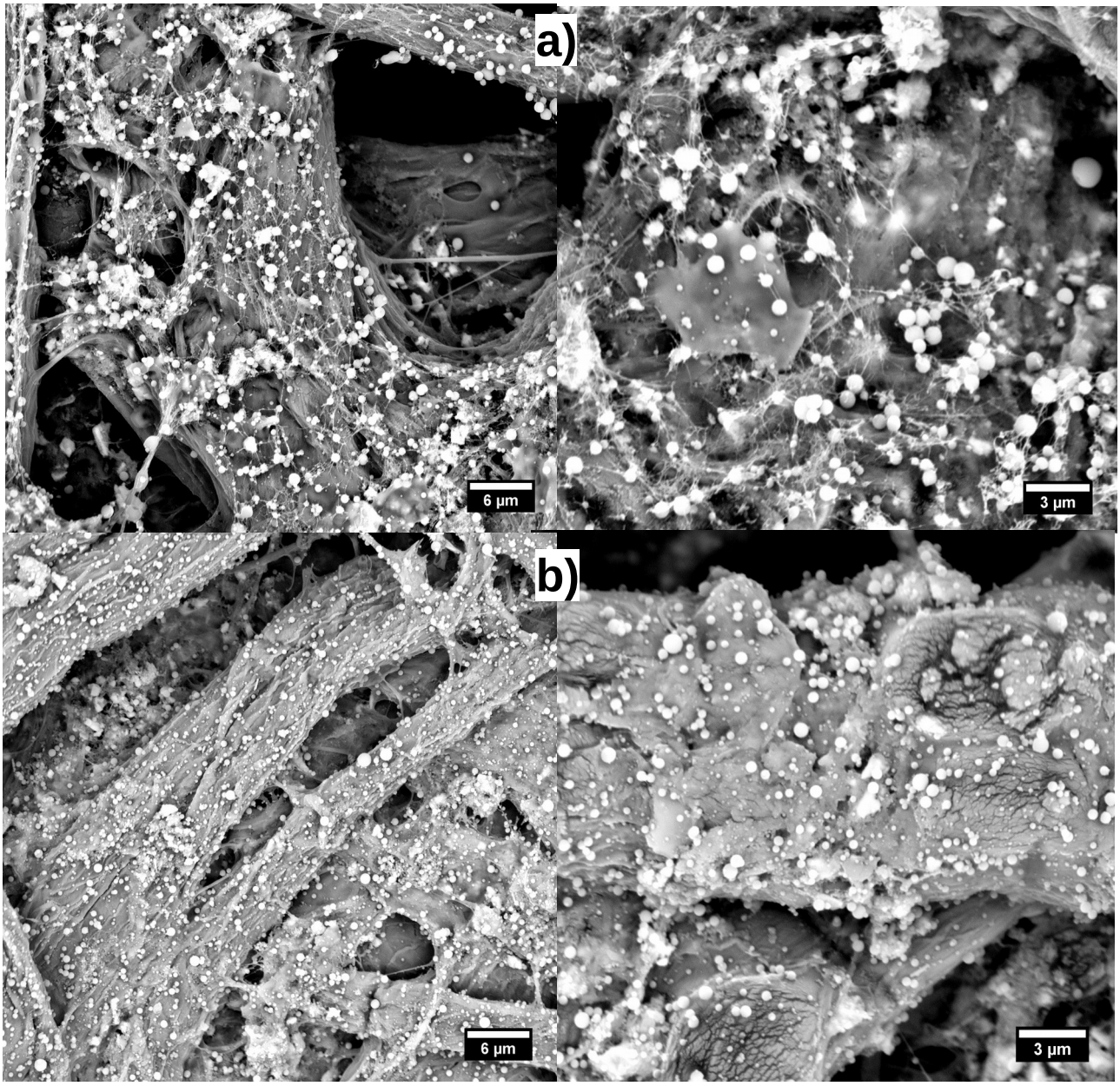

Fig. 16: SEM micrographs of HA 0,6 MDa H2O:IPA 10:7 2,3 wt.% solution fibers; a) non-oxidized HA, spinning voltage 20 kV b) HA-ox, spinning voltage 15,8 kV

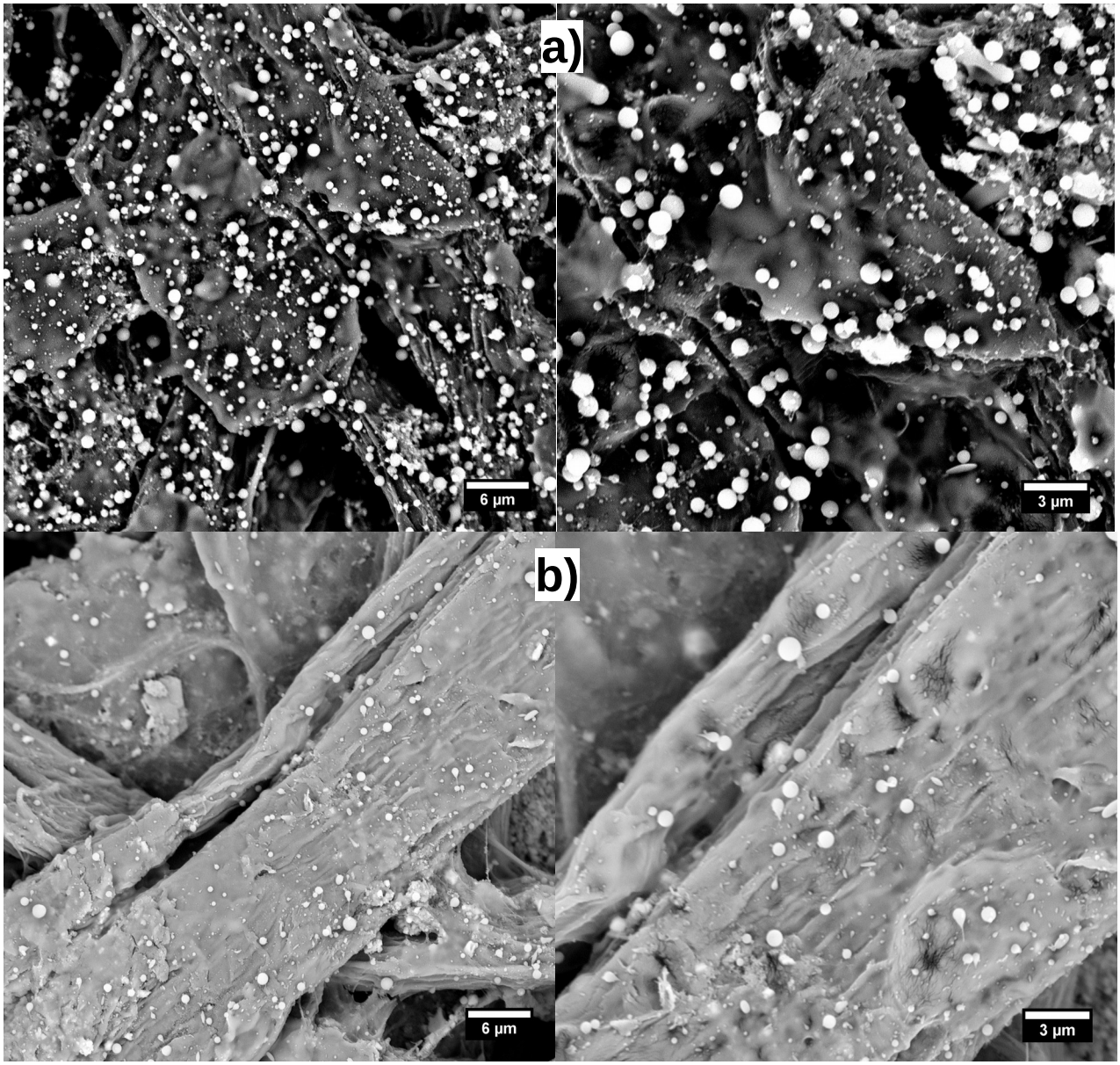

Fig. 17: SEM micrographs of HA 0,6 MDa H2O:IPA 10:7 1,3 wt.% solution fibers, a) non-oxidized HA, spinning voltage 16,2 kV b) HA-ox, spinning voltage 16,4 kV

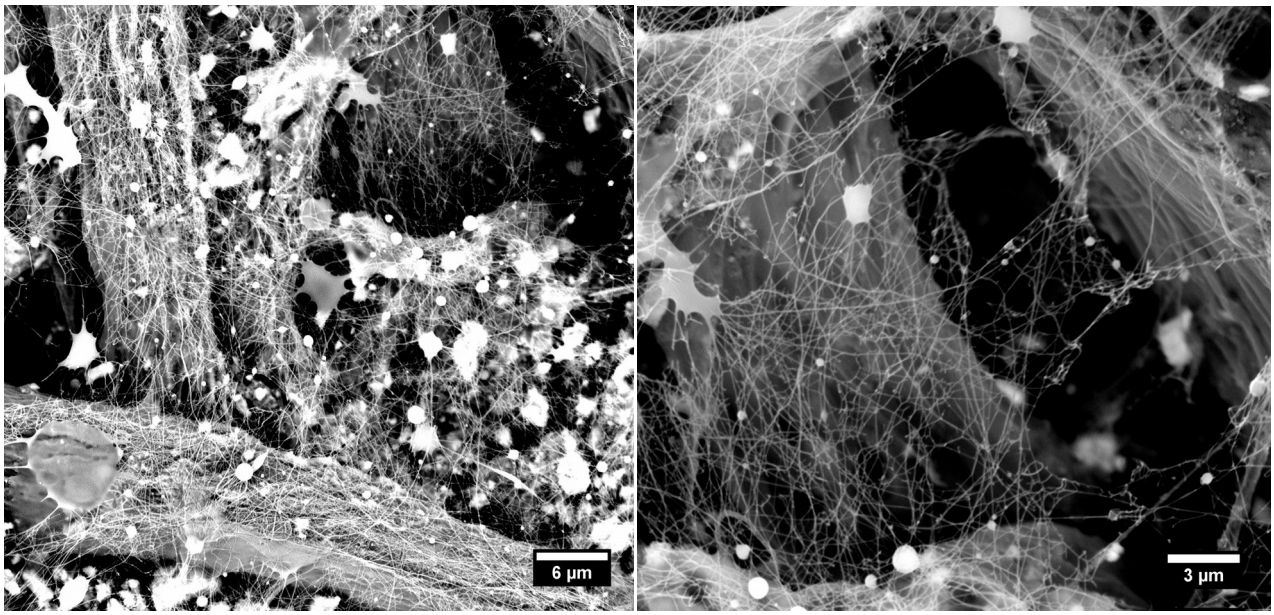

Fig. 18: SEM micrographs of HA 1,18 MDa H2O:IPA 10:7 2,9 wt.% solution fibers, spinning voltage 24 kV

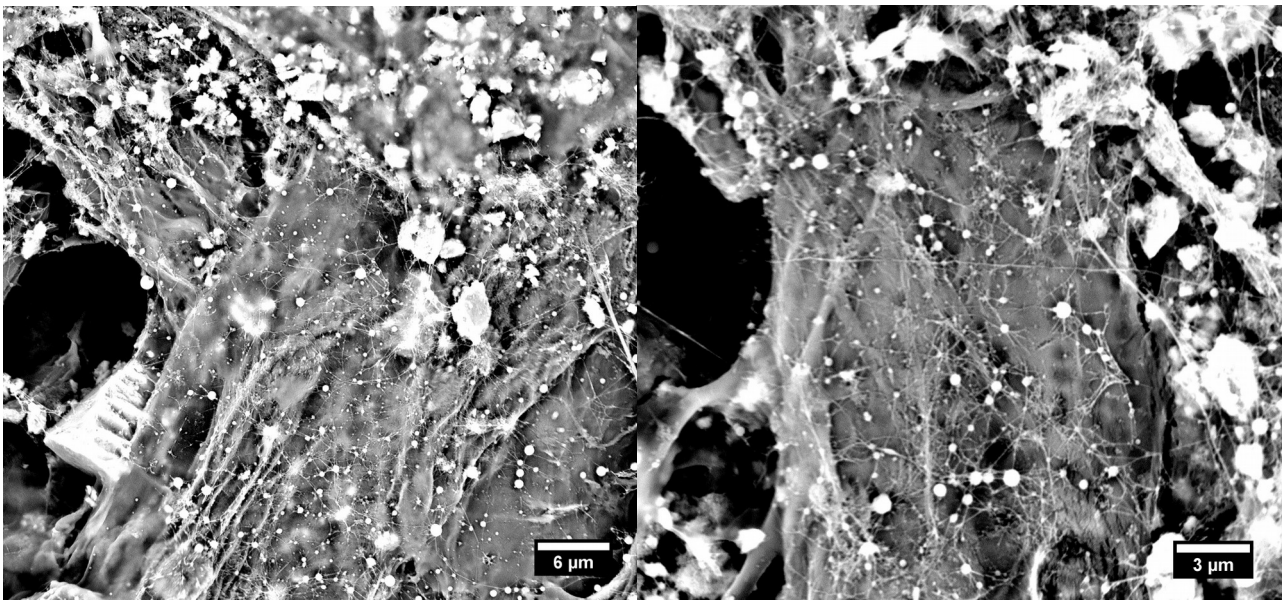

Fig. 19: SEM micrographs of HA 1,18 MDa H2O:IPA 10:7 1,2 wt.% solution fibers, spinning voltage 16,3 kV

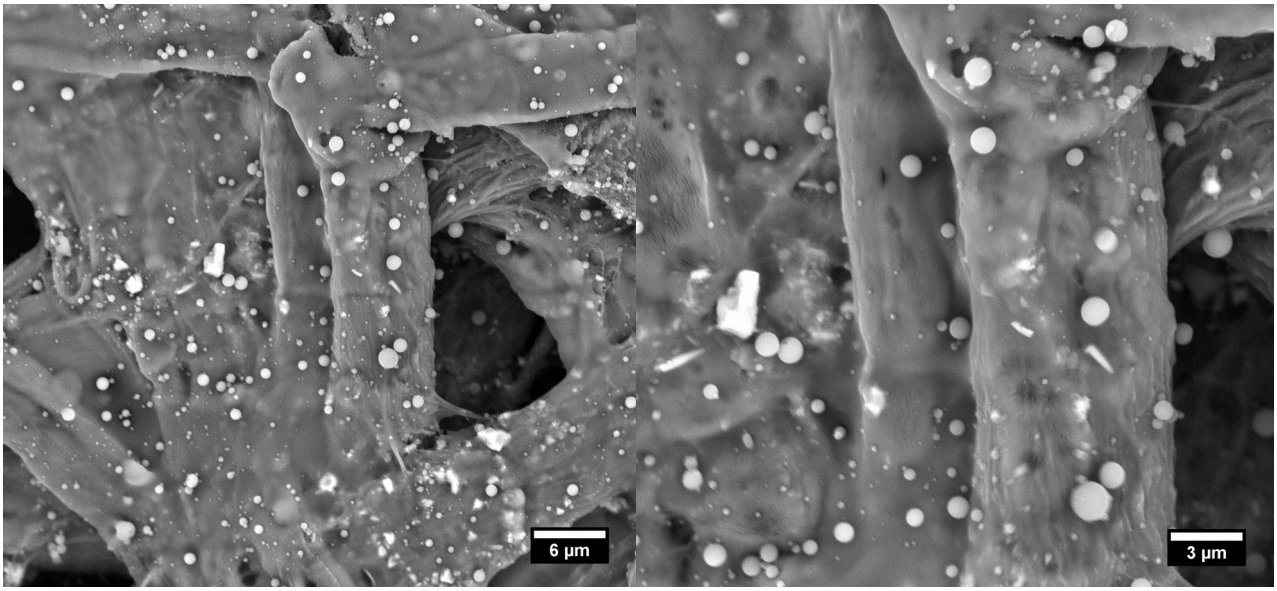

Fig. 20: SEM micrographs of HA 1,18 MDa H2O:IPA 10:7 1,0 wt.% solution fibers, spinning voltage 19,0 kV

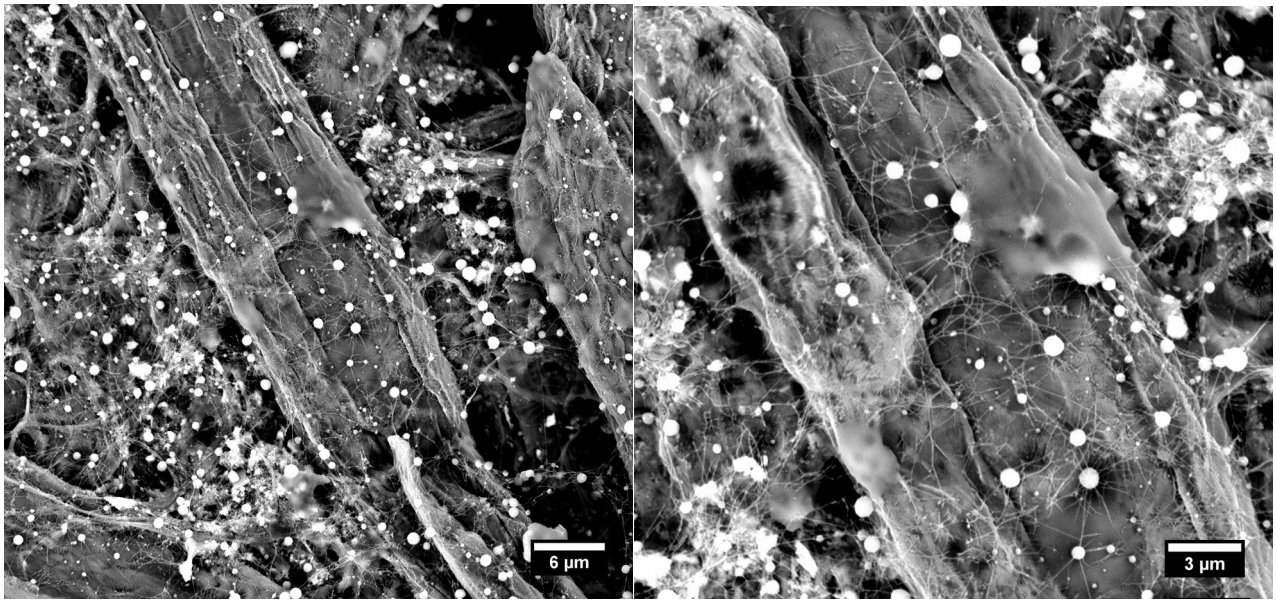

Fig. 21: SEM micrographs of HA 0,6 MDa H2O:EtOH:MeOH 5:5:1 2,8 wt.% solution fibers, spinning voltage 19,1 kV

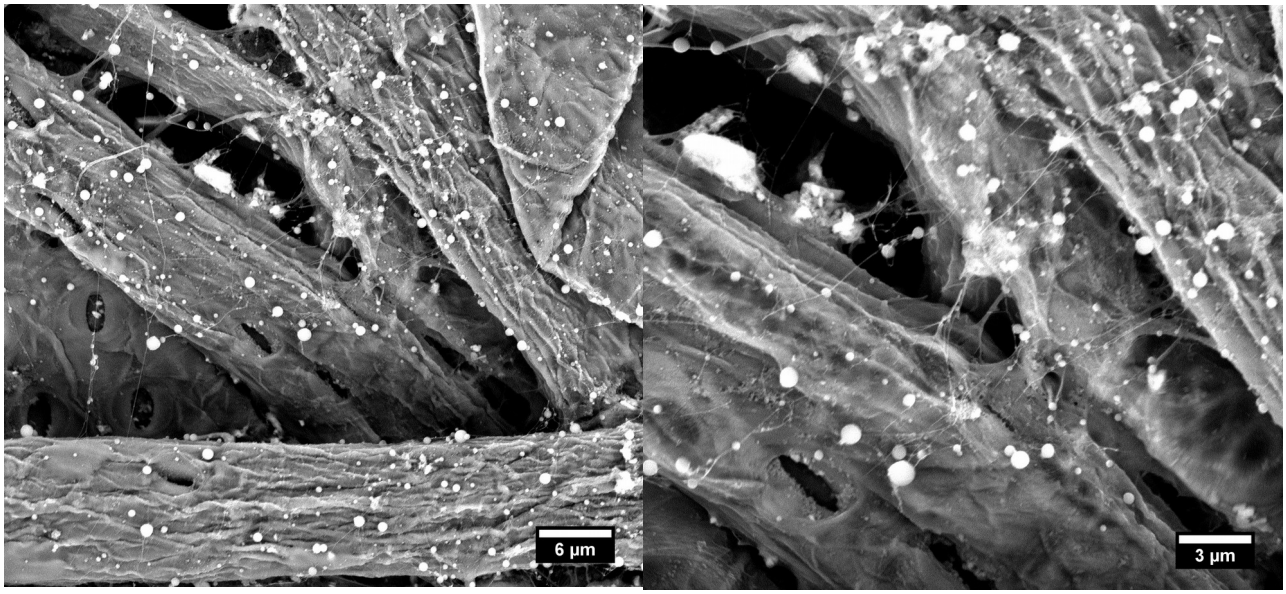

Fig. 22: SEM micrographs of HA 0,6 MDa H2O:EtOH:MeOH 5:5:1 2,4 wt.% solution fibers, spinning voltage 16,5 kV

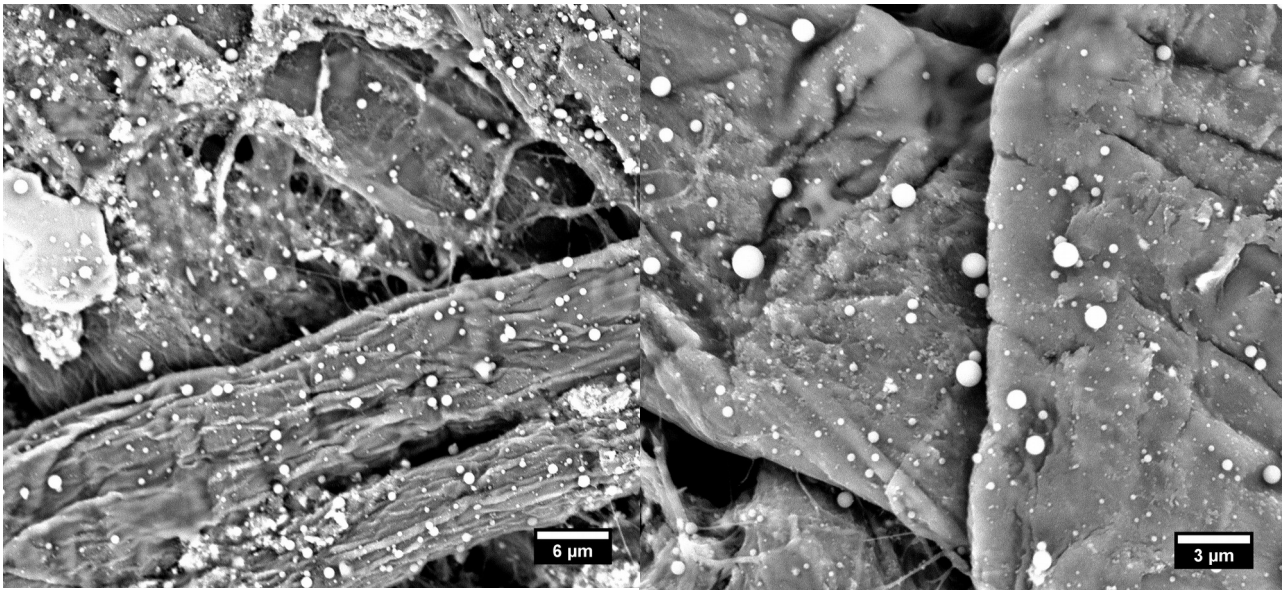

Fig. 23: SEM micrographs of HA 0,6 MDa H2O:EtOH:MeOH 5:5:1 0,7 wt.% solution fibers, spinning voltage 14,9 kV

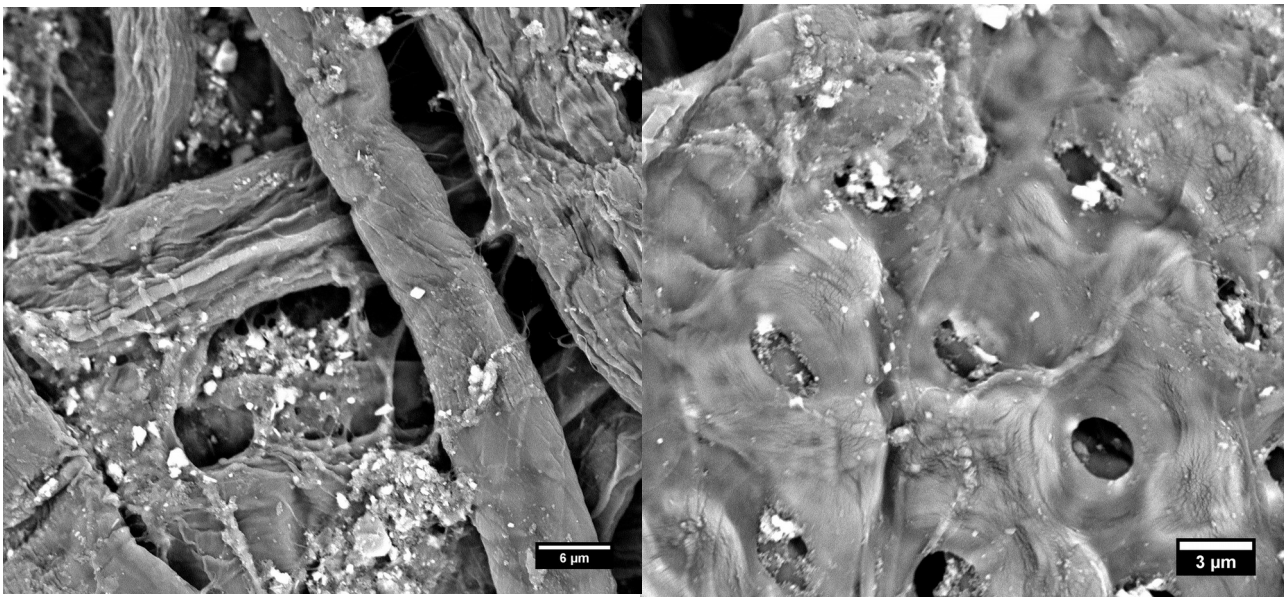

Fig. 24: SEM micrographs of HA 1,18 MDa H2O:EtOH:MeOH 5:5:1 2,3 wt.% solution fibers, spinning voltage 29,2 kV

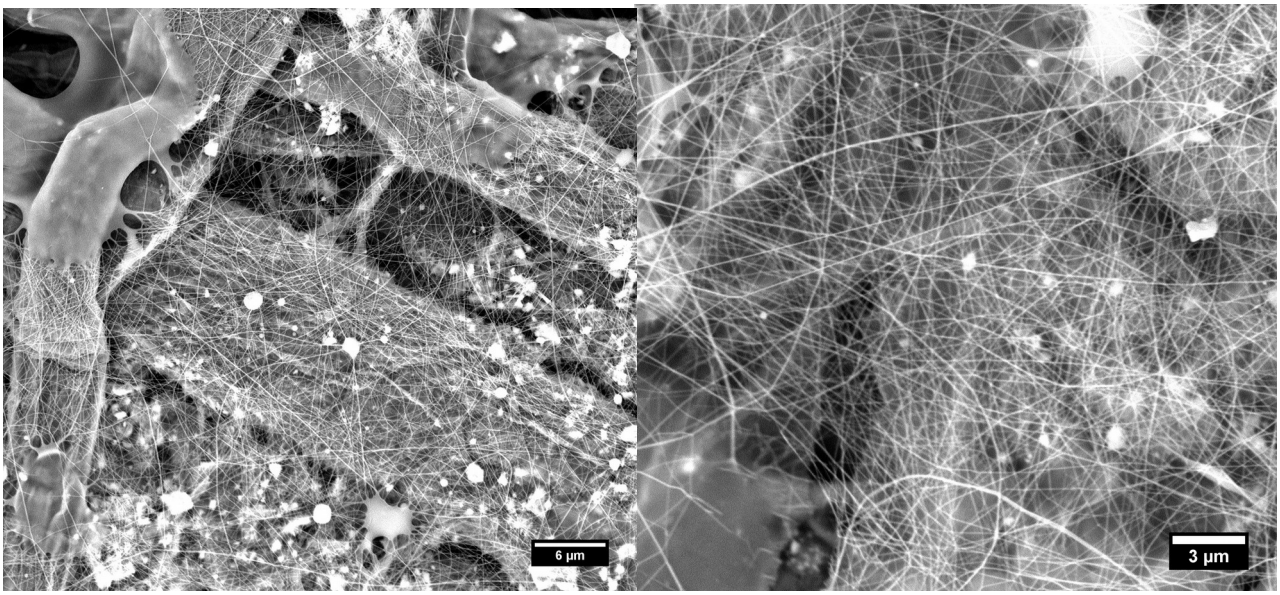

Fig. 25: SEM micrographs of HA 1,18 MDa H2O:EtOH:MeOH 5:5:1 2,2 wt.% solution fibers, spinning voltage 22,9 kV

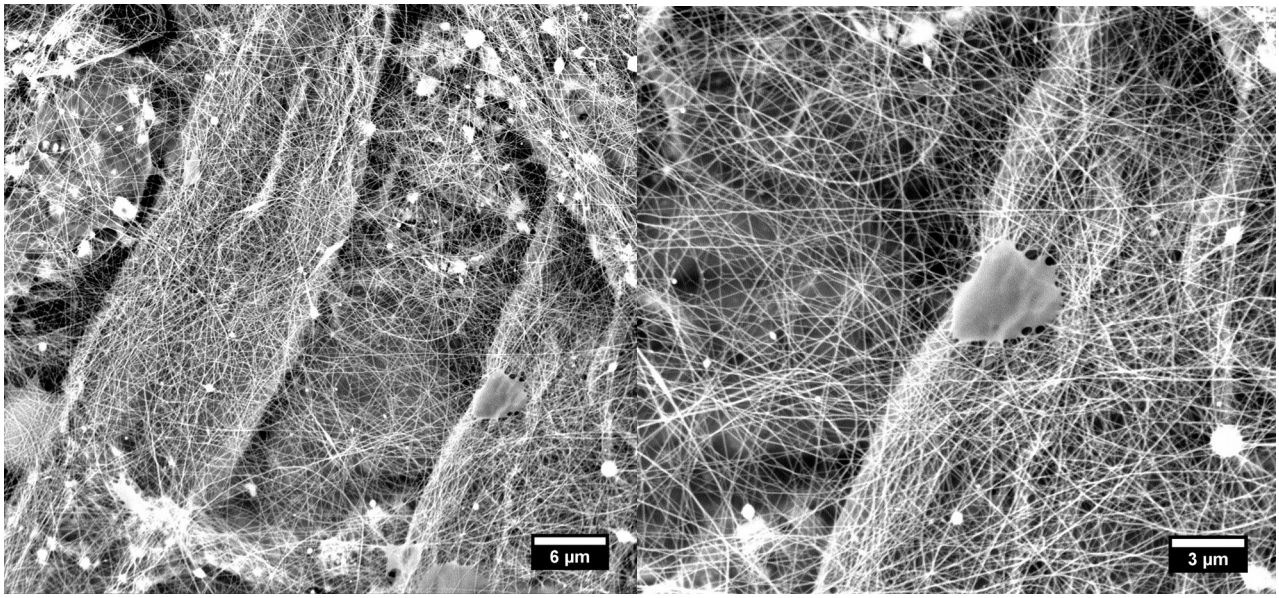

Fig. 26: SEM micrographs of HA 1,18 MDa H2O:EtOH:MeOH 5:5:1 1,5 wt.% solution fibers, spinning voltage 19,2 kV

Table 2: Morphology analysis of single Mw HA electrospinning products

Solvent mixture	Molecular weight [kDa]	Concentration [wt.%]	Spinning voltage [kV]	Product form	Diameter [µm]
H_2O:IPA 10:7	**600**	3,2 - non-oxidized	20,5	Spherical particles Fibers	0,3 – 0,6 0,04 – 0,1
		3,2 - oxidized	17,1	Spherical particles	0,1 – 0,6
		2,3 - non-oxidized	20,0	Spherical particles Fibers	0,3 – 1,0 0,06 – 0,1
		2,3 - oxidized	15,8	Spherical particles	0,3 – 0,8
		1,3 - non-oxidized	16,2	Spherical particles Fibers	0,4 – 1,2 0,05 – 0,1
		1,3 - oxidized	16,4	Spherical particles	0,2 – 0,5
	1 180	2,9	24,0	Fibers	0,05 – 0,09
		1,2	16,3	Spherical particles Fibers	0,3 – 0,8 0,06 – 1,0
		1	19,0	Spherical particles	0,7 – 1,1
H_2O:EtOH: MeOH 5:5:1	**600**	2,8	19,1	Spherical particles Fibers	0,4 – 1,0 0,05 – 0,07
		2,4	16,5	Spherical particles Fibers	0,2 – 0,8 0,05 – 0,07
		0,7	14,9	Spherical particles	0,3 – 1,4
	1 180	2,3	29,2	Elongated beads	0,2 – 0,4
		2,2	22,9	Fibers	0,05 – 0,08
		1,5	19,2	Fibers	0,05 – 0,1

Table 3: Characteristics of electrospinnable single M_w HA solutions

Solvent mixture	M_w [kDa]	Concentration [wt.%]	Density [g·cm^{-3}]	Surface tension [mN·m^{-1}]	Conductivity [µS·cm^{-1}]
H_2O:IPA at weight ratio 10:7	600	3,2	0,937043	27±1	854±2
		2,3	0,925345	25,0±0,5	568,4±0,4
		1,3	0,942085	26,2±0,3	465±1
	1 180	2,9	0,934543	24±3	682±2
		1,2	0,933866	28±2	386±2
		1,0	0,935955	27,1±0,5	343±2
H_2O:EtOH: MeOH at weight ratio 5:5:1	600	2,8	0,905499	32,3±0,9	740±8
		2,4	0,919826	30,5±0,5	748±1
		0,7	0,908960	30,2±0,8	249±1
	1 180	2,3	0,917288	27,4±0,8	704±1
		2,2	0,907604	28±2	616±1
		1,5	0,906813	27,6±0,9	459,3±0,7

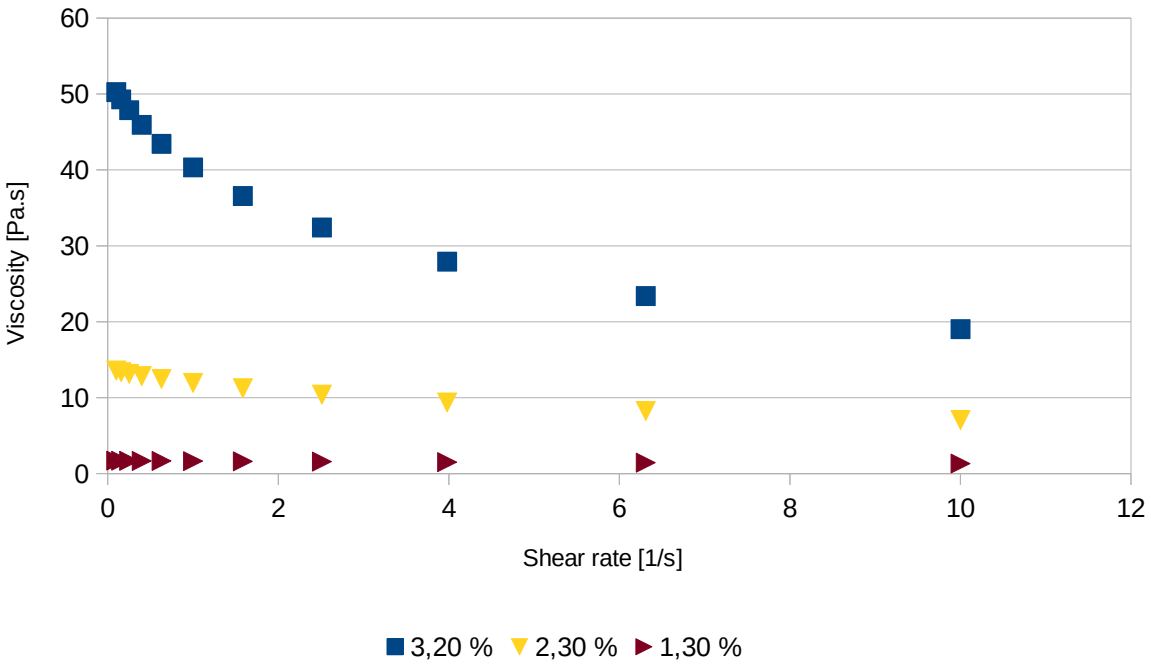

Fig. 27: Viscosity of 0,6 MDa HA in H2O:IPA 10:7 solution as a function of shear rate

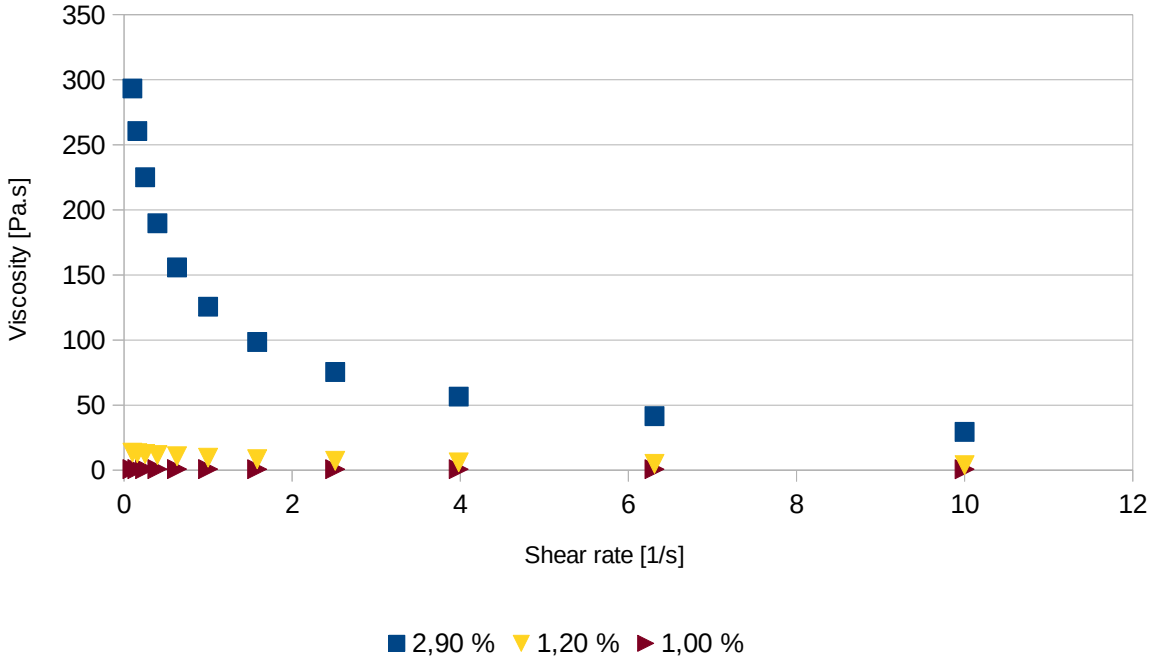

Fig. 28: Viscosity of 1,18 MDa HA in H2O:IPA 10:7 solution as a function of shear rate

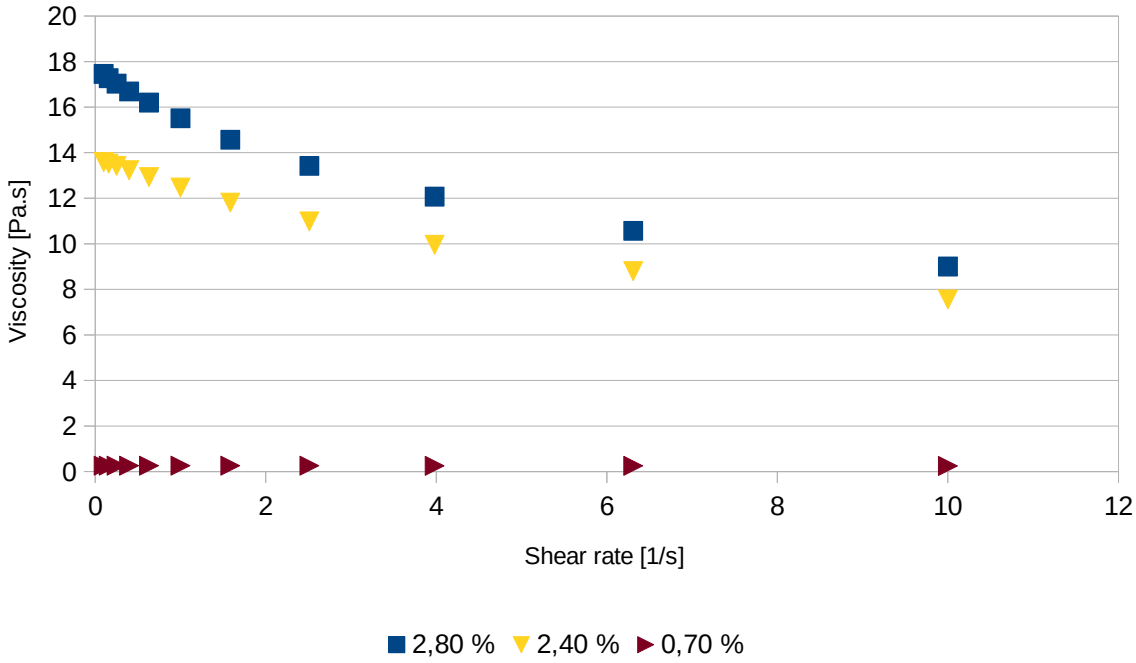

Fig. 29: Viscosity of 0,6 MDa HA in H2O:EtOH:MeOH 5:5:1 solution as a function of shear rate

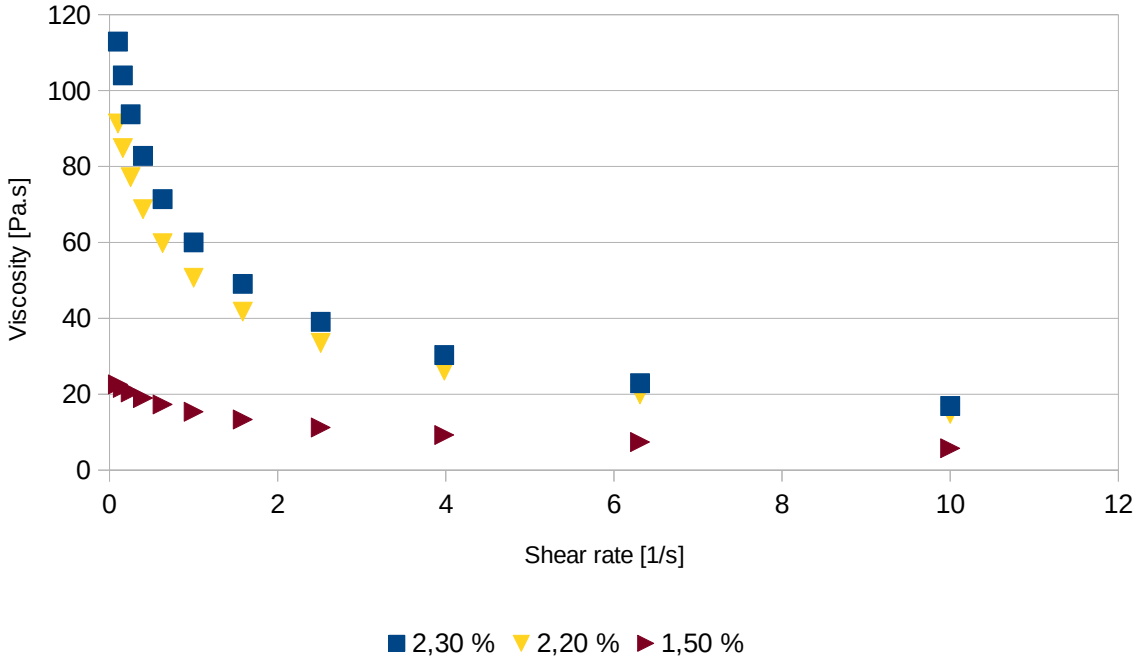

Fig. 30: Viscosity of 1,18 MDa HA in H2O:EtOH:MeOH 5:5:1 solution as a function of shear rate

7.2 Mixed Mw HA solutions

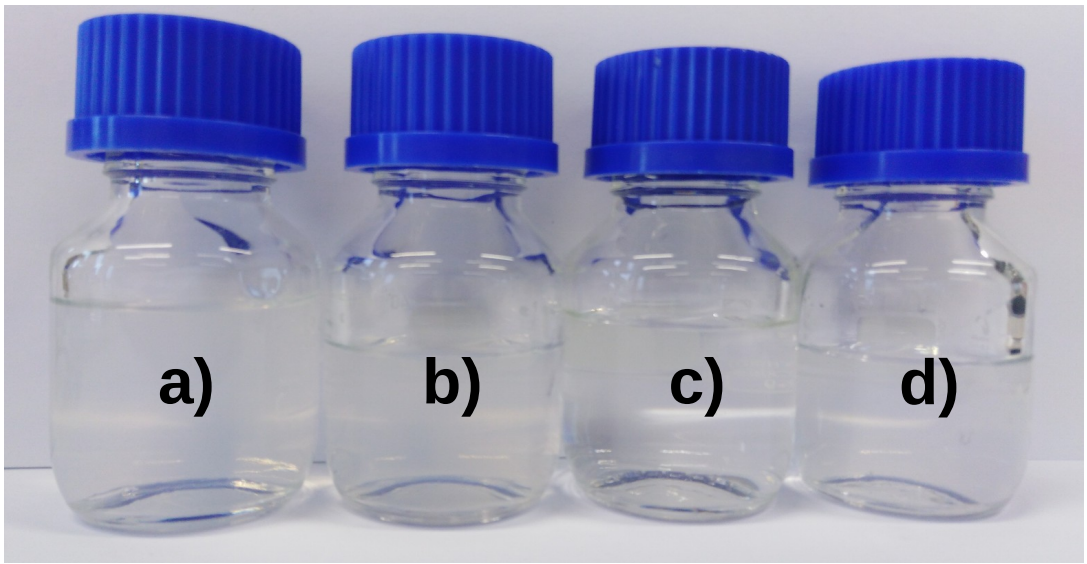

Fig. 31: Solutions of mixed Mw HA in H2O:EtOH 4:3, a) HA 124 kDa, 243 kDa, 370 kDa, 600 kDa – 4,3 wt.%, b) HA 124 kDa, 243 kDa, 370 kDa, 600 kDa – 3,5 wt.%, c) HA 124 kDa, 243 kDa, 370 kDa, 600 kDa – 1,0 wt.%, d) HA 124 kDa, 243 kDa, 370 kDa, 600 kDa, 1 180 kDa, 1 500 kDa – 3,5 wt.%

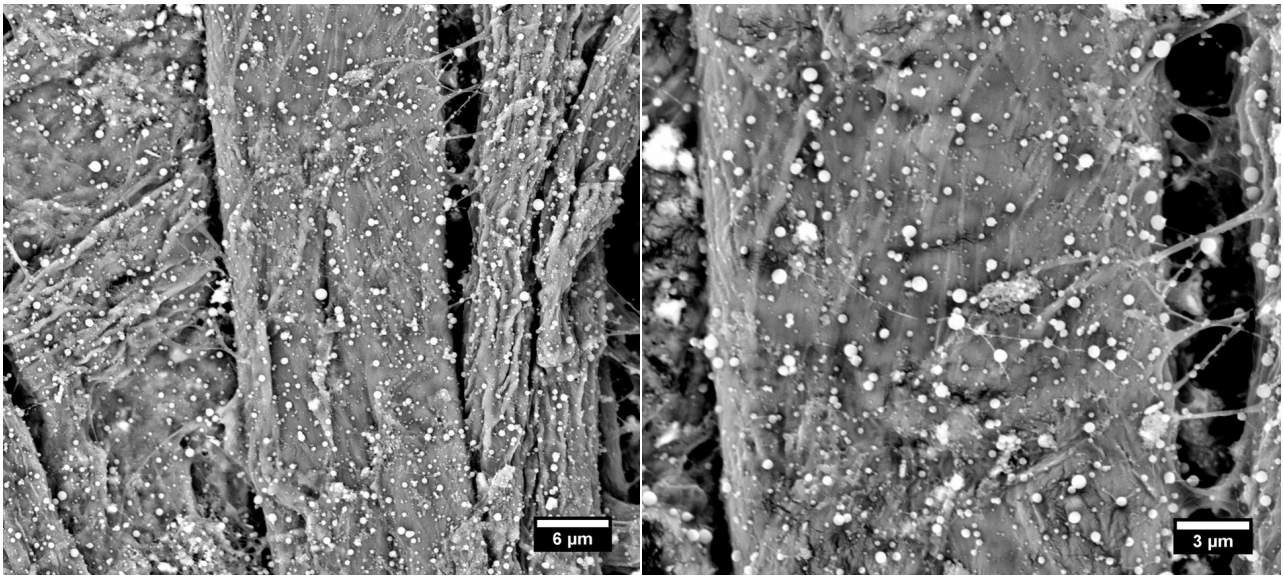

Fig. 32: SEM micrographs of mixed Mw (124 kDa, 243 kDa, 370 kDa, 600 kDa) HA H2O:EtOH 4:3 4,3 wt.% solution fibers, spinning voltage 18,5 kV

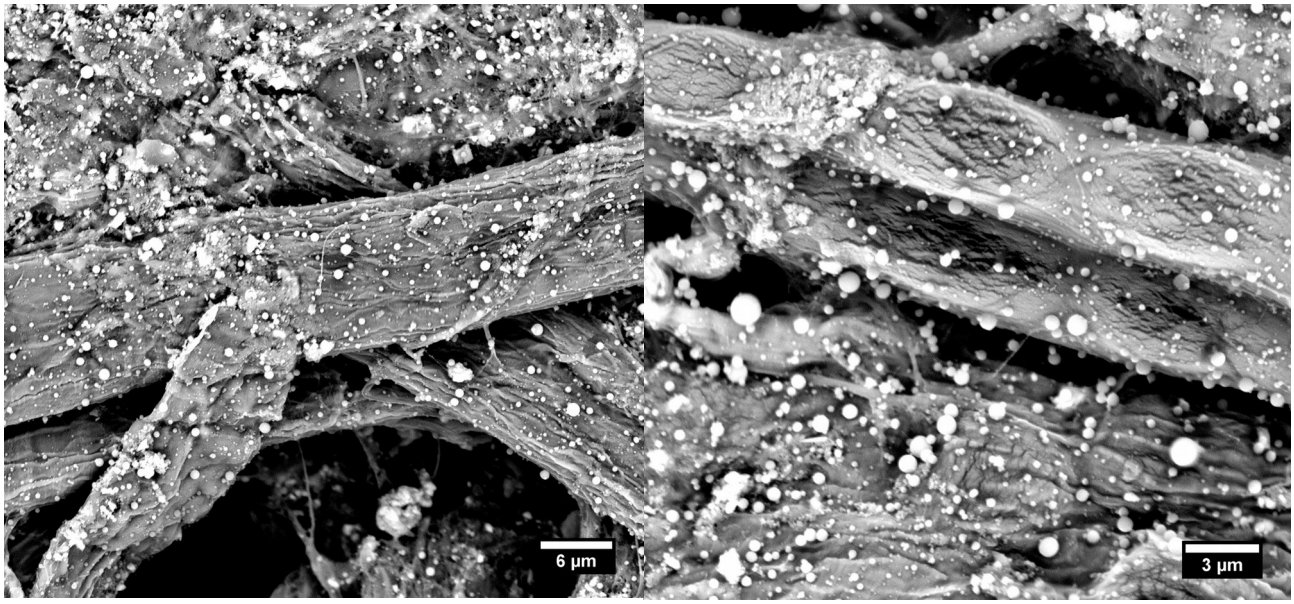

Fig. 33: SEM micrographs of mixed Mw (124 kDa, 243 kDa, 370 kDa, 600 kDa) HA H2O:EtOH 4:3 3,5 wt.% solution fibers, spinning voltage 16,9 kV

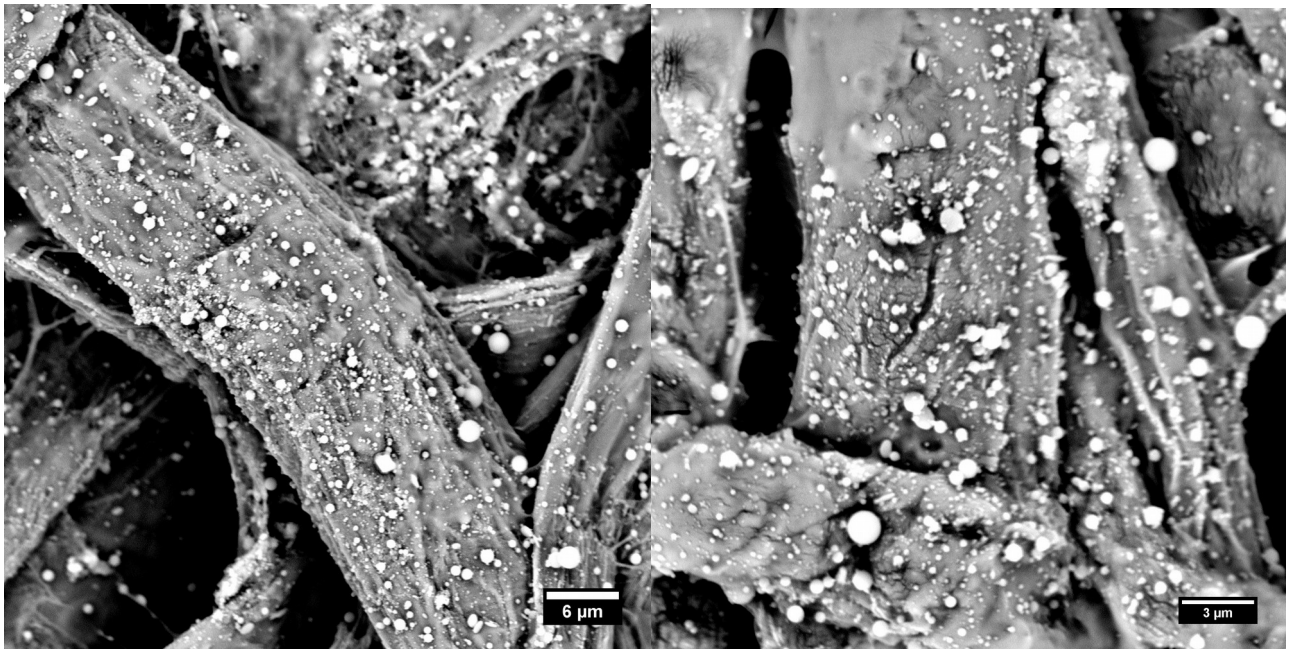

Fig. 34: SEM micrographs of mixed Mw (124 kDa, 243 kDa, 370 kDa, 600 kDa) HA H2O:EtOH 4:3 1,0 wt.% solution fibers, spinning voltage 21,2 kV

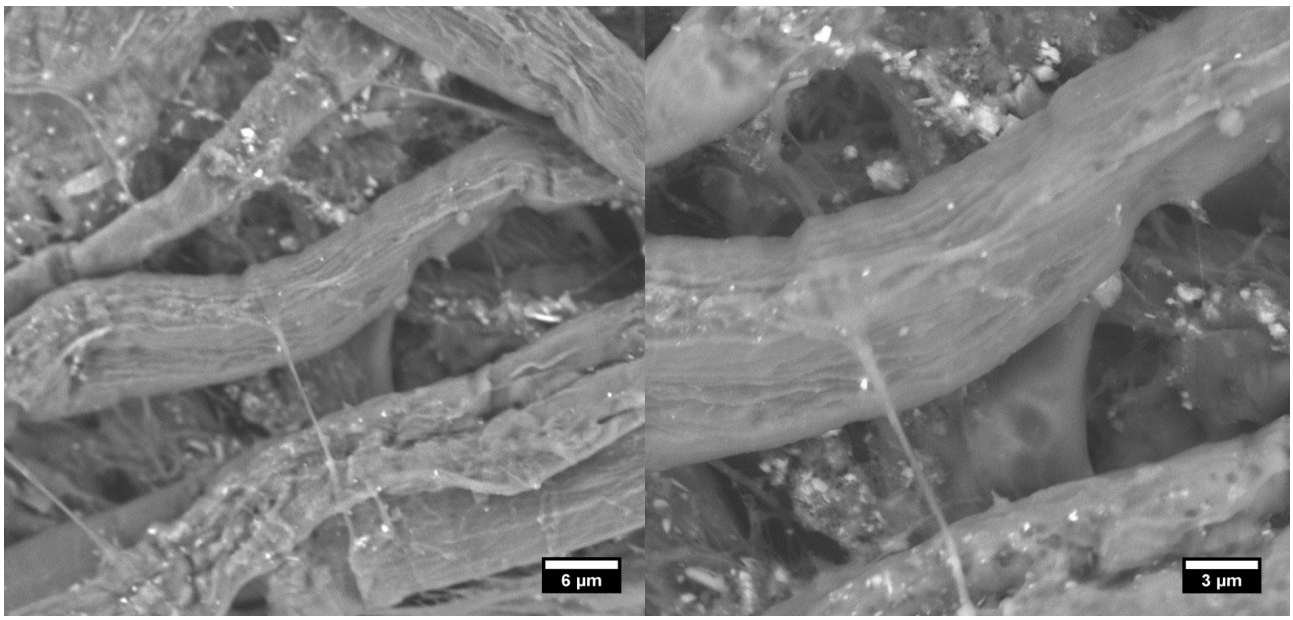

Fig. 35: SEM micrographs of mixed Mw (124 kDa 243 kDa, 370 kDa, 600 kDa, 1 180 kDa, 1 500 kDa) HA in H2O:EtOH 4:3 3,5 wt.% solution fibers, spinning voltage 20,2 kV

Table 4: Morphology analysis of mixed M_w HA electrospinning products

HA M_w [kDa]	Concentration [wt.%]	Spinning voltage [kV]	Product form	Diameter [µm]
124; 243; 370; 600	4,3	18,5	Spherical particles Fibers	0,1 – 0,7 0,05 – 0,09
	3,5	16,9	Spherical particles	0,2 – 0,7
	1,0	21,2	Spherical particles	0,2 – 0,5
124; 243; 370; 600; 1 180; 1 500	3,5	20,2	Elongated beads	0,1 – 0,3

Table 5: Characteristics of HA solution containing Mw 128 kDa, 243 kDa, 370 kDa and 600 kDa at weight ratio 1:1:1:1 in H2O:EtOH 4:3 solvent mixture

Concentration [wt.%]	Density [g·cm^{-3}]	Surface tension [mN·m^{-1}]	Conductivity [µS·cm^{-1}]
4,3	0,930287	27,0±0,2	1136±4
3,5	0,935694	27,9±0,2	1090±5
1,0	0,939916	28,8±0,6	432±1

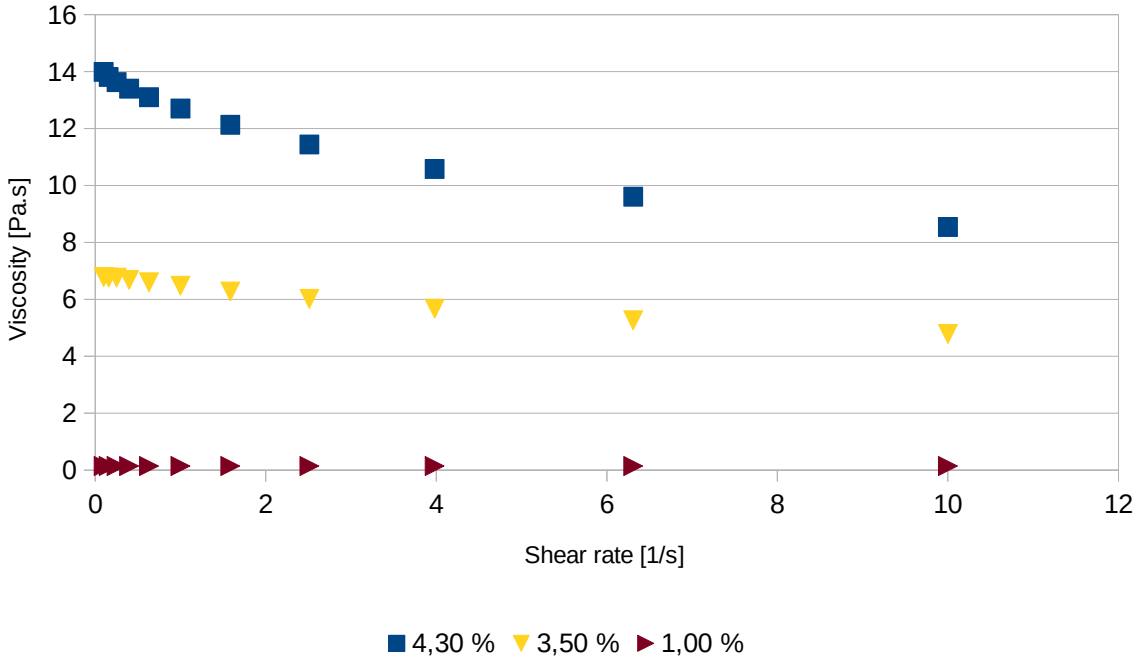

Fig. 36: Viscosity of HA of mixed Mw in H2O:EtOH 4:3 solution as a function of shear rate

7.3 HA/PEO bi-component blend solutions

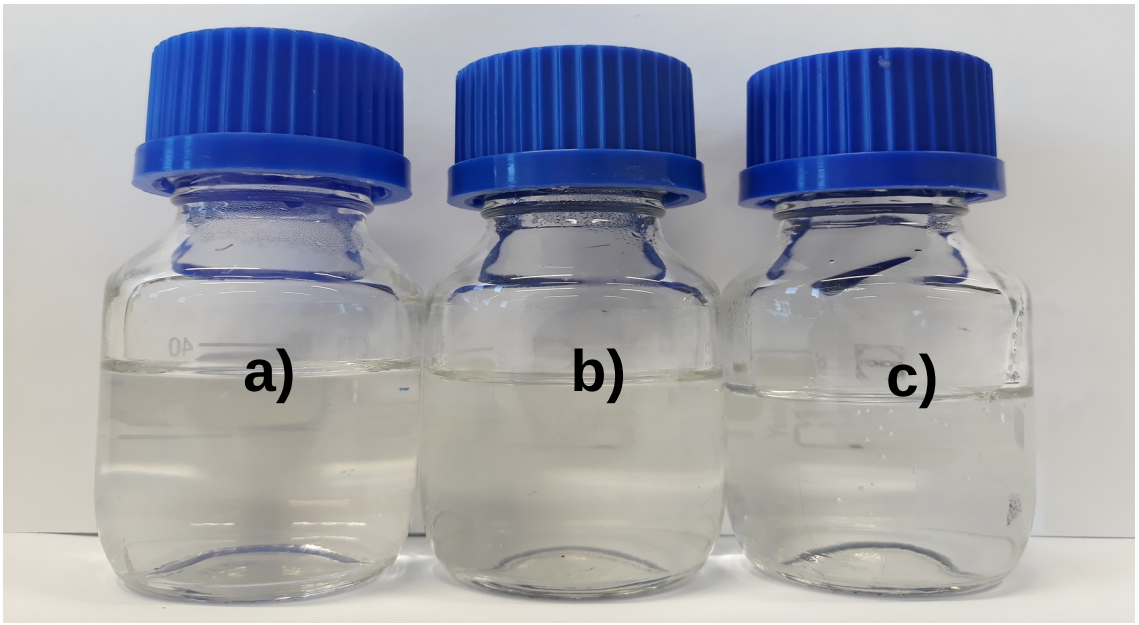

Fig. 37: PEO 300 kDa/HA blend solutions; a) HA 243 kDa, b) HA 370 kDa, c) HA 600 kDa

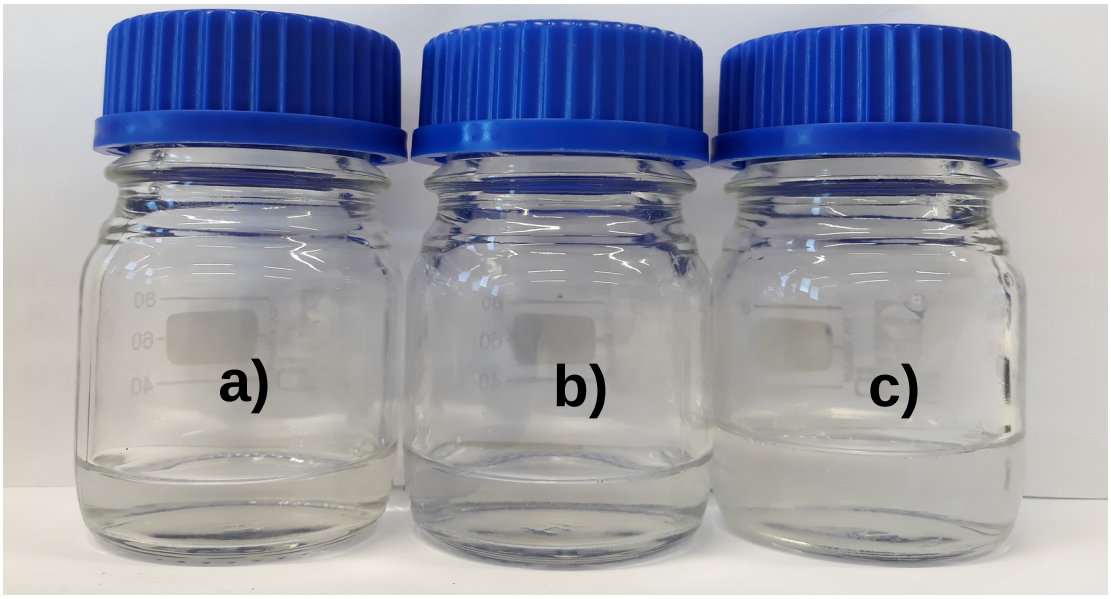

Fig. 38: PEO 600 kDa/HA blend solutions; a) HA 243 kDa, b) HA 370 kDa, c) HA 600 kDa

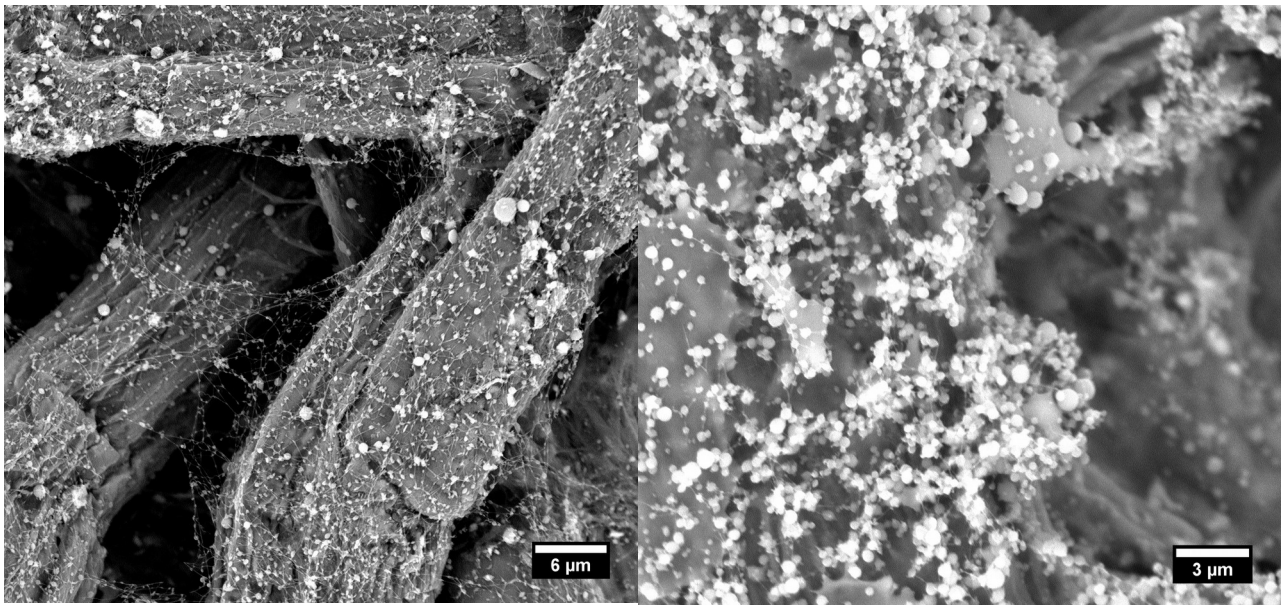

Fig. 39: SEM micrographs of PEO 300 kDa and HA 243 kDa solution fibers, spinning voltage 18,2 kV

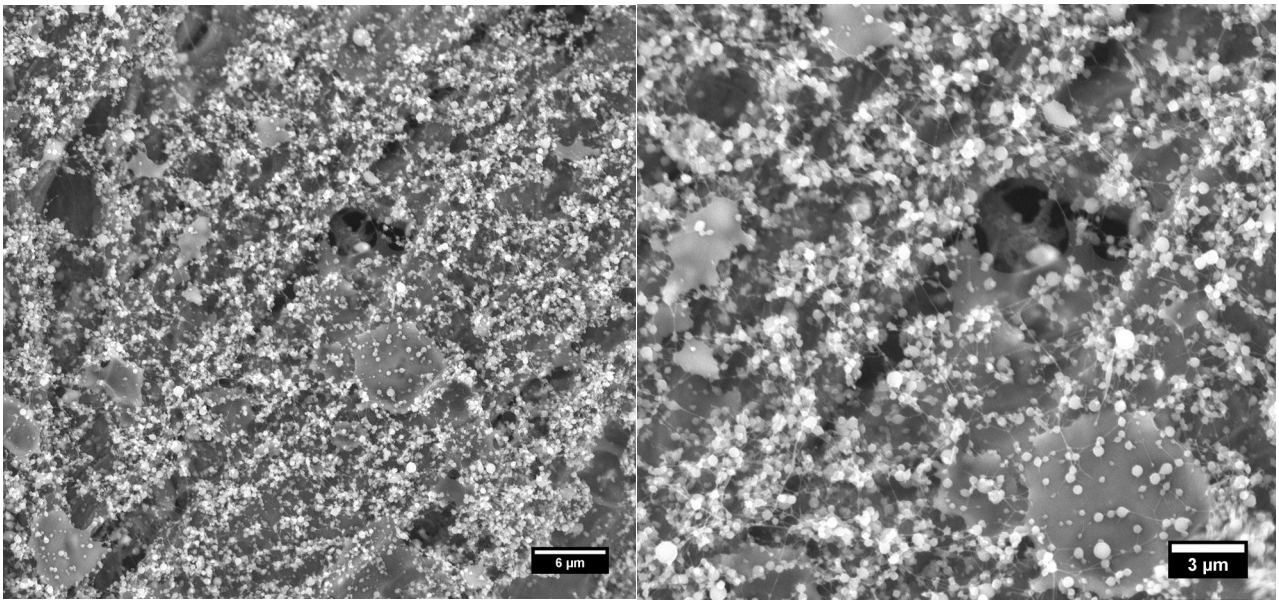

Fig. 40: SEM micrographs of PEO 300 kDa and HA 370 kDa solution fibers, spinning voltage 18,2 kV

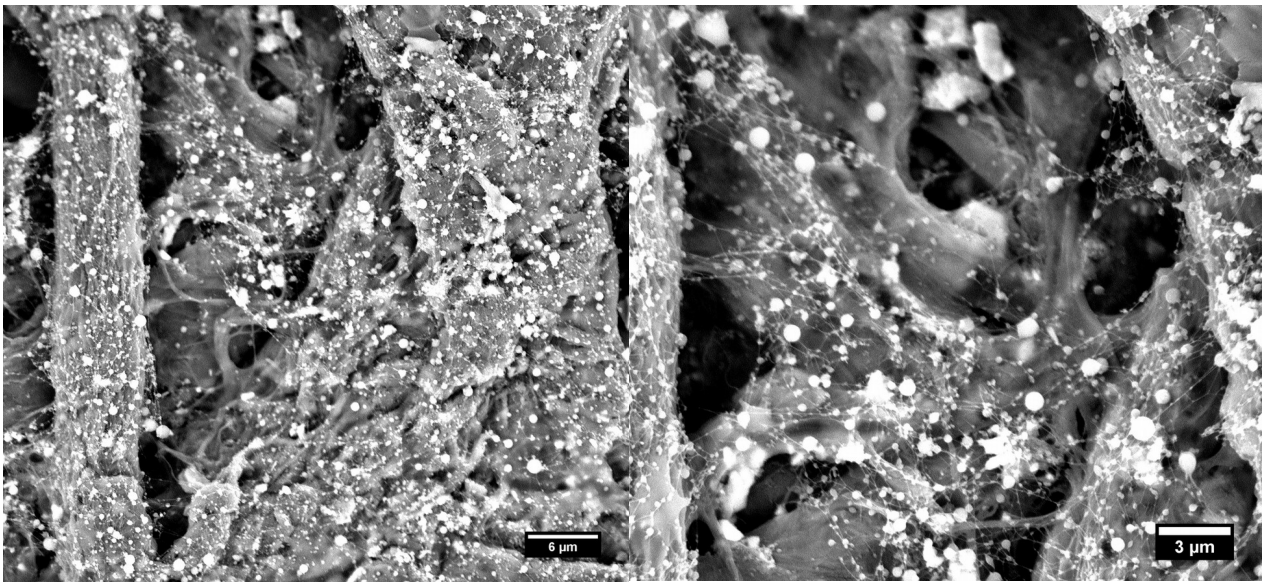

Fig. 41: SEM micrographs of PEO 300 kDa and HA 600 kDa solution fibers, spinning voltage 18,2 kV

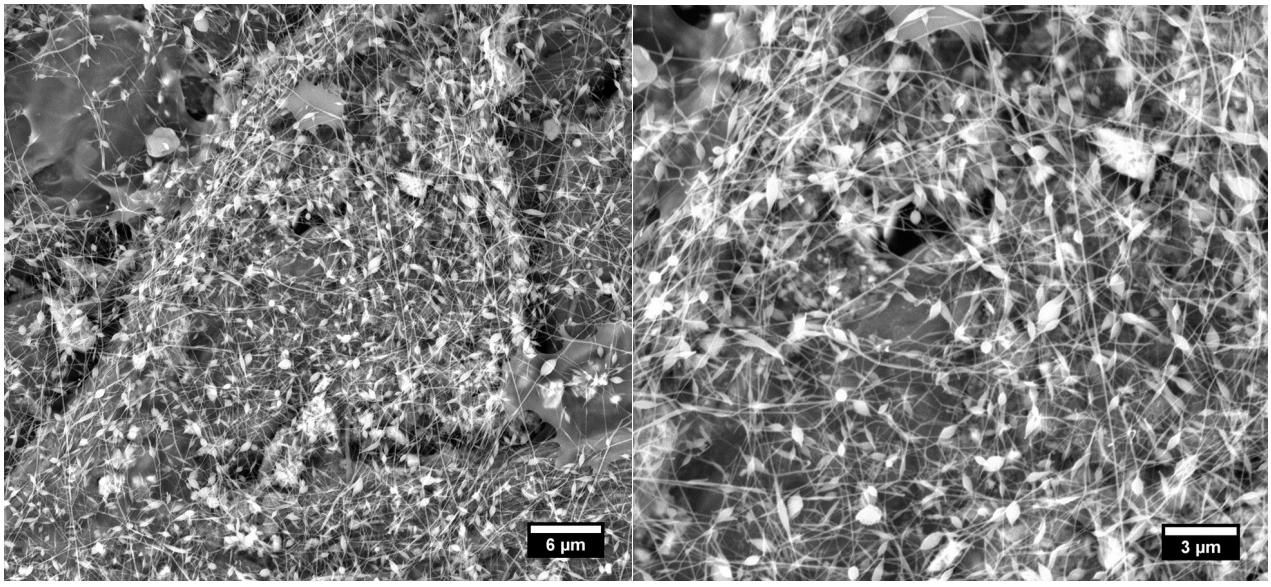

Fig. 42: SEM micrographs of PEO 600 kDa and HA 243 kDa solution fibers, spinning voltage 24,5 kV

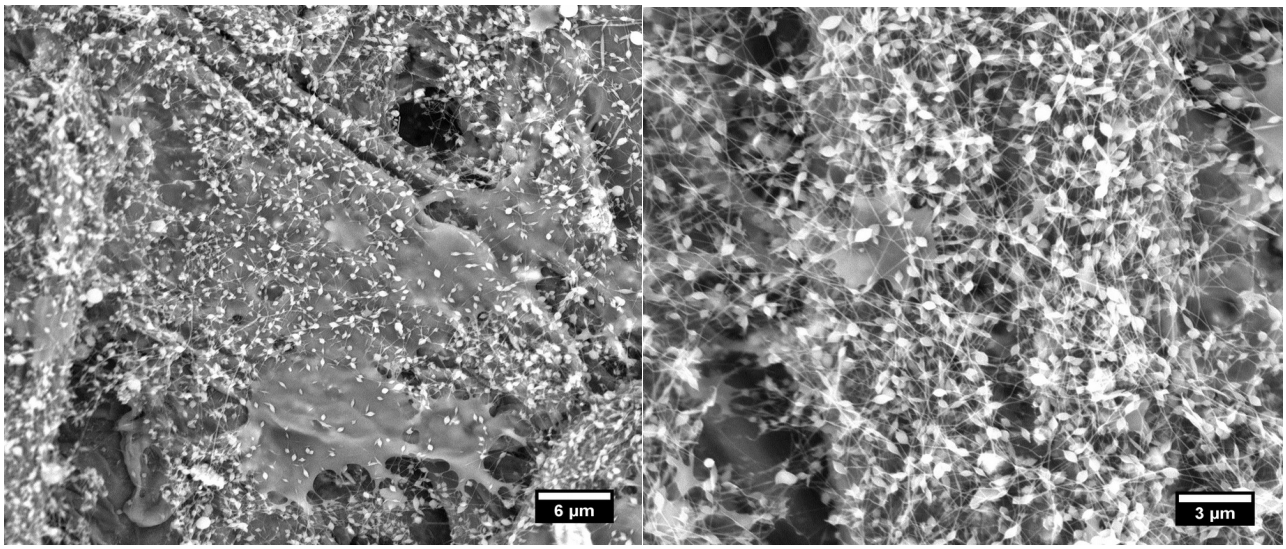

Fig. 43: SEM micrographs of PEO 600 kDa and HA 370 kDa solution fibers, spinning voltage 24,5 kV

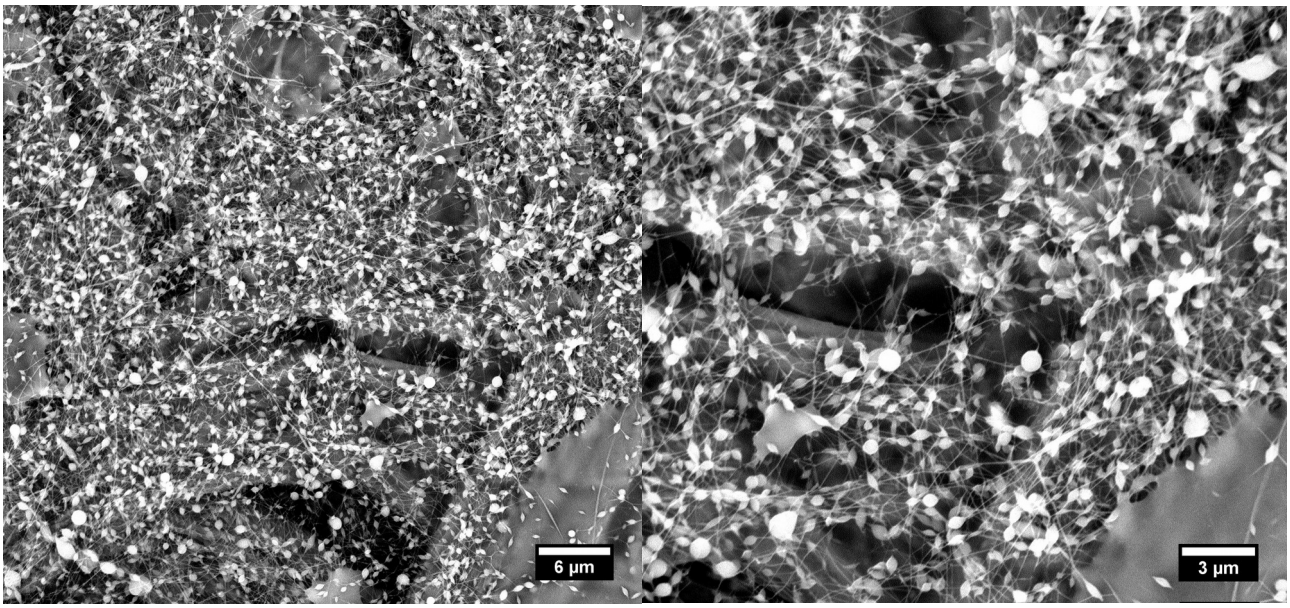

Fig. 44: SEM micrographs of PEO 600 kDa and HA 600 kDa solution fibers, spinning voltage 24,5 kV

Table 6: Morphology analysis of PEO/HA electrospinning products

PEO M_w [kDa]	HA M_w [kDa]	Spinning voltage [kV]	Product form	Diameter [µm]
300	**243**	18,2	Bead-on-string	0,25 – 0,5 0,02 – 0,05
	370	18,2	Bead-on-string	0,3 – 0,5 0,03 – 0,07
	600	18,2	Bead-on-string	0,2 – 0,6 0,04 – 0,1
600	**243**	24,5	Bead-on-string	0,2 – 0,7 0,05 – 0,1
	370	24,5	Bead-on-string	0,3 – 0,6 0,05 – 0,1
	600	24,5	Bead-on-string	0,3 – 0,6 0,03 – 0,09

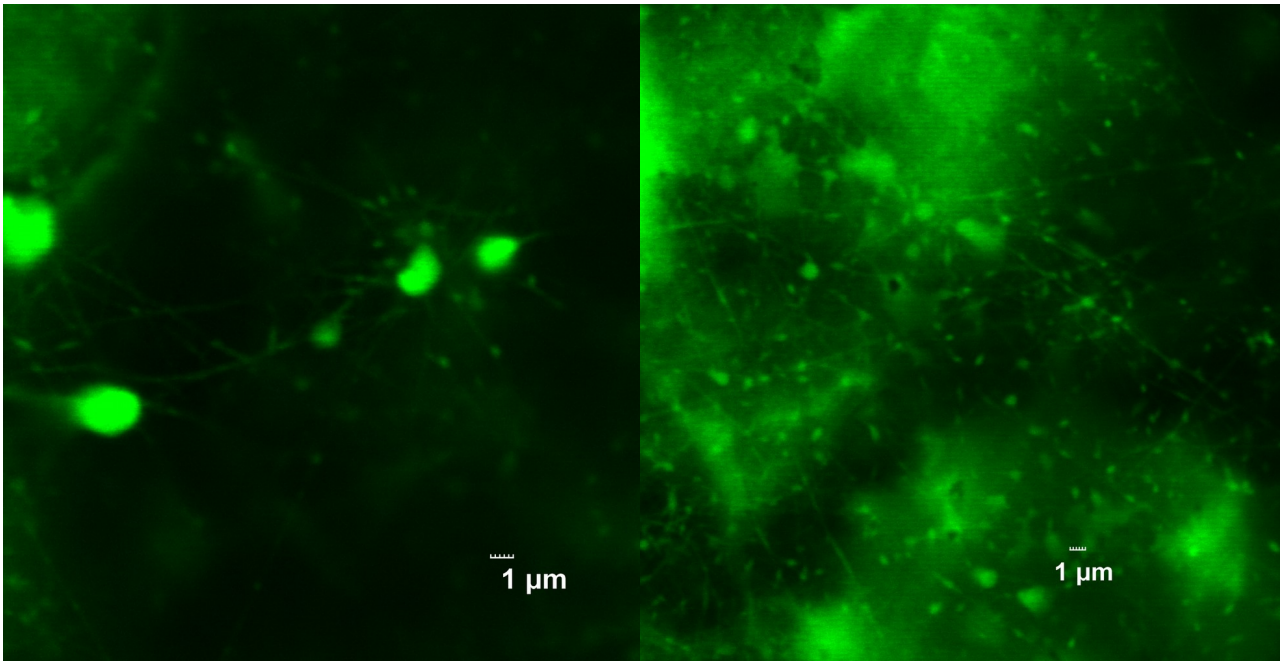

Fig. 45: Fluorescence confocal microscopy micrographs of HA-NB 600 kDa and PEO 600 kDa 2 wt.% aqueous solution, spinning voltage 24,5 kV

Table 7: Characteristics of electrospinnable HA/PEO blend solutions

PEO M_w [kg·mol^{-1}]	HA M_w [kg·mol^{-1}]	Density [g·cm^{-3}]	Surface Tension [mN·m^{-1}]	Conductivity [µS·cm^{-1}]
300	243	1,003294	46±2	1284±8
	370	1,003525	49,3±0,2	1255±7
	600	1,003597	49±2	1241±6
600	243	1,003816	51±2	1312±4
	370	1,003769	52±2	1258±3
	600	1,003638	54±1	1213±3

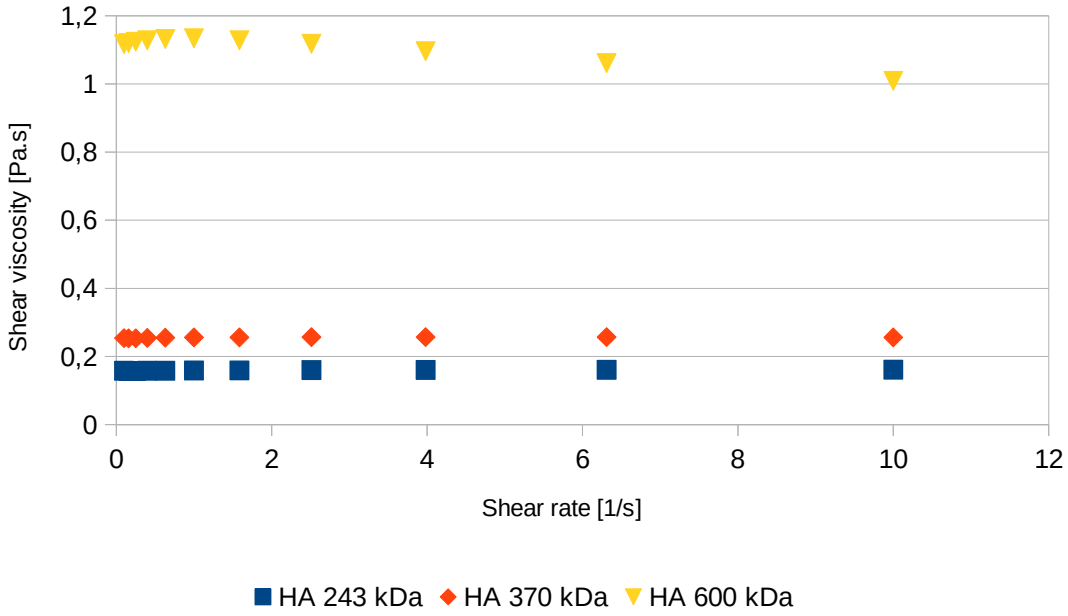

Fig. 46: Viscosity of HA and 300 kDa PEO bi-component solutions as a function of shear rate

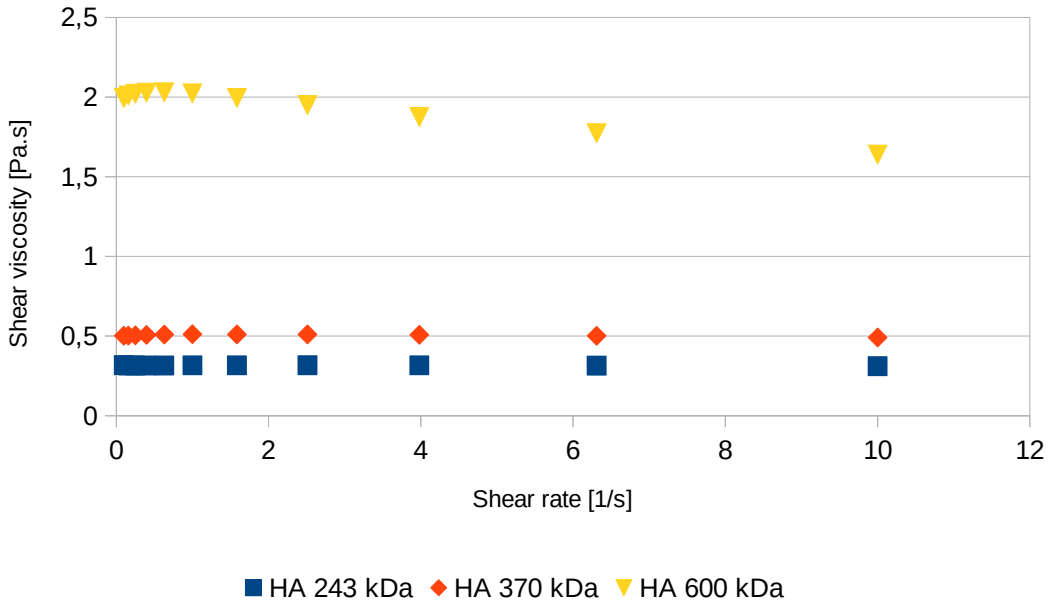

Fig. 47:Viscosity of HA and 600 kDa PEO bi-component solutions as a function of shear rate

7.4 HA/PVA bi-component blend solutions

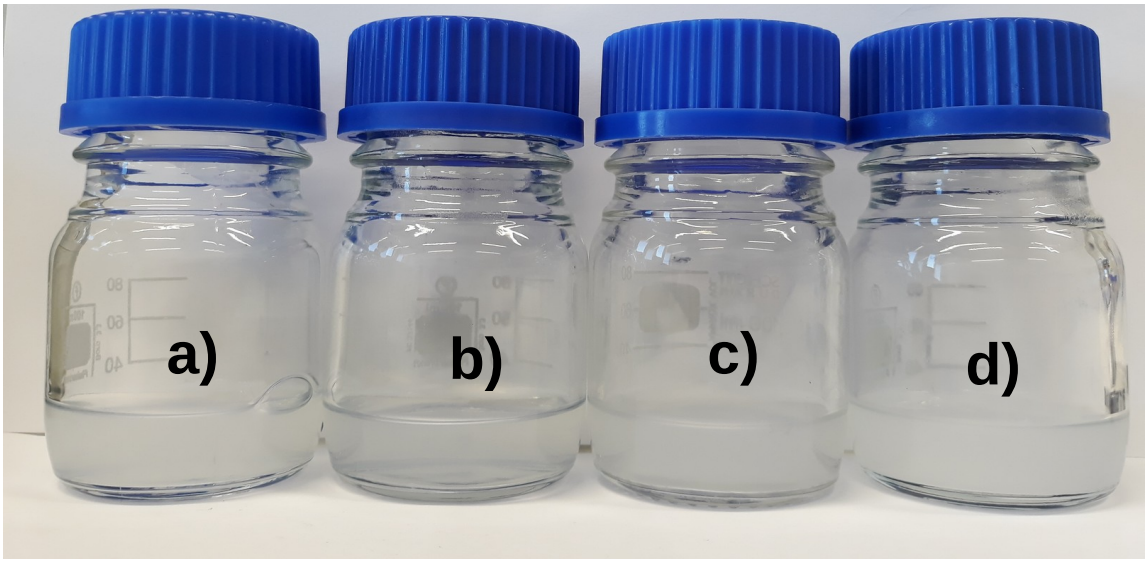

Fig. 48: PVA 89-98 kDa/HA 600 kDa blend solutions; a) 0,006 wt.% BAC , b) 0,013 wt.% BAC, c) 0,033 wt.% BAC, d) 0,065 wt.% BAC

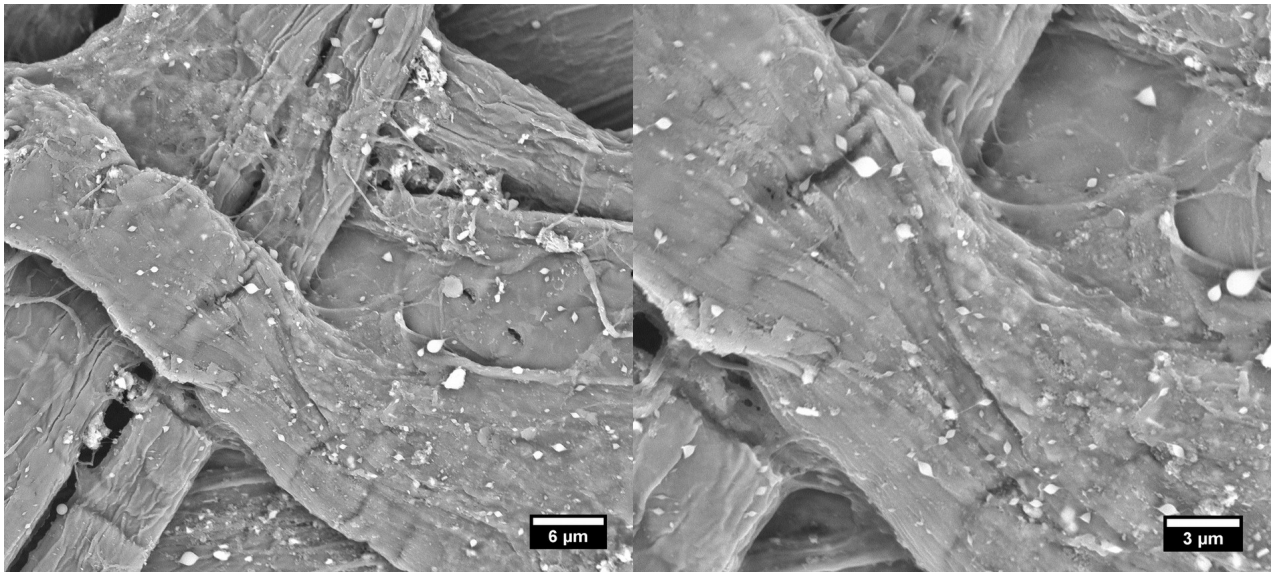

Fig. 49: SEM micrographs of PVA 89-98 kDa and HA 600 kDa solution with 0,006 wt.% BAC fibers, spinning voltage 20,4 kV

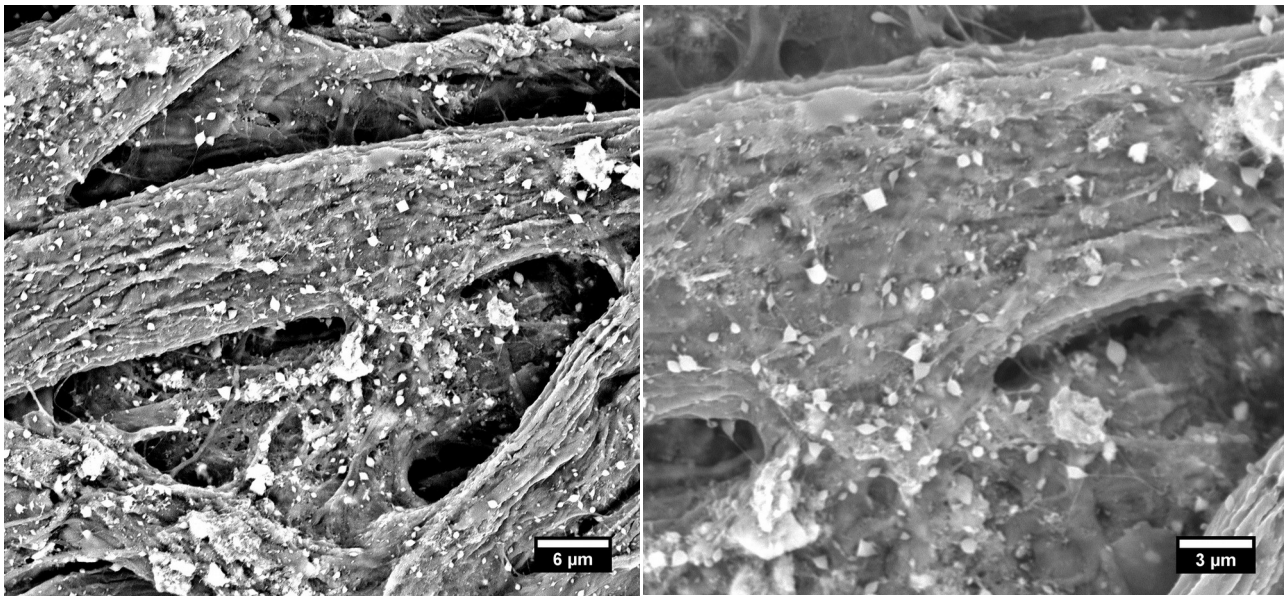

Fig. 50: SEM micrographs of PVA 89-98 kDa and HA 600 kDa solution with 0,013 wt.% BAC fibers, spinning voltage 18,8 kV

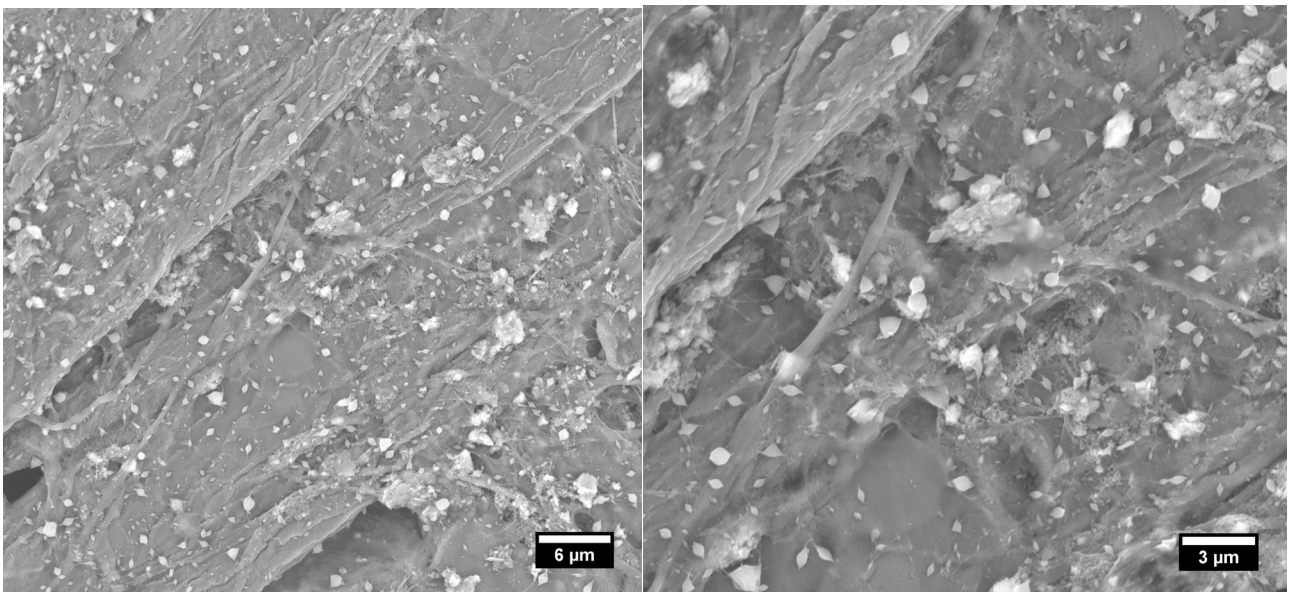

Fig. 51: SEM micrographs of PVA 89-98 kDa and HA 600 kDa solution with 0,033 wt.% BAC fibers, spinning voltage 17,5 kV

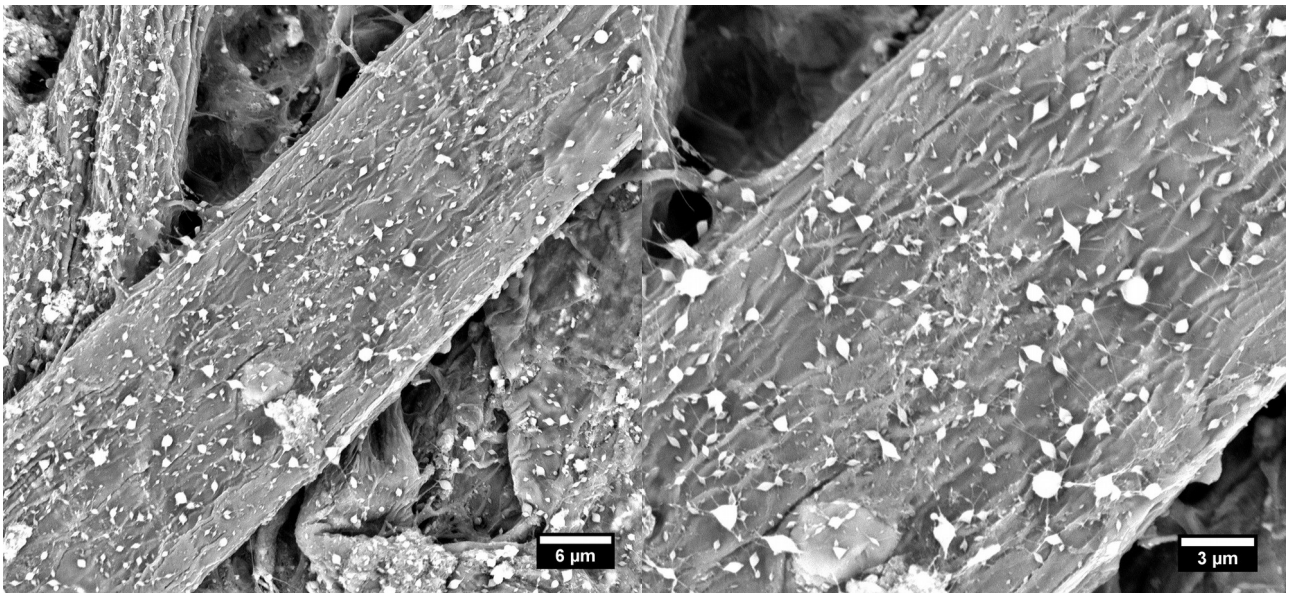

Fig. 52: SEM micrographs of PVA 89-98 kDa and HA 600 kDa solution with 0,065 wt.% BAC fibers, spinning voltage 15,9 kV

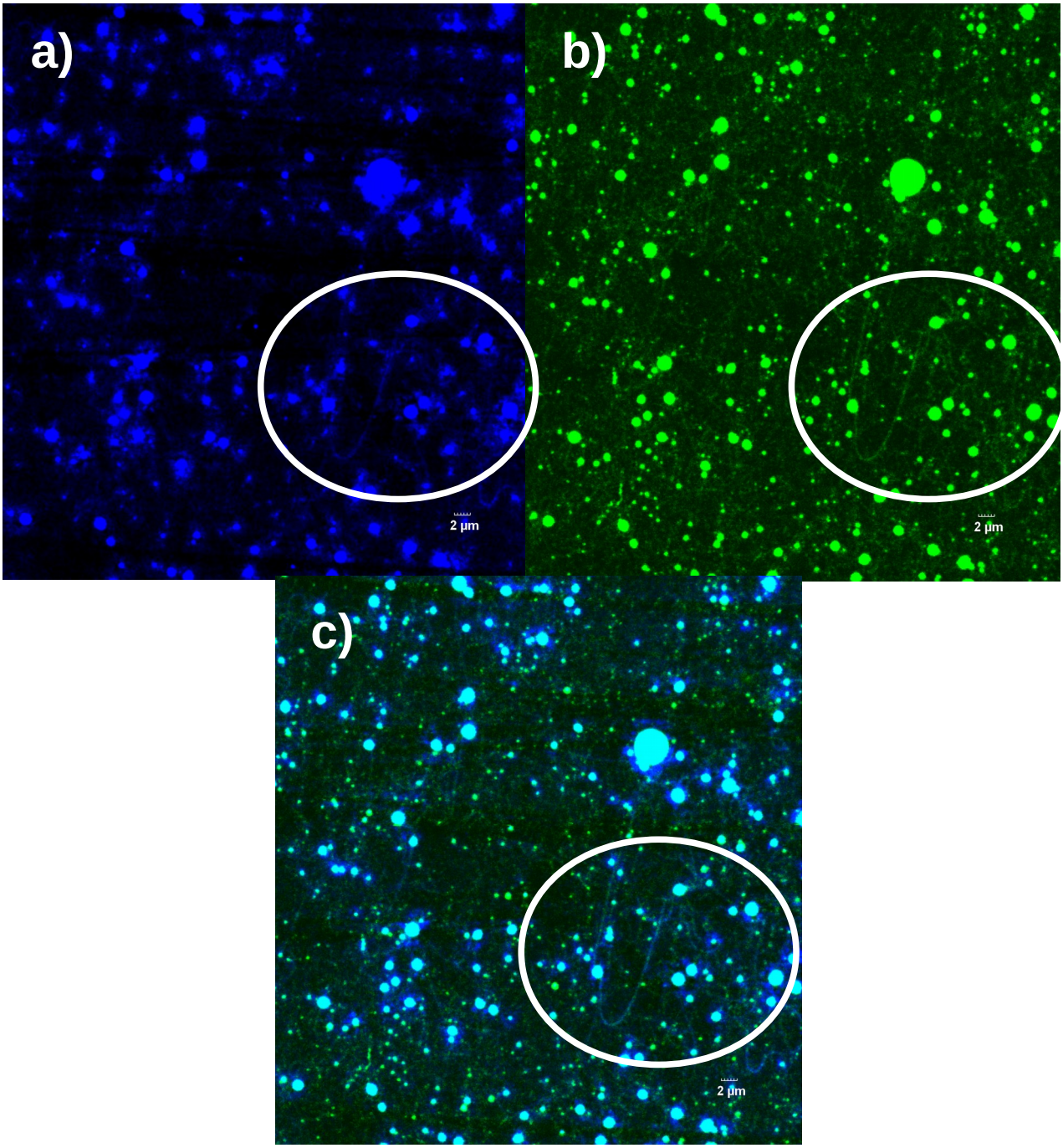

Fig. 53: Fluorescence confocal microscopy micrographs of PVA-FITC and HA-NB solution with 0,065 wt.% BAC fibers, spinning voltage 18,1 kV, a) PVA-FITC visible (excitation wavelength 488 nm), b) HA-NB visible (excitation wavelength 640 nm), c) both PVA-FITC and HA-NB visible (combined excitation wavelengths)

Table 8: Morphology analysis of PVA/HA electrospinning products

	BAC [wt.%]	Spinning voltage [kV]	Product form	Diameter [µm]
HA 600 kDa 1,1 wt.% **PVA 89-90 kDa 0,44 wt.%**	0,006	20,4	Elongated beads	0,1 – 0,5
	0,013	18,8	Bead-on-string	0,3 – 0,7 0,05 – 0,1
	0,033	17,5	Bead-on-string	0,1 – 0,8 0,03 – 0,06
	0,065	15,9	Bead-on-string	0,2 – 0,6 0,06 – 0,1

Table 9: Characteristics of electrospinnable HA/PVA blend solutions with BAC addition

	BAC [wt.%]	Density [g·cm^{-3}]	Surface Tension [mN·m^{-1}]	Conductivity [µS·cm^{-1}]
HA 600 kDa 1,1 wt.% **PVA 89-90 kDa 0,44 wt.%**	0,006	1,002793	43,7±0,9	1473±7
	0,013	1,002755	42,6±0,2	1496±2
	0,033	1,002924	41,4±0,6	1513±4
	0,065	1,002823	41,1±0,2	1546±4

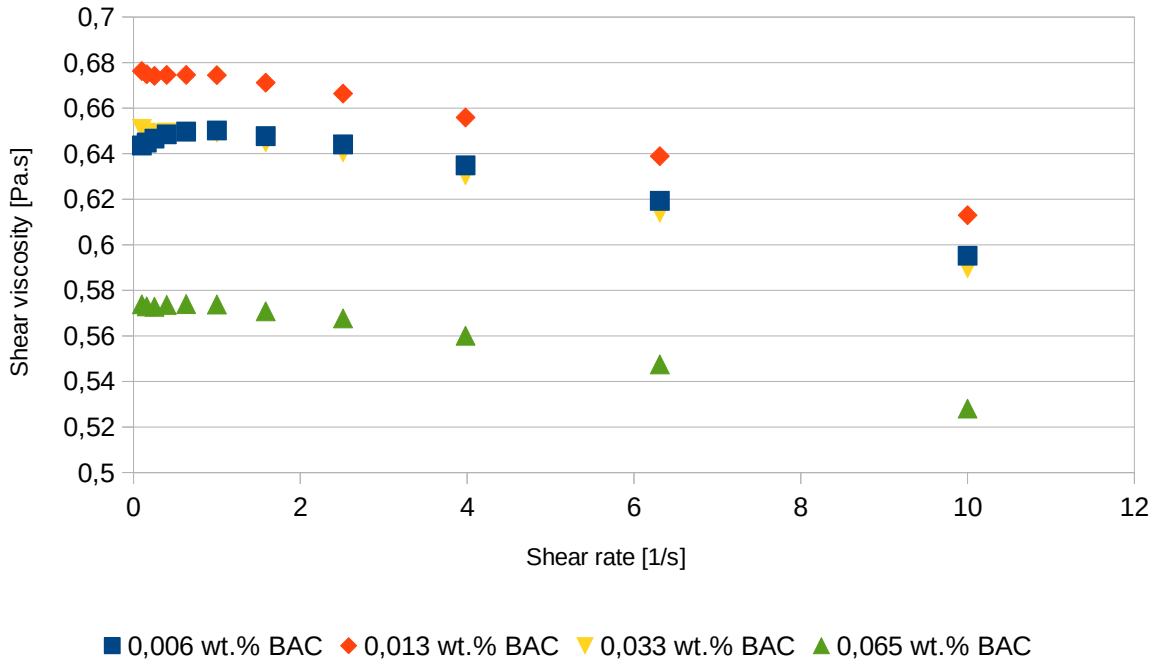

Fig. 54: Viscosity of HA/PVA bi-component solutions with addition of BAC as a function of shear rate

8 DISCUSSION

The experiments described in previous section were designed to find conditions allowing electrospinning of solutions containing HA. The solutions were characterized, emphasizing the parameters which are connected to electrospinning performance according to experts. The result will be discussed in the following sections.

8.1 Electrospinning of single M_w HA

HA of 0,6 MDa and 1,18 MDa were spun from two different solvent mixtures – water and IPA, and water, EtOH and MeOH. These systems were chosen with respect to literature, corresponding to findings of Luo et al., 2010 [29]. The selected solvent systems are presented in Teas graph below. The fractional parameters values are taken from Gardon and Teas, 1976, and Barton, 1983 [79], [80]. It was not possible to spun pure HA from water only, presumably due to high surface tension and water being a good solvent to HA. This causes the polymer chains to unwind, possibly leading to lower number of physical knots in low concentration solutions.

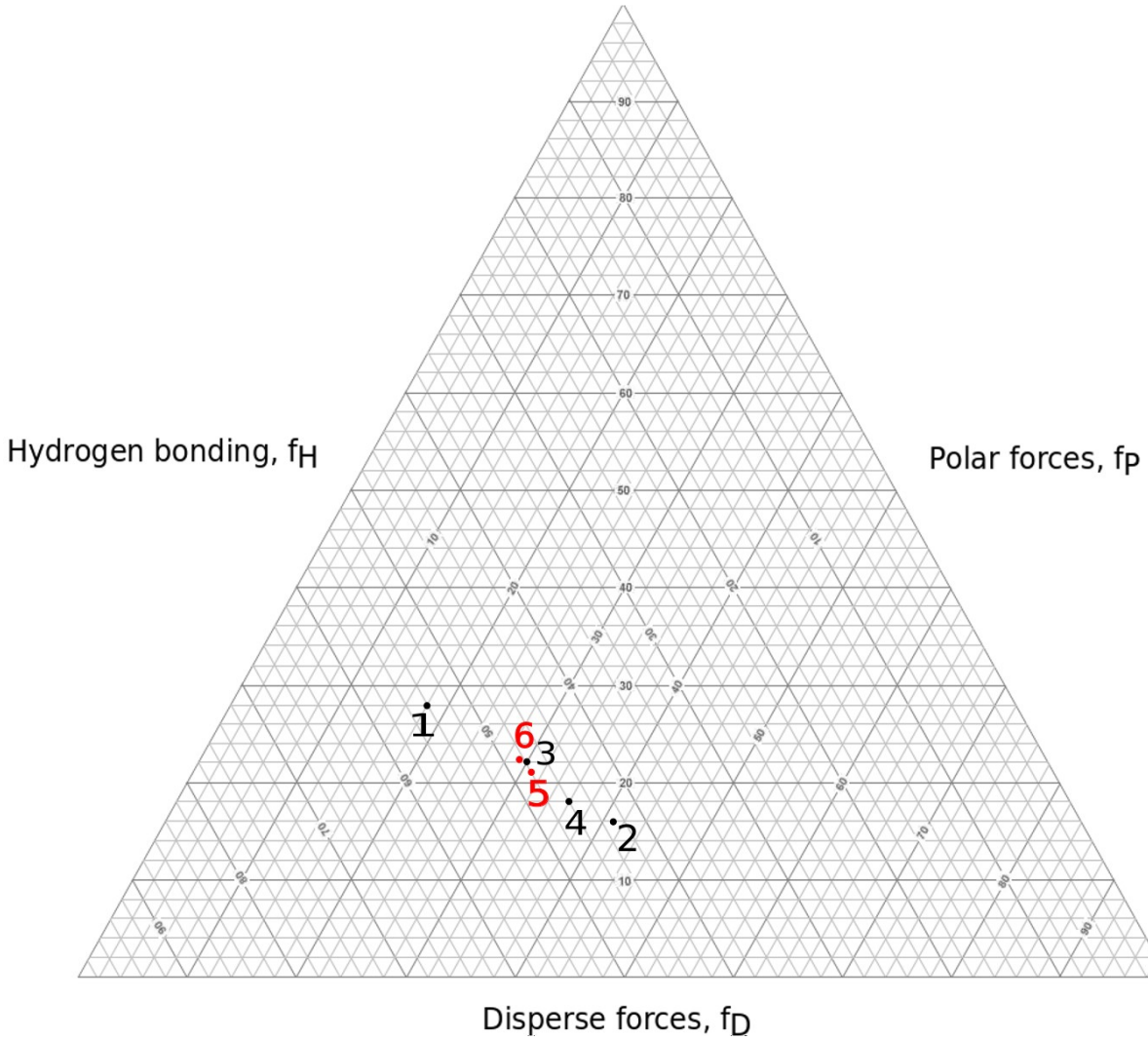

Fig. 55: Solvents and solvent mixtures represented in Teas graph; 1 – water, 2 – IPA, 3 – MeOH, 4 – EtOH, 5 – H2O:IPA 10:7, 6 – H2O:EtOH:MeOH 5:5:1

The solvent mixtures are very close in Teas graph, therefore similar solubility and behavior during electrospinning for all the solvent mixtures can be assumed. However, the experiments show

differences in the process, which will be discussed later. All the solvent mixtures allow the polymer to be dissolved without precipitation. The solutions turbidity is higher compared to water solutions of HA (see figs. 11-14), suggesting stronger polymer-polymer interactions to be present.

Spinning product morphology

The upper and lower limiting concentration was found for all solvent mixtures respective to HA M_w. The upper limiting concentration is around 3 wt.%, the lower is about 1 wt.%. It is rather difficult to draw conclusions on the influence of concentration on the fiber morphology, as the resulting structure is rather similar in most cases. It can be seen that some of the limiting concentrations represent the very transition from electrospinning to electrospraying (HA 0,6 MDa in H2O:IPA, concentration 1,3 wt.% - fig. 17; HA 0,6 MDa in H2O:EtOH:MeOH, concentration 0,7 wt.% - fig. 23; HA 1,18 MDa in H2O:EtOH:MeOH, concentration 2,3 wt.% - fig. 24).

The SEM micrographs show H2O:IPA solutions to have higher tendency to form beaded structures than H2O:EtOH:MeOH solutions. It can be clearly seen especially in the case of 0,6 MDa HA (see figs. 15-17, 21-23). It is clear from SEM micrographs that 1,18 MDa HA shows lower tendency to form beaded structures. On the other hand, concentration of 1,18 MDa HA had to be lower compared to 0,6 MDa HA to ensure smooth electrospinning process. That causes faster material consumption. The spinning voltage was significantly higher for 1,18 MDa HA solutions (maximum 20,5 kV for 0,6 MDa vs. 24 kV for 1,18 MDa in H2O:IPA solutions, and 19,1 kV for 0,6 MDa vs. 29,2 kV for 1,18 MDa for H2O:EtOH:MeOH solutions). This is possibly due to higher viscosity compared to 0,6 MDa HA solutions. The polymer concentration affects the yield of nanofibers and the tendency to form beads, however, no significant shift in sizes of nanofibers or beads was found.

Oxidized 0,6 MDa HA was electrospun as well to see the effect of chemical modification on fiber morphology. SEM micrographs show that oxidized HA has higher tendency to form beaded structures (see figs. 15-17), but also requires lower spinning voltage (maximum 20,5 for non-oxidized HA vs. 17,1 for HA-ox; see table 2). It is possible that higher concentration could stabilize the spinning process. That would make HA-ox a more desirable material to use in electrospinning application.

Solution parameters

The effect of polymer concentration on solution density is rather insignificant in all cases. The density is governed mainly by the solvents, which is clear in comparison of respective solvent systems - H2O:EtOH:MeOH system provides lower density solutions than H2O:IPA system.

Surface tension of the spinning solutions drops significantly compared to water solutions of HA. According to measurements of Jurošková, 2017, this is around 70 mN·m-1 [81], while in alcohol based solutions used in the current thesis, the surface tension is roughly 25 $mN \cdot m^{-1}$ – 30 $mN \cdot m^{-1}$. No dependence on HA concentration can be drawn from the results listed in table 3. This may be caused by little concentration range. Nevertheless, it is safe to assume that in the case of solutions used in the experimental work presented earlier, the surface tension is governed by the solvents. There is no significant difference in surface tension of respective solvent system. This fact is most likely coincidental.

We can see a steep drop in conductivity with decrease of HA concentration due to polyionic nature of HA. The conductivity drops with increase in HA molecular weight. This can be explained by the

fact that in solutions of different M_w polymer with the same polymer weight fraction, the molar fraction is lower for the polymer of higher M_w. This causes the electrolytic balance to be reached at lower dissociation of the HA molecules. Conductivity is also affected by the solvents. It is comparatively higher in H2O:EtOH:MeOH solvent system than in H2O:IPA solvent system (see table 3).

Shear viscosity is clearly a function of molecular weight and polymer concentration, with growing trend in both cases (see figs. 27-30). For 1,18 MDa HA it increased as high as 6 times compared to 0,6 MDa HA in the highest electrospinnable concentration. The magnitude of decrease with decreasing concentration depends on the respective polymer M_w – solvent system. The highest concentration of HA displays non-newtonian behavior regardless of HA M_w and solvent system. The viscosity curve was measured at low shear rates (0,1 s^{-1} – 10 s^{-1}) due to focus on electrospinning onset. At the formation of Taylor cone, the shear rates should be low, even negligible. Therefore non-newtonian behavior does not affect the onset of electrospinning. In jet spinning, elongation stress is applied to the forming fiber, therefore elongation viscosity is an important parameter in this part of the process. However, the elongation behavior of the jet is not within the scope of the current thesis.

The limiting parameters in electrospinning of HA are presumed to be viscosity in upper limiting concentration, and chain entanglement in lower limiting concentration. The experiments show that there is a significant difference in viscosity of upper limiting concentration solutions of HA with different M_w. This would suggest the limiting factor is not viscosity per se, but rather complex combination of intermolecular interactions, affecting ionic strength of the solution, polymer chain configuration and other parameters. As for the lower limiting concentration, it needs to be clarified whether the transition from electrospinning to electrospraying is caused by insufficient chain entanglement, or by significant decrease in conductivity, which leads to higher tendency to undergo Rayleigh instability.

8.2 Electrospinning of mixed M_w HA

Mixing high M_w and low M_w HA reduces the viscosity significantly, which leads to possibility of maintaining the electrospinning onset at higher weight concentration of the polymer. According to Palangetic et al., 2014, higher polydispersity leads to lower tendency to form beaded structures [21]. Mixing of several molecular weights simulates a highly polydisperse polymer system, therefore positive effects are expected.

Spinning product morphology

SEM micrographs show higher tendency to form beaded structures than in the case of single M_w HA (see figs. 32-34). Fibers and bead-on-string structures are very scarce. The particles have nearly spherical shape and their size is not affected significantly by the solution concentration. To address the problem of particle formation, high M_w HA (1,18 MDa and 1,5 MDa) was added to the mix at the concentration 3,5 wt.%. Although this adjustment did not lead to process stabilization, a certain progress can be seen. While in mixed M_w HA solution without HA over 1 MDa the particles are spherical, strongly elongated beads are found upon the addition of HA over 1 MDa (see fig. 34). The diameter of the beads decreased significantly in comparison to solutions without high M_w HA. This would suggest necessity of high M_w fractions of HA to be present electrospinning solution in

order to stabilize the jet. The effect of several M_w present in a solution on electrospinning process needs to be studied further to be fully understood.

Solution parameters

Surface tension shows a slight increase with the decrease of concentration. A similar findings were published by Ribeiro et al., 2007, for hyaluronan saline solutions above entanglement concentration [82]. Nonogaki et al., 2000, studied hyaluronan bi-layer formation in saturated bovine serum, and found a decrease in surface tension as the migration with increase in hyaluronan concentration. They assume this behavior to be a result of increase in negative charge amount on the surface [83]. The conclusions of these papers may not be valid in the present case, as they used hyaluronan instead of hyaluronic acid, and the solvent was different from the ones used in the current thesis. However, the entanglement concentration theory is in agreement with spinnability theory, as was described in 1.4.1. It is clear that more investigation on this issue is necessary.

As in the single M_w HA systems, density is not affected by the polymer concentration. Conductivity shows the same trend as in single M_w HA systems, as it decreases with HA concentration (see table 5). It exceeds the single M_w HA systems greatly due to higher concentrations, and possibly due to presence of low M_w HA chains, which effectively increase the overall molar fraction of HA in the solution. A different solvent mixture may be another aspect governing the conductivity. Shear viscosity decreases with decrease of polymer concentration, and it is significantly lower in comparison to single M_w HA solutions (see fig. 36). Compared to single M_w HA systems, the non-newtonian behavior is less distinct.

8.3 The influence of HA M_w on HA/PEO bi-component solutions and their spinnability

HA/PEO mixtures were spun from aqueous solutions in order to find influence of HA M_w on electrospinning of the mixture. The concentration of polymers was adjusted to 2 wt.% and their ratio was 1:1. The spinning voltage was kept at a steady value for each PEO M_w series in order to exclude as many influences as possible. Clear polymer solutions were obtained (figs. 37,38).

Spinning product morphology

All of the HA/PEO bi-component solutions give bead-on-string structured mats. No significant difference in diameter of either beads or strings can be found with respect to HA M_w at chosen conditions. There is a clear difference in the morphology of the beads when 300 kDa and 600 kDa PEO solutions are compared (figs. 39-44). In 300 kDa PEO solutions, the beads tend to form into almost spherical shapes, and in many cases connect several fibers together. In 600 kDa PEO solutions, high elongation is evident and the beads. This would suggest possibility of different original phenomenon leading to beads formation. The spherical particles connected with fibers present in 300 kDa PEO solutions (see figs. 39-41) may be a result of electric field induced elongation acting on electrosprayed particles. Bead-on-string structures created by 600 kDa PEO solutions (see figs. 42-44) are typically a result of electric field induced undulations appearing on originally uniform jet. This phenomenon is briefly described in section 1.1.2 of this thesis. However, the origin of the instabilities in the current experiments has to be further confirmed. The differences in diameter of structures obtained from 300 kDa and 600 kDa PEO solutions respectively is inconclusive (see table 6). Spinning voltage of 600 kDa PEO solutions was

necessary to be higher than for 300 kDa PEO solutions. This can be assigned to higher viscosity of 600 kDa PEO solutions.

HA-NB (M_w = 600 kDa) was spun from a blend with 600 kDa PEO, and then examined using fluorescent confocal microscope. Fig. 45 clearly shows that both beads and nanofibers contain HA. Unfortunately, it is not possible to confirm core-shell structure of the fibers, as the dimension of the layers would be below resolution of the microscope. On account of non-fluorescence of PEO, it is very difficult to be distinguished in presence of fluorescent HA.

Solution parameters

Neither HA M_w, nor PEO M_w have any effect on solution density. This is likely due to very low polymer concentration (2 wt.%), at which the solution's density is governed solely by the solvent, in this case water. The density of solutions is indeed very close to density of water at 25°C, which is 0,99704 $g \cdot cm^{-3}$ [84].

Surface tension of the solutions is affected by the polymer M_w. Solutions of 300 kDa PEO have lower surface tension in comparison to 600 kDa PEO solutions. Regardless of PEO M_w, the surface tension rises with higher HA M_w (see table 7). The cause of this shift is yet to be determined. In comparison to pure water (about 70 $mN \cdot m^{-1}$, [81]), surface tension decreased significantly in HA/PEO solutions (54 $mN \cdot m^{-1}$ – 46 $mN \cdot m^{-1}$). It should be noted that the surface tension of HA/PEO bi-component solution is significantly higher compared to HA solutions discussed in 8.1 and 8.2. The obvious explanation is difference in solvent choice.

Solution conductivity decreases with the increase of HA M_w. The possible cause of this phenomenon was discussed in 8.1. The drop in conductivity appears to be steeper in 600 kDa PEO solutions compared to 300 kDa PEO solutions. PEO might influence the conductivity of aqueous solutions due to dissociation of -OH groups, however, this effect is probably negligible in presence of highly dissociating HA molecules.

Shear viscosity of solutions increases with increasing HA M_w. A jump in shear viscosity was observed for solution with 600 kDa HA (see figs. 46,47). Solutions concentration was set at 2 wt.% mainly to ensure spinnability of 600 kDa HA, the solutions with lower HA M_w were spinnable at higher concentrations as well. The steep increase in viscosity is probably the cause of decreased spinnability of the solutions. All solutions act as newtonian fluids in the chosen range of shear rates.

8.4 The influence of BAC concentration on spinnability of HA/PVA bi-component solutions

HA/PVA aqueous electrospinnable solutions were found experimentally. Addition of small amount of BAC was found to be necessary to facilitate stability of the spinning process. In order to determine the influence of BAC concentration, four solutions with different amount of BAC were spun at the same processing parameters (spinning voltage and tip-to-collector distance). It should be noted that turbidity of the solutions increases with increase of BAC concentration and partial precipitation can be observed in 0,065 wt.% BAC solution (see fig. 48), in agreement with Gřundělová et al., 2013, [78]. Further increase of BAC concentration would therefore be counterproductive. Thus it is safe to assume that BAC induces higher polymer-polymer interactions, leading to coiling and microscopic clumps to be formed, therefore effectively creating low quality solvent.

Spinning product morphology

Bead-on-string structures were obtained from all the solutions except for 0,006 wt.% BAC solution, which formed only particles, although these also show clear signs of elongation (see figs. 49-52). There is no significant difference in diameter of neither beads or strings with respect to BAC concentration. The tendency to form beaded structures is rather high in all the solutions, but the amount of fibers formed increases with the increase in BAC concentration. Higher concentration of BAC leads to multiple Taylor cone formation, therefore increasing the yield of electrospun structures. Increase in BAC concentration causes a notable decrease in spinning voltage required (see table 8). It is ought to remember that any assumption made on account of the current experiments is valid only in the range of BAC concentrations used. As stated earlier, high concentrations of BAC lead to complete precipitation of HA and would disrupt the electrospinning process.

PVA-FITC and HA-NB were spun to determine the inner structure of the fibers using fluorescence confocal microscopy. Fig. 53 a) and b) clearly show that both polymers are present in the fibers, as well as in the beads. Fig. 53 c) shows a combination of both fluorescent polymers. The results could mean that in some fibers, PVA-FITC prevails over HA-NB and vice versa, or, in case of core-shell structure, a different shell material in respective fibers. Unfortunately, it is not possible to determine whether the morphology is truly core-shell, since the resolution is insufficient.

Solution parameters

No effect of BAC concentration on solution density was found. The density is very close to density of pure water at 25°C (see 8.3), therefore it can be assumed that the main contribution to the solution density is the one of the solvent, i.e. water.

BAC, being a surface active substance, affects the surface tension of the solution by definition. A slight decrease in surface tension is observed with increase of BAC concentration (45 $mN \cdot m^{-1}$ – 41 $mN \cdot m^{-1}$), which is an expected outcome (see table 9). The decrease in surface tension is likely the cause of decrease in spinning voltage (20 kV to 16 kV). It should be noted that surface tension (40 $mN \cdot m^{-1}$ – 45 $mN \cdot m^{-1}$) decreased slightly compared to HA/PEO bi-component solutions (45 $mN \cdot m^{-1}$ – 55 $mN \cdot m^{-1}$). It is still significantly higher than surface tension of HA alcohol based solutions (25 $mN \cdot m^{-1}$ – 30 $mN \cdot m^{-1}$), and significantly lower than pure water surface tension (about 70 $mN \cdot m^{-1}$, [81]).

BAC as an ionic substance should have an effect on solution conductivity as well. This can be clearly seen in table 9. The conductivity increases with increase of BAC concentration. The increase in conductivity is probably to be accounted for the decrease in tendency to form beaded structures. In comparison to HA/PEO solutions, the conductivity is higher, although the amount of HA in respective bi-component solutions is comparable. This could be the result of combined effect of BAC dissociation, and dissociation of partner polymer, i.e. PVA, or PEO respectively.

Shear viscosity of HA/PVA solutions containing 0,006 wt.% BAC, 0,013 wt.% BAC, and 0,33 wt.% BAC is not affected by BAC concentration in any way. However, solution containing 0,063 wt.% BAC shows a significant drop in shear viscosity (fig. 54). This is likely due to partial precipitation of polymer in this solution. All solutions display almost newtonian behavior in the chosen range of shear rates.

CONCLUSION

In the current Master's thesis, solutions containing HA were spun into nanofibers via DC electric field. The polymer was either HA alone, or a combination of HA/PEO or HA/PVA respectively.

For pure HA solutions, solvent mixtures were found which facilitate electrospinning process to occur. These solvent mixtures are H2O:IPA 10:7, H2O:EtOH:MeOH 5:5:1, and H2O:EtOH 4:3. The last was used for solutions containing mixture of high M_w HA and low M_w HA. Upper and lower concentration limit was found for each respective solution. The lower limiting factor appears to be either insufficiency of polymer chain entanglements, or low conductivity. Viscosity appears to be logical candidate for upper limiting factor, however, great variety in viscosity of upper limiting concentration solutions was observed in the current thesis. Therefore, the upper limiting factor is yet to be determined.

HA/PEO and HA/PVA bi-component blend water solutions were successfully spun. In HA/PEO solutions, PEO of 600 kDa gave more uniform bead-on-string structures than PEO of 300 kDa solutions. No influence of HA M_w on spinning product morphology was found in the experiments. Fluorescence confocal microscopy of fibers containing HA-NB proved presence of HA in both fibers, and beads. For HA/PVA electrospinning, addition of small amount of BAC was necessary. All of the solutions produced beaded, or bead-on-string structures. BAC concentration closest to critical micelar concentration (0,065 wt.%) provided the highest fiber-to-beads ratio. Fluorescence confocal microscopy of fibers containing HA-NB and PVA-FITC proved presence of both polymers in fibers, as well as beads.

To conclude, the most significant results of the current thesis are the following:

a) single M_w HA is possible to be electrospun from solutions containing alcohols, as listed earlier; higher M_w HA (1 180 kDa) shows lower tendency to form beaded structures than lower M_w HA (600 kDa),

b) mixed M_w HA can be electrospun from H2O:EtOH solution, but the tendency to form spherical particles is higher than in solutions containing single M_w HA,

c) bi-component blend solutions containing HA and PEO/PVA respectively can be electrospun, resulting in bead-on string structures,

d) bi-component blends of HA/PEO can be electrospun as water solutions; higher PEO M_w (600 kDa) provides more uniform products than lower PEO M_w (300 kDa),

e) bi-component blends of HA/PVA can be electrospun as water solutions with the addition of small amount of BAC; the best results are reached when BAC concentration is closest to critical micelar concentration.

The reasons for the phenomena described in experimental part of the current thesis need further investigation. Let this thesis be an experimental insight into possibilities of HA electrospinning.

BIBLIOGRAPHY

[1] J. F. Cooley, “Apparatus for electrically dispersing fluids,” 692631, 1902.

[2] W. J. Morton, “Method of dispersing fluids,” 705691, 1902.

[3] G. Taylor, “Disintegration of water drops in an electric field,” *Proceeding R. Soc. A*, no. February, pp. 383–397, 1964.

[4] S. Agarwal, J. H. Wendorff, and A. Greiner, “Use of electrospinning technique for biomedical applications,” *Polymer (Guildf).*, vol. 49, no. 26, pp. 5603–5621, 2008.

[5] K. Yong, L. Jeong, Y. Ok, S. Jin, and W. Ho, “Electrospinning of polysaccharides for regenerative medicine,” *Adv. Drug Deliv. Rev.*, vol. 61, no. 12, pp. 1020–1032, 2009.

[6] M. Kitsara, O. Agbulut, D. Kontziampasis, Y. Chen, and P. Menasché, “Fibers for hearts: A critical review on electrospinning for cardiac tissue engineering,” *Acta Biomaterialia*. 2017.

[7] A. Rogina, “Electrospinning process: Versatile preparation method for biodegradable and natural polymers and biocomposite systems applied in tissue engineering and drug delivery,” *Appl. Surf. Sci.*, vol. 296, pp. 221–230, 2014.

[8] S. Vikram and R. Vasanthakumari, “Assessment on the Release of Magnetite Nanoparticles Embedded with PVA Nanofiber in Hydrodynamics,” vol. 41, pp. 31–41, 2016.

[9] L. Burke *et al.*, “In-situ synthesis of magnetic iron-oxide nanoparticle-nano fi bre composites using electrospinning,” *Mater. Sci. Eng. C*, vol. 70, pp. 512–519, 2017.

[10] D. K. Kim, M. Hwang, and J. P. F. Lagerwall, “Liquid crystal functionalization of electrospun polymer fibers,” *J. Polym. Sci. Part B Polym. Phys.*, vol. 51, no. 11, pp. 855–867, 2013.

[11] I. C. Um, D. Fang, B. S. Hsiao, A. Okamoto, and B. Chu, “Electro-Spinning and Electro-Blowing of Hyaluronic Acid,” *Biomacromolecules*, vol. 5, pp. 1428–1436, 2004.

[12] E. K. Brenner, J. D. Schiffman, E. A. Thompson, L. J. Toth, and C. L. Schauer, “Electrospinning of hyaluronic acid nanofibers from aqueous ammonium solutions,” *Carbohydr. Polym.*, 2012.

[13] Y. Liu, G. Ma, D. Fang, J. Xu, H. Zhang, and J. Nie, “Effects of solution properties and electric field on the electrospinning of hyaluronic acid,” *Carbohydr. Polym.*, vol. 83, no. 2, pp. 1011–1015, 2011.

[14] D. Lukáš *et al.*, “Physical principles of electrospinning (electrospinning as a nano-scale technology of the twenty-first century),” *Text. Prog.*, vol. 41, no. 2, pp. 59–140, 2009.

[15] R. M. Pashley, *On the Surface of Things*. Ballan: Connor Court Publishing Ltd., 2012.

[16] D. Lukas, A. Sarkar, P. Pokorny, and V. Dyke, “Self-organization of jets in electrospinning from free liquid surface: A generalized approach,” *J. Appl. Phys.*, vol. 103, pp. 1–7, 2008.

[17] T. Miloh, B. Spivak, and A. L. Yarin, “Needleless electrospinning : Electrically driven instability and multiple jetting from the free surface of a spherical liquid layer,” *J. Appl. Phys.*, vol. 106, 2009.

[18] M. E. Helgeson, K. N. Grammatikos, J. M. Deitzel, and N. J. Wagner, “Theory and kinematic measurements of the mechanics of stable electrospun polymer jets,” *Polymer (Guildf).*, vol. 49, no. 12, pp. 2924–2936, 2008.

[19] A. Y. Malkin, A. Arinstein, and V. G. Kulichikhin, “Polymer extension flows and instabilities,” *Prog. Polym. Sci.*, vol. 39, no. 5, pp. 959–978, 2014.

[20] S. L. Shenoy, W. D. Bates, H. L. Frisch, and G. E. Wnek, “Role of chain entanglements on fiber formation during electrospinning of polymer solutions: Good solvent, non-specific polymer-polymer interaction limit,” *Polymer (Guildf).*, vol. 46, no. 10, pp. 3372–3384, 2005.

[21] L. Palangetic, N. K. Reddy, S. Srinivasan, R. E. Cohen, G. H. McKinley, and C. Clasen, “Dispersity and spinnability: Why highly polydisperse polymer solutions are desirable for electrospinning,” *Polymer (Guildf).*, 2014.

[22] J. H. Jeans, *The Mathematical Theory of Electricity and Magnetism*. Cambridge: Cambridge University Press, 1908.

[23] D. H. Reneker and A. L. Yarin, “Electrospinning jets and polymer nanofibers,” *Polym. with aligned carbon Nanotub. Act. Compos. Mater.*, vol. 49, no. 10, pp. 2387–2425, 2008.

[24] W. E. Teo and S. Ramakrishna, “A review on electrospinning design and nanofibre assemblies,” *Nanotechnology*, vol. 17, no. 14, 2006.

[25] R. Nayak, R. Padhye, I. L. Kyratzis, Y. B. Truong, and L. Arnold, “Recent advances in nanofibre fabrication techniques,” *Text. Res. J.*, 2012.

[26] I. Alghoraibi and S. Alomari, *Different methods for nanofibers design and fabrication*. 2018.

[27] J. W. Gibbs, “A method of geometrical representation of the thermodynamic properties of substances by means of surfaces,” *Trans. Connect. Acad.*, vol. 2, no. December, pp. 382–404, 1873.

[28] P. J. Flory, *Principles of Polymer Chemistry*. Ithaca, NY: Cornell University Press, 1953.

[29] C. J. Luo, M. Nangrejo, and M. Edirisinghe, “A novel method of selecting solvents for polymer electrospinning,” *Polymer (Guildf).*, vol. 51, no. 7, pp. 1654–1662, 2010.

[30] A. Y. Malkin *et al.*, “Spinnability of Dilute Polymer Solutions,” *Macromolecules*, vol. 50, no. 20, pp. 8231–8244, 2017.

[31] C. Tanford, *Physical Chemistry of Macromolecules*. New York: Wiley, 1961.

[32] B. L. Hager, G. C. Berry, and H.-H. Tsai, “Moderately concentrated solutions of polystyrene. II. Integrated-intensity light scattering as a function of concentration, temperature, and molecular weight,” *J. Polym. Sci. Part B Polym. Phys.*, vol. 25, no. 2, 1987.

[33] S. L. Shenoy, W. D. Bates, and G. Wnek, “Correlations between electrospinnability and physical gelation,” *Polymer (Guildf).*, vol. 46, no. 21, pp. 8990–9004, 2005.

[34] J. M. Deitzel, J. Kleinmeyer, D. Harris, and N. C. Beck Tan, “The effect of processing variables on the morphology of electrospun nanofibers and textiles,” *Polymer (Guildf).*, 2001.

[35] H. Semat and R. Katz, “Electrical Conduction in Liquids and Solids,” in *Physics*, New York: Rinehart & Company, Inc., 1958.

[36] J. Novák, L. Bartovská, I. Cibulka, and V. Dohnal, *Fyzikální chemie*. Praha, 2008.

[37] P. Peer, “Rheological Characterization of Polymer Solutions with Respect to Quality of Electrospinning Process,” Thomas Bata University in Zlín, 2015.

[38] A. L. Yarin, S. Koombhongse, and D. H. Reneker, “Bending instability in electrospinning of nanofibers,” *J. Appl. Phys.*, 2001.

[39] L. Vysloužilová *et al.*, “Needleless coaxial electrospinning: A novel approach to mass production of coaxial nanofibers,” *Int. J. Pharm.*, vol. 516, no. 1–2, pp. 293–300, 2017.

[40] Y. J. Chiu *et al.*, “Fabrication and Thermal Insulation Properties of Bamboo-Shaped Polymer Fibers by Selective Solvent Vapor Annealing,” *Macromol. Rapid Commun.*, vol. 1800424, pp. 1–7, 2018.

[41] J. Yoon, H. S. Yang, B. S. Lee, and W. R. Yu, “Recent Progress in Coaxial Electrospinning: New Parameters, Various Structures, and Wide Applications,” *Adv. Mater.*, vol. 30, no. 42, pp. 1–23, 2018.

[42] Q. Gao, J. Luo, X. Wang, C. Gao, and M. Ge, “Novel hollow α-Fe2O3 nanofibers via electrospinning for dye adsorption,” *Nanoscale Res. Lett.*, 2015.

[43] J. P. F. Lagerwall, “Switchable and responsive liquid crystal-functionalized microfibers produced via coaxial electrospinning,” *Proc. Spie*, vol. 8279, no. February 2012, 2012.

[44] A. L. Yarin, “Coaxial electrospinning and emulsion electrospinning of core – shell fibers,” *Polym. Adv. Technol.*, vol. 22, no. April 2010, pp. 310–317, 2011.

[45] E. Kostakova, L. Meszaros, and J. Gregr, “Composite nanofibers produced by modified needleless electrospinning,” *Mater. Lett.*, vol. 63, no. 28, pp. 2419–2422, 2009.

[46] H. Ma, G. Chen, J. Zhang, Y. Liu, J. Nie, and G. Ma, “Facile fabrication of core-shell polyelectrolyte complexes nanofibers based on electric field induced phase separation,” *Polymer (Guildf).*, vol. 110, pp. 80–86, 2017.

[47] E. A. Buyuktanir, M. W. Frey, and J. L. West, “Self-assembled, optically responsive nematic liquid crystal/polymer core-shell fibers: Formation and characterization,” *Polymer (Guildf).*, vol. 51, no. 21, pp. 4823–4830, 2010.

[48] A. V. Bazilevsky, A. L. Yarin, and C. M. Megaridis, “Co-electrospinning of core-shell fibers using a single-nozzle technique,” *Langmuir*, vol. 23, no. 5, pp. 2311–2314, 2007.

[49] C. G. Reyes, A. Sharma, and J. P. F. Lagerwall, “Non-electronic gas sensors from electrospun mats of liquid crystal core fibres for detecting volatile organic compounds at room temperature,” *Liq. Cryst.*, vol. 43, no. 13–15, 2016.

[50] J. Wang, A. Jákli, and J. L. West, “Liquid crystal/polymer fiber mats as sensitive chemical sensors,” *J. Mol. Liq.*, vol. 267, pp. 490–495, 2018.

[51] S. Manmohan, “Requirement for Fiber Forming Polymer,” *https://www.scribd.com/document/136844033/Requirement-for-Fiber-Forming-Polymer*, 2013. [Online]. Available: https://www.scribd.com/document/136844033/Requirement-for-Fiber-Forming-Polymer.

[52] G. Kogan, L. Šoltés, R. Stern, and P. Gemeiner, “Hyaluronic acid: A natural biopolymer with a broad range of biomedical and industrial applications,” *Biotechnol. Lett.*, vol. 29, no. 1, pp. 17–25, 2007.

[53] “Polymer Properties Database.” [Online]. Available: https://polymerdatabase.com/index.html. [Accessed: 02-Jan-2019].

[54] R. Uppal, G. N. Ramaswamy, C. Arnold, R. Goodband, and Y. Wang, “Hyaluronic acid nanofiber wound dressing-production, characterization, and in vivo behavior,” *J. Biomed. Mater. Res. - Part B Appl. Biomater.*, vol. 97 B, no. 1, pp. 20–29, 2011.

[55] S. J. Eichhorn, J. W. S. Hearle, M. Jaffe, and T. Kikutani, *Handbook of Textile Fibre Structure*. 2009.

[56] S. E. M. Selke and J. D. Culter, *Plastics Packaging - Properties, Processing, Applications, and Regulations*, 3rd ed. Hanser Publishers, 2016.

[57] J. G. Pritchard, *Poly(vinyl alcohol)*, 1st ed. London: Macdonald & Co. Ltd., 1970.

[58] J. Grufíková, “The Influence of PEO Source on Nanofiber Layer Preparation,” Brno University of Technology, 2017.

[59] D. B. Braun and M. R. Rosen, “27. Polyethylene Oxide,” in *Rheology Modifiers Handbook - Practical Use and Application*, William Andrew Publishing, 2000.

[60] M. N. Subramanian, *Polymer Blends and Composites - Chemistry and Technology*. John Wiley & Sons, 2017.

[61] E. Bingham and B. Cohrssen, “Polyoxyethylene,” in *Patty’s Toxicology (6th Edition) Volumes 1-6*, John Wiley & Sons, 2012.

[62] S. G. Kumbar, C. T. Laurencin, and M. Deng, *Natural and Synthetic Biomedical Polymers*. Elsevier, 2014.

[63] G. Yan *et al.*, “Self-assembly of electrospun polymer nanofibers: A general phenomenon generating honeycomb-patterned nanofibrous structures,” *Langmuir*, vol. 27, no. 8, pp. 4285–4289, 2011.

[64] W. K. Son, J. H. Youk, T. S. Lee, and W. H. Park, “The effects of solution properties and polyelectrolyte on electrospinning of ultrafine poly (ethylene oxide) fibers,” vol. 45, pp. 2959–2966, 2004.

[65] F. Brochard and P. G. de Gennes, “Spreading laws for liquid polymer droplets: interpretation of the ‘foot,’” *J. Phys.*, vol. 45, no. June, pp. 597–602, 1984.

[66] P. G. de Gennes, “Wetting: statics and dynamics,” *Rev. Mod. Phys.*, vol. 57, no. 3, 1985.

[67] I. Newton, *Philosophiae Naturalis Principia Mathematica*. J. Societatis Regiae ac Typis J. Streater, 1687.

[68] A. C. Merrington, *Viscometry*. London: Edward Arnold & Co., 1949.

[69] S. C. Moldoveanu and V. David, “Short Overviews of Analytical Techniques Not Containing an Independent Separation Step,” in *Selection of the HPLC Method in Chemical Analysis*, Elsevier Inc., 2017.

[70] R. Kazys, R. Sliteris, R. Rekuviene, E. Zukauskas, and L. Mazeika, “Ultrasonic Technique for Density Measurement of Liquids in Extreme Conditions,” *Sensors*, vol. 15, pp. 19393–19415, 2015.

[71] A. Furtado, E. Batista, I. Spohr, and E. Filipe, “Measurement of density using oscillation-type density meters. Calibration , traceability and Uncertainties,” 2009.

[72] L. Reimer, *Scanning electron microscopy: physics of image formation and microanalysis*, 2nd ed. Berlin: Springer, 1998.

[73] S. W. Paddock, *Confocal microscopy: methods and protocols*, 2nd ed. New York: Humana Press, 2013.

[74] R. L. Price and W. G. Jerome, *Basic confocal microscopy*. New York: Springer, 2011.

[75] G. Huerta-Angeles, M. Němcová, E. Příkopová, D. Šmejkalová, M. Pravda, and V. Velebný, “Reductive alkylation of hyaluronic acid for the synthesis of biocompatible hydrogels by click chemistry,” *Carbohydr. Polym.*, vol. 90, pp. 1704–1711, 2012.

[76] D. Šmejkalová *et al.*, “Hyaluronan polymeric micelles for topical drug delivery,” *Carbohydr. Polym.*, vol. 156, pp. 86–96, 2017.

[77] Y. Kaneo, S. Hashihama, A. Kakinoki, and T. Tanaka, “Pharmacokinetics and Biodisposition of Poly (vinyl alcohol) in Rats and Mice,” *Drug Metab. Pharmacokinet.*, vol. 20, no. 6, pp. 435–442, 2005.

[78] L. Gřundělová, A. Mráček, V. Kašpárková, A. Minařík, and P. Smolka, “The influence of quarternary salt on hyaluronan conformation and particle size in solution,” *Carbohydr. Polym.*, vol. 98, pp. 1039–1044, 2013.

[79] J. L. Gardon and J. P. Teas, “Characterization of Coatings: Physical Techniques,” in *Treatise on Coatings*, 2nd ed., New York: Marcel Dekker, 1976.

[80] A. Barton, *Handbook of Solubility Parameters*. CRC Press, 1983.

[81] D. Jurošková, “Charakterizace hyaluronanu sodného ve vodných roztocích a na fázových rozhraních,” Thomas Bata University in Zlín, 2017.

[82] W. Ribeiro, L. Mata, and B. Saramago, “Effect of Concentration and Temperature on Surface Tension of Sodium Hyaluronate Saline Solutions,” vol. 94, no. 11, pp. 7014–7017, 2007.

[83] T. Nonogaki, S. Xu, S. Kugimiya, S. Sato, I. Miyata, and M. Yonese, “Two Dimensional Auto-Organized Nanostructure Formation of Hyaluronate on Bovine Serum Albumin Monolayer and Its Surface Tension,” no. 17, pp. 4272–4278, 2000.

[84] G. E. Totten, S. R. Westbrook, and R. J. Shah, *Fuels and Lubricants Handbook - Technology, Properties, Performance, and Testing: (MNL 37WCD)*. ASTM International, 2003.

LIST OF ABBREVIATIONS

HA	Hyaluronic acid
DC	Direct current
AC	Alternating current
M_w	Molecular weight
PMSQ	Polymethylsilsesquioxane
EtOH	Ethanol
PVA	Polyvinyl alcohol
PEO	Poly(ethylene oxide)
FDA	United States Food and Drug Administration
DMF	N,N - dimethylformamide
SEM	Scanning Electron Microscopy
DEMI	Demineralized
IPA	Propan-2-ol
MeOH	Methanol
BAC	Benzethonium chloride
4-Ac-TEMPO	4-acetamido-TEMPO
DMSO	Dimethylsulfoxide
FITC	Fluorescein isothyocyanite isomer
HA-ox	Oxidized HA
PVA-FITC	FITC labeled PVA
HA-NB	Nile Blue labeled HA

LIST OF FIGURES

Fig. 1: Taylor cone scheme.…… **14**

Fig. 2: A scheme of electrospinning jet path.…… **16**

Fig. 3: Conventional DC electrospinning setup scheme.…….... **18**

Fig. 4: Teas graph – a ternary plot designed to depict fractional solubility parameters of solvents derived from Hansen solubility parameters.…….. **21**

Fig. 5: Co-axial electrospinning setup scheme.…….... **24**

Fig. 6: A scheme of core-shell electrospinning of an emulsion.…… **25**

Fig. 7: HA structure formula.…….. **26**

Fig. 8: PVA structure formula.…….... **27**

Fig. 9: PEO structure formula.…….. **28**

Fig. 10: Electrospinning device used in experimental part of the current thesis (high voltage power supply not in picture).…….. **35**

Fig. 11: Solutions of 0,6 MDa HA in H_2O:IPA 10:7, a) 3,2 wt.%, b) 2,3 wt.%, c) 1,3 wt.%.…... **37**

Fig. 12: Solutions of 1,18 MDa HA in H_2O:IPA 10:7, a) 2,9 wt.%, b) 1,2 wt.%, c) 1,0 wt.%.….. **37**

Fig. 13: Solutions of 0,6 MDa HA in H_2O:EtOH:MeOH 5:5:1, a) 2,8 wt.%, b) 2,4 wt.%, c) 0,7 wt.%.…….... **38**

Fig. 14: Solutions of 1,18 MDa HA in H_2O:EtOH:MeOH 5:5:1, a) 2,3 wt.%, b) 2,2 wt.%, c) 1,5 wt.%.…….. **38**

Fig. 15: SEM micrographs of HA 0,6 MDa H_2O:IPA 10:7 3,2 wt.% solution fibers; a) non-oxidized HA, spinning voltage 20,5 kV b) HA-ox, spinning voltage 17,1 kV.…… **39**

Fig. 16: SEM micrographs of HA 0,6 MDa H_2O:IPA 10:7 2,3 wt.% solution fibers; a) non-oxidized HA, spinning voltage 20 kV b) HA-ox, spinning voltage 15,8 kV.…… **40**

Fig. 17: SEM micrographs of HA 0,6 MDa H_2O:IPA 10:7 1,3 wt.% solution fibers, a) non-oxidized HA, 16,2 kV b) HA-ox, spinning voltage 16,4 kV.…… **41**

Fig. 18: SEM micrographs of HA 1,18 MDa H_2O:IPA 10:7 2,9 wt.% solution fibers, spinning voltage 24 kV.…….. **42**

Fig. 19: SEM micrographs of HA 1,18 MDa H_2O:IPA 10:7 1,2 wt.% solution fibers, spinning voltage 16,3 kV.…….. **42**

Fig. 20: SEM micrographs of HA 1,18 MDa H_2O:IPA 10:7 1,0 wt.% solution fibers, spinning voltage 19,0 kV.…….. **43**

Fig. 21: SEM micrographs of HA 0,6 MDa H_2O:EtOH:MeOH 5:5:1 2,8 wt.% solution fibers, spinning voltage 19,1 kV.…….. **43**

Fig. 22: SEM micrographs of HA 0,6 MDa H_2O:EtOH:MeOH 5:5:1 2,4 wt.% solution fibers, spinning voltage 16,5 kV.…….. **44**

Fig. 23: SEM micrographs of HA 0,6 MDa H_2O:EtOH:MeOH 5:5:1 0,7 wt.% solution fibers, spinning voltage 14,9 kV.…….. **44**

Fig. 24: SEM micrographs of HA 1,18 MDa H_2O:EtOH:MeOH 5:5:1 2,3 wt.% solution fibers, spinning voltage 29,2 kV.… **45**

Fig. 25: SEM micrographs of HA 1,18 MDa H_2O:EtOH:MeOH 5:5:1 2,2 wt.% solution fibers, spinning voltage 22,9 kV.… **45**

Fig. 26: SEM micrographs of HA 1,18 MDa H_2O:EtOH:MeOH 5:5:1 1,5 wt.% solution fibers, spinning voltage 19,2 kV.… **46**

Fig. 27: Viscosity of 0,6 MDa HA in H_2O:IPA 10:7 solution as a function of shear rate.… **48**

Fig. 28: Viscosity of 1,18 MDa HA in H_2O:IPA 10:7 solution as a function of shear rate.… **49**

Fig. 29: Viscosity of 0,6 MDa HA in H_2O:EtOH:MeOH 5:5:1 solution as a function of shear rate.… **49**

Fig. 30: Viscosity of 1,18 MDa HA in H_2O:EtOH:MeOH 5:5:1 solution as a function of shear rate.… **50**

Fig. 31: Solutions of mixed M_w HA in H_2O:EtOH 4:3, a) HA 124 kDa, 243 kDa, 370 kDa, 600 kDa – 4,3 wt.%, b) HA 124 kDa, 243 kDa, 370 kDa, 600 kDa – 3,5 wt.%, c) HA 124 kDa, 243 kDa, 370 kDa, 600 kDa – 1,0 wt.%, d) HA 124 kDa, 243 kDa, 370 kDa, 600 kDa, 1 180 kDa, 1 500 kDa – 3,5 wt.%.… **50**

Fig. 32: SEM micrographs of mixed M_w (124 kDa, 243 kDa, 370 kDa, 600 kDa) HA H_2O:EtOH 4:3 4,3 wt.% solution fibers, spinning voltage 18,5 kV.… **51**

Fig. 33: SEM micrographs of mixed M_w (124 kDa, 243 kDa, 370 kDa, 600 kDa) HA H_2O:EtOH 4:3 3,5 wt.% solution fibers, spinning voltage 16,9 kV.… **51**

Fig. 34: SEM micrographs of mixed M_w (124 kDa, 243 kDa, 370 kDa, 600 kDa) HA H_2O:EtOH 4:3 1,0 wt.% solution fibers, spinning voltage 21,2 kV.… **52**

Fig. 35: SEM micrographs of mixed M_w (124 kDa 243 kDa, 370 kDa, 600 kDa, 1 180 kDa, 1 500 kDa) HA in H_2O:EtOH 4:3 3,5 wt.% solution fibers, spinning voltage 20,2 kV.… **52**

Fig. 36: Viscosity of HA of mixed molecular weights in H_2O:EtOH 4:3 solution as a function of shear rate.… **53**

Fig. 37: PEO 300 kDa/HA blend solutions; a) HA 243 kDa, b) HA 370 kDa, c) HA 600 kDa.… **54**

Fig. 38: PEO 600 kDa/HA blend solutions; a) HA 243 kDa, b) HA 370 kDa, c) HA 600 kDa.… **54**

Fig. 39: SEM micrographs of PEO 300 kDa and HA 243 kDa solution fibers, spinning voltage 18,2 kV.… **55**

Fig. 40: SEM micrographs of PEO 300 kDa and HA 370 kDa solution fibers, spinning voltage 18,2 kV.… **55**

Fig. 41: SEM micrographs of PEO 300 kDa and HA 600 kDa solution fibers, spinning voltage 18,2 kV.… **56**

Fig. 42: SEM micrographs of PEO 600 kDa and HA 243 kDa solution fibers, spinning voltage 24,5 kV.… **56**

Fig. 43: SEM micrographs of PEO 600 kDa and HA 370 kDa solution fibers, spinning voltage 24,5 kV.… **57**

Fig. 44: SEM micrographs of PEO 600 kDa and HA 600 kDa solution fibers, spinning voltage 24,5 kV.… **57**

Fig. 45: Fluorescence confocal microscopy micrographs of HA-NB 600 kDa and PEO 600 kDa 2 wt.% aqueous solution, spinning voltage 24,5 kV.……. **58**

Fig. 46: Viscosity of HA and 300 kDa PEO bi-component solutions as a function of shear rate.……. **59**

Fig. 47: Viscosity of HA and 600 kDa PEO bi-component solutions as a function of shear rate.……. **59**

Fig. 48: PVA 89-98 kDa/HA 600 kDa blend solutions; a) 0,006 wt.% BAC , b) 0,013 wt.% BAC, c) 0,033 wt.% BAC, d) 0,065 wt.% BAC.……. **60**

Fig. 49: SEM micrographs of PVA 89-98 kDa and HA 600 kDa solution with 0,006 wt.% BAC fibers, spinning voltage 20,4 kV.……. **60**

Fig. 50: SEM micrographs of PVA 89-98 kDa and HA 600 kDa solution with 0,013 wt.% BAC fibers, spinning voltage 18,8 kV.……. **61**

Fig. 51: SEM micrographs of PVA 89-98 kDa and HA 600 kDa solution with 0,033 wt.% BAC fibers, spinning voltage 17,5 kV.……. **61**

Fig. 52: SEM micrographs of PVA 89-98 kDa and HA 600 kDa solution with 0,065 wt.% BAC fibers, spinning voltage 15,9 kV.……. **62**

Fig. 53: Fluorescence confocal microscopy micrographs of PVA-FITC and HA-NB solution with 0,065 wt.% BAC fibers, spinning voltage 18,1 kV, a) PVA-FITC visible (excitation wavelength 488 nm), b) HA-NB visible (excitation wavelength 640 nm), c) both PVA-FITC and HA-NB visible (combined excitation wavelength).…… **63**

Fig. 54: Viscosity of HA/PVA bi-component solutions with addition of BAC as a function of shear rate.…… **64**

Fig. 55: Solvents and solvent mixtures represented in Teas graph; 1 – water, 2 – IPA, 3 – MeOH, 4 – EtOH, 5 – H_2O:IPA 10:7, 6 – H_2O:EtOH:MeOH 5:5:1.…… **65**

LIST OF TABLES

Table 1: Contents of HA/PVA blend solutions with addition of BAC.……...**35**

Table 2: Morphology analysis of single M_w HA electrospinning products.……..**47**

Table 3: Characteristics of electrospinnable single M_w HA solutions.……...**48**

Table 4: Morphology analysis of mixed M_w HA electrospinning products.……..**53**

Table 5: Characteristics of HA solution containing M_w 128 kDa, 243 kDa, 370 kDa and 600 kDa at weight ratio 1:1:1:1 in H_2O:EtOH 4:3 solvent mixture.……...**53**

Table 6: Morphology analysis of PEO/HA electrospinning products.……...**58**

Table 7: Characteristics of electrospinnable HA/PEO blend solutions.……...**59**

Table 8: Morphology analysis of PVA/HA electrospinning products.……....**64**

Table 9: Characteristics of electrospinnable HA/PVA blend solutions with BAC addition.……**64**